UNIVERSIDAD DE CHILE
FACULTAD DE CIENCIAS FÍSICAS Y MATEMÁTICAS
DEPARTAMENTO DE INGENIERÍA ELÉCTRICA

DEVELOPMENT OF MODULAR COMPONENTS FOR RADIO ASTRONOMICAL RECEIVERS IN THE BANDS Q (30–50 GHZ) AND W (80–110 GHZ).

TESIS PARA OPTAR AL GRADO DE DOCTOR EN INGENIERÍA ELÉCTRICA

CLAUDIO FELIPE JARUFE TRONCOSO

PROFESOR GUÍA:
FAUSTO PATRICIO MENA MENA

MIEMBROS DE LA COMISIÓN:
LEONARDO BRONFMAN AGUILO
NICOLAS REYES GUZMAN
RODRIGO REEVES DÍAZ
JOSÉ SILES PÉREZ
DANIELLE AMANDA GEORGE

Este trabajo ha sido parcialmente financiado por el proyecto Gemini-Conicyt 32130023, Centro Basal de Astronomía y Tecnologías Afines (CATA), "Programa de Formacion de Capital Humano Avanzado" de CONICYT y el Comité Mixto ESO-Chile

SANTIAGO DE CHILE
2018

Abstract

This work presents the design, construction and characterization of devices for radio astronomy receivers in the Q (30-50 GHz) and W (80-110 GHz) bands. On one hand, the device developed for the Q band is of interest for band 1 of the Argentinian-Brazilian telescope LLAMA (Long Latin American Array). On the other hand, the W band components can be used in the band 3 of LLAMA or in a possible upgrade of the Southern Millimeter Wave Telescope (SMWT) which is maintained by our group.

For the Q band, a low noise amplifier was designed and constructed using a hybrid scheme: integration of a high electronic mobility transistor (HEMT) and a commercial monolithic microwave integrated circuit (MMIC). With this amplifier, noise temperatures less than 20 K and gain greater than 30 dB can be obtained.

In the W band several components have been developed. First, commercial MMIC amplifiers from the OMMIC and HRL companies were packaged. When measured at 15 K, these low noise amplifiers have noise temperatures below 100 K and gains above 17 dB. Given their commercial availability they are suitable to be used as a second amplifier in a receiver. Secondly, using commercial Schottky diodes, sub-harmonic mixers have been manufactured. Development techniques have varied from the use of discrete components to the design of MMICs to reduce the size of the mixers. The aforementioned components have been assembled in a small compact module that can be used as a down-conversion stage. This module has a noise temperature lower than 800 K and gain greater than 2 dB at room temperature. Finally, a slot antenna whose profile has been optimized to improve its main characteristics (reflections, bandwidth, cross polarization and beam symmetry) was built. Among the antennas of its type, this is the only one that has an optimized profile which has permitted to obtain the best performance achieved so far.

RESUMEN DE LA TESIS
PARA OPTAR AL GRADO DE
DOCTOR EN INGENIERIA ELECTRICA
POR: CLAUDIO FELIPE JARUFE TRONCOSO
FECHA: 16 DE ABRIL DE 2018
PROF. GUIA: SR. FAUSTO PATRICIO MENA.

DESARROLLO DE COMPONENTES MODULARES PARA RECEPTORES RADIOASTRNOMICOS EN LAS BANDAS Q (30-50GHz) Y W(80-110GHz).

Este trabajo presenta el diseño, construcción y caracterización de dispositivos para receptores radioastronómicos en las bandas Q (30-50 GHz) y W (80-110 GHz). Por un lado, el dispositivo desarrollado para la banda Q es de interés para la banda 1 del telescopio argentino-brasileño LLAMA (Long Latin American Array). Por otro lado, los componentes de banda W pueden ser utilizados en la banda 3 de LLAMA o en posibles mejoras para el Telescopio Austral de Ondas Milimétricas (SMWT) que es mantenido por nuestro grupo.

Para la banda Q, se diseñó y construyó un amplificador de bajo ruido utilizando un esquema hibrido de integración. Se integró un transistor de alta movilidad electrónica (HEMT) y un circuito integrado monolítico de microondas (MMIC) obtenido comercialmente. Con este diseño una temperatura de ruido inferior a 20 K y una ganancia superior a 30 dB pueden ser obtenidas.

En la banda W se desarrollaron varios componentes. En primer lugar, se empaquetaron amplificadores comerciales MMIC de las compañías OMMIC y HRL. Al ser medidos a 15 K estos amplificadores de bajo ruido alcanzaron temperaturas de ruido menores a 100 K y ganancias superiores a 17 dB. Dada su disponibilidad comercial se determinó que son apropiados para ser utilizados como segundo amplificador en un receptor. Segundo, utilizando diodos Schottky comerciales, se fabricaron mezcladores sub-armónicos que cubren la banda W extendida. Las técnicas de desarrollo han variado desde el uso de componentes discretos hasta el diseño de MMICs para reducir el tamaño de los mezcladores. Los componentes mencionados previamente han sido ensamblados en un módulo compacto que puede ser utilizado en la etapa de mezcla de frecuencias. Este módulo posee una temperatura de ruido menor a 800 K y ganancia superior a 2 dB a temperatura ambiente. Finalmente, se construyó una antena de ranura cuyo perfil ha sido optimizado para mejorar sus principales características (reflexiones, ancho de banda, polarización cruzada y simetría de haz). Entre las antenas de su tipo, esta es la única que posee un perfil optimizado lo que ha permitido obtener el mejor funcionamiento alcanzado hasta el momento.

This thesis is dedicated to my family for their invaluable support and understanding through all these years, specially to my wife Carola and my two little stars: Samir and Mila.

Contents

1 Introduction **1**
- 1.1 Astronomical relevance of the Q and W Bands . . . 1
- 1.2 Heterodyne Receivers . . . 2
  - 1.2.1 Receiver Noise . . . 4
- 1.3 Focal Plane Imaging Arrays . . . 4
- 1.4 Millimeter-Wave Mixers . . . 6
- 1.5 Low Noise Amplifiers . . . 7
- 1.6 Hypothesis . . . 7
- 1.7 Objectives . . . 8
- 1.8 Outline of this thesis . . . 8

2 Tapered Slot Antennas **9**
- 2.1 Introduction . . . 9
- 2.2 Design . . . 10
  - 2.2.1 Antenna Design . . . 10
  - 2.2.2 Transition from Slot Line to Waveguide . . . 16
  - 2.2.3 Clamping of the Antenna . . . 18
- 2.3 Construction and Measurements . . . 18
- 2.4 Conclusion . . . 19

3 Mixers **26**
- 3.1 Introduction . . . 26
- 3.2 Single-Ended diode mixer . . . 27
- 3.3 Sub-harmonic Mixers . . . 28
- 3.4 Schottky Diodes . . . 29
- 3.5 W-Band Mixer . . . 31
  - 3.5.1 UMS Diodes . . . 31
  - 3.5.2 Design . . . 31
  - 3.5.3 Construction and Measurement . . . 34
- 3.6 Band-2+3 Mixers . . . 36
  - 3.6.1 Design . . . 36
  - 3.6.2 Construction and measurement . . . 38
- 3.7 MMIC Mixer . . . 38
  - 3.7.1 Design . . . 38
- 3.8 Conclusions . . . 46

4 Low Noise Amplifiers **47**
4.1 High Electron-Mobility Transistors (HEMTs) . . . 47
4.1.1 HEMT Modelling . . . 48
4.2 Design of Low Noise Amplifiers . . . 49
4.2.1 Design of a Single Stage Amplifier . . . 49
4.2.2 Noise . . . 50
4.2.3 Stability . . . 51
4.3 Q-Band LNA . . . 51
4.3.1 Single Transistor . . . 52
4.3.2 MMIC . . . 52
4.3.3 Input and Output Lines . . . 54
4.3.4 Matching Lines . . . 54
4.3.5 Mechanical Design . . . 55
4.3.6 Measurements . . . 55
4.3.7 Cryo3 + MMIC Amplifier . . . 59
4.4 W-Band LNA . . . 60
4.4.1 Waveguide to microstrip transition: . . . 62
4.4.2 Noise measurement . . . 63
4.5 Conclusions . . . 68

5 Compact down-converter module **69**
5.1 Introduction . . . 69
5.2 Construction . . . 69
5.3 Measurements . . . 70
5.4 Conclusions . . . 72

6 Conclusions and Future Work **73**

Bibliography **75**

List of Tables

1.1 Molecular transitions at Q and W bands. Data taken from [1]. 2
1.2 ALMA frequency bands and noise requirements. The fourth column presents the minimum noise temperature at the maximum frequency of the band. . . 5

2.1 Comparison of W-Band Tapered-Slot Antennas 10
2.2 Corrugation effect 16

3.1 Available power for the LO 35

4.1 CGY2122 bias point for room temperature noise measurement 59
4.2 CGY2122 bias point for cryogenic measurement 59

Chapter 1

Introduction

In the last decades Northern Chile has become the preferred/chosen site to place Astronomical Observatories. The main reasons to choose Chile are the exceptional atmospheric conditions of the skies, adequate access conditions, view of almost the entire sky and operational ease for continuous use of large facilities.

During the last years the Chilean science community has drawn its attention towards the construction of state of the art radiotelescopes, joining efforts to develop national astronomical instrumentation in order to provide solutions for astronomical receivers. In this context the Millimetre Wave Laboratory at Universidad de Chile designs, builds and test receivers for use in radio astronomy with a focus on academic and technological research activities.

Here we present a thesis aiming to design, fabricate and measure receiver components for astronomical receivers in the millimeter wave range, specifically between 9 mm and 3 mm, known as Q(30-50 GHz) and W(75-110 GHz) bands. The frequency band around 60 GHz will no be treated because it is not used for ground based radio astronomy due to the oxygen attenuation.

1.1 Astronomical relevance of the Q and W Bands

The discovery of interstellar molecules and the establishment of the field of astrochemistry began in the 1970s with the discovery of carbon monoxide (CO) in the Orion Nebula [2]. Then, in the 1980s, the observation of NH3, H2CO, HCN, H2S, SO2 and other molecules changed the image astronomers had of interstellar space. The dynamics and chemistry associated with star formation can be understood by tracing molecular line emissions in dense molecular clouds within our galaxy. The most important lines detected in the bands Q and W are presented on table 1.1.

The most abundant molecular gas in the universe is molecular Hydrogen (H_2). It is found in great quantities in stars and gas giant planets. Molecular clouds of H_2 are associated with star formation. Regrettably its transition lines are weak and hard to detect. A tracer

Table 1.1: Molecular transitions at Q and W bands. Data taken from [1].

Molecule	Frequency [GHz]
CH_3CCH	34.183
SO	36.202
HC_3N	36.392
HCS	42.674
SiO	43.122
C_3H_2	46.755
CS	48.991
SiO	86.243
HCN	88.632
HCO^+	89.189
N_2H^+	93.174
$^{12}C^{18}0$	109.782
$^{12}C^{17}0$	112.359
$^{12}C^{16}0$	115.271

for H_2 is CO, the second most abundant molecule in the space, its rotational lines emit at frequencies $n \times 115$ GHz with $n = 1, 2, ...$ being the rotational energy levels.

Molecular lines from distant galaxies can also be observed. Due to the expansion of the universe spectral lines are redshifted by a factor shown in equation 1.1.

$$z = \frac{f_{emmited} - f_{observed}}{f_{observed}} \tag{1.1}$$

The study of molecular hydrogen in high red-shift galaxies is a key to understand the star-formation process of early galaxies. For instance, CO emissions with $z = 6.4$ have been observed at 46.6, 93.2 and 108.7 GHz [3].

1.2 Heterodyne Receivers

By observing electromagnetic radiation received from astronomical source scientist can have an insigth into the physical processes involved in the generation of such radiation [4]. Since the distance between the source and the receiver are huge, these receivers must be extremely sensitive. Therefore, all the losses in the receiver must be kept to a minimum while maintaining a high gain.

At millimeter wavelengths one of the most typical receivers is the heterodyne receiver

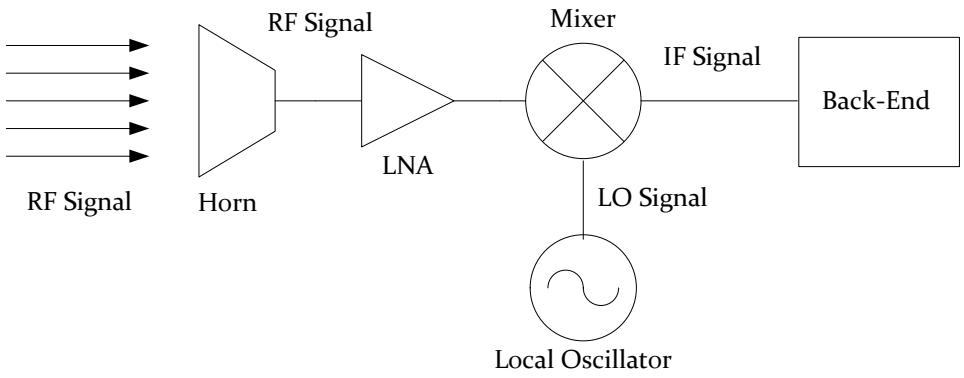

Figure 1.1: Heterodyne Receiver diagram

[5]. The main characteristic of this type of receiver is that they convert the incoming high frequency signal to a lower frequency signal called Intermediate Frequency (IF) preserving the amplitude and phase information of the spectral line. With the IF signal it is easier to work because the losses are lower and the components can be cheaper. If the IF signal is low enough it can be processed directly using the analogue to digital converters of the back-end electronics. When a high IF frequency is used a second downconversion can be added in the receiver architecture. Figure 1.1 shows the basic schematic of a heterodyne receiver.

The incoming radiation (RF signal) is collected by an antenna (usually a horn) which confines the radiation inside a waveguide. The signal is, then, directed to a Low Noise Amplifier (LNA) that amplifies the signal adding minimum noise. The amplified signal is down-converted to a lower frequency using a mixer. This frequency conversion is achieved by supplying to the mixer the local oscillator (LO). The mixer output is a new signal that has one of the resulting frequencies equal to the difference in frequency between the LO and RF signals. At higher frequencies the architecture can be slightly modified. Above 120 GHz efficient amplification is not yet possible and down conversion with Superconductor-Insulator-Superconductor tunnel junction (SIS) [6] or Hot Electron Bolometers (HEB) [7] mixers is performed before amplification. During this work an amplifier stage based on High Electron Mobility Transistors (HEMTs) was used due their ease of operation, lower cryogenic requirements and potentially lower noise when considering the complete system.

An important output signal to be considered in a mixer is the image. This signal is $2\omega_{IF}$ away from the RF signal and is converted to the same IF frequency as the RF. Noise and unwanted signals present at the image will degrade the receiver performance. The frequency band above the LO is called the Upper Side Band (USB) and the one below the LO is called the Lower Side Band (LSB). Filters can be used to avoid this situation and allow only the desired RF signal to be processed by the mixer.

1.2.1 Receiver Noise

All electronic devices generate some amount of noise. There are many noise sources, like shot noise [8] and flicker noise [9], but the most important in radio astronomy is the thermal noise because it can be minimized by cooling down the electrical components [10] [11]. The thermal noise power depends only on the frequency bandwidth (B) and the physical temperature (T) and is given by

$$P = kTB, \tag{1.2}$$

where k is the Boltzmann constant.

The noise temperature, T_{noise}, is used to characterize the receiver's noise level. It is given by the physical temperature a resistance in front of the receiver would have to get the measured output noise power considering a noiseless receiver. The noise temperature of a cascade of electronic components is given by [12]:

$$T_{receiver} = T_1 + \frac{T_2}{G_1} + \frac{T_3}{G_1 G_2} + ... + \frac{T_n}{\Pi G_{\mathrm{i}}} \tag{1.3}$$

where T_{i} and G_{i} are the noise temperature and gain, respectively, of each cascade stage. It can be seen that using a high-gain amplifier, the noise temperature of a receiver is completely dominated by the noise contribution of this amplifier.

The minimum power a system can detect is determined by the receiver's noise level. This noise can be minimized using low noise detectors and cooling down the complete receiver to avoid thermal noise. The theoretical minimum noise temperature of a heterodyne receiver is given by [13]:

$$T_{rec} > \frac{h\nu}{2k} \tag{1.4}$$

Table 1.2 presents the noise figure requirements of the ALMA receivers at each frequency band [14].

1.3 Focal Plane Imaging Arrays

Focal plane arrays are of increasing interest for the radio astronomy community. The potential of synchronous image sampling, in which post processing can be applied to a large number of array elements simultaneously has generated a high level of enthusiasm. Multi-beam imaging systems can observe extended astronomical sources faster than traditional single beam or phased array telescopes, maintaining a comparable level of performance than single beam

Table 1.2: ALMA frequency bands and noise requirements. The fourth column presents the minimum noise temperature at the maximum frequency of the band.

ALMA Band	Frequency Range [GHz]	Receiver SSB Noise Temperature in the complete band	Minimum noise Temperature at F_{max}	Receiver technology
1	31.3-45	28K	1.2K	HEMT
2	67-90	50K	2.15K	HEMT
3	84-116	62K	2.78K	SIS
4	125-169	85K	4.05K	SIS
5	163-211	108K	5.06K	SIS
6	211-275	138K	6.59K	SIS
7	275-373	221K	8.94K	SIS
8	385-500	147K	11.99K	SIS
9	602-720	263K	17.27K	SIS
10	787-950	345K	22.78K	SIS

systems [15]. Since millimeter and submillimeter receivers are approaching their sensitivity limit, building a multi-beam detector can increase the mapping speed.

Multi-beam systems have already been built and are under operation. For example, at the James Clerk Maxwell Telescope, the Heterodyne Array Program B-Band (HARP-B) system uses 16 independent high performance pixels each with its own independent heterodyne receiver chain operating between 325-375 GHz [16]. Another implementation of multibeam receiver is located at the 30-m IRAM telescope in Spain. This system is composed of 117 independent beam pixels [17] operating at 230 GHz. Each receiver is a simple bolometer so there is no spectral information from the source. In Chile, the Cerro Chajnantor Atacama Telescope (CCAT-p) is a proposed telescope to be built with high continuum sensitivity at submillimeter wavelengths. With the CCAT-p Heterodyne Array Instrument (CHAI) working with 32 pixels at 460 and 830 GHz, CCAT will be faster than ALMA when mapping continuum [18]. In the frequency band of interest some examples can be mentioned: Argus instrument is a 16 pixels array working from 85 to 116 GHz [19], IRAM 30m receiver has an array of 25 pixels operating from 80 to 116 GHz [20].

An increase in the number of elements in the array results in higher performance. Therefore the array elements must be relatively cheap and easy to manufacture while retaining high coupling efficiency to ensure that a large number of elements can be used.

For a large number of pixels it is necessary for each element to be very small . Because of this the construction of the receivers is challenging and the solutions have ranged from modular designs to embedded designs [21]. Usually in a heterodyne receiver like the one shown in figure 1.1 the amplifier and mixing stages are separated, enlarging the receiver. To increase the number of elements it is highly desirable to assemble the amplifier and the

mixer into a single block [22] [23] or even on a single chip [24] [25]. Furthermore the antenna responsible for coupling the single beam into each pixel of the receiver can also be integrated [26].

1.4 Millimeter-Wave Mixers

Mixers are one of the main parts of a heterodyne receiver because they can convert the frequency of the input signal. To achieve the downconversion effect a non-linear element is needed, typically the two most common devices used at millimeter wavelengths are:

- Schottky diodes: Mixers based on this type of diodes operates well either at cryogenic or room temperatures being simpler to integrate in a heterodyne receiver. These diodes are used to built mixers up to THz frequencies. Reference [27] presents a receiver based in a solid-state planar Schottky diode working in the 1.2 THz range with noise temperature of 2800 K and a conversion loss of 10.5 dB measured at room temperature. Even at higher frequencies, a GaAs monolithic membrane-diode (MOMED) structure has also been measured as a 2.25 THz Schottky diode mixer [28].
- Superconductor-Insulator-Superconductor (SIS) tunnel junction diodes: Mixers based on SIS junctions are often used for millimeter and submillimeter wavelength due their remarkably sensitivity. This type of diodes requires cooling to cryogenic temperatures to operate, restricting their use. As an example, ALMA Band-10 (787 to 950 GHz) SIS mixers have a noise temperature below 240 K in the whole band [29]. The operating frequency of the SIS mixers is limited by the superconducting material of the electrodes. The critical temperature of the material is related to the gap frequency of the material. Above this frequency the photon energy is larger than the "binding" energy of the Cooper pairs and the electrodes loose their superconducting properties when radiated. For Niobium this frequency is 700 GHz. For frequencies above 1 THz HEB are used for heterodyne detection. The Herschel-Heterodyne Instrument for the Far-Infrared (HIFI) uses HEB mixers for the bands above 1.4 THz obtaining 1000 K of noise temperature [30].

To obtain low noise in the complete receiver two alternatives are commonly used for the first element in the receiver chain: LNAs based on HEMTs operating at 15 K and SIS mixers operating at 4 K. At frequencies below 120 GHz the noise of HEMT based LNAs is lower than that of SIS mixers [31]. Considering that the cryogenic system to operate SIS mixers requires more cooling power, operating at higher temperature provides an advantage for LNAs at these frequencies. In this thesis we will focus in W-band components and therefore SIS mixers will not be treated.

In our effort to build a small compact downconverter for W-band a small mixer is needed. Currently, different mixer configuration (sub-harmonic, balanced and others) are commercially available up to 110 GHz but they are already packaged in big blocks. Therefore, it is necessary to build our own mixers at the laboratory. We will focus on diode mixers based on Schottky diodes due to their commercial availability.

1.5 Low Noise Amplifiers

Low noise amplifiers are one of the most important elements in heterodyne receivers for frequencies below 120 GHz. At these frequencies the performance of LNAs is better than SIS mixers in terms of sensitivity and bandwidth without the need of cooling down to 4 K. In this situation, the noise of the LNA dominates the noise of the complete receiver as explained in section 1.2.1.

At millimeter wavelengths LNAs are based on High Electron Mobility Transistors (HEMTs). The first HEMTs were based in AlGaAs/GaAs hetero-junctions over GaAs substrate. Using this kind of hetero-structures a high mobility was achieved. To increase the electron mobilty Indium was added in the channel. Unfortunately, Indium lattice constant does not match AlGaAs and GaAs, then only a thin layer of In can be used. This type of heterostructures are known as pseudomorphic HEMTs (p-HEMTs). The p-HEMT structure was improved creating a structure of InAlAs/InGaAs/InAlAs over GaAs. By adding a buffer layer of InAlAs the lattice constants of both the GaAs and the InGaAs channel can be matched. To increase the In content even more, InP HEMTs were fabricated using a heterostructure based on AlAs/InGaAs/InAlAs over a InP substrate. The increase in In content allowed this type of HEMTs to achieve lower noise and greater mobility than GaAs p-HEMTs [32].

Currently MMICs based on InP HEMTs have achieved the lowest noise temperatures. At W band several examples of low noise amplifiers using InP HEMTs can be found in the literature. In [33] noise temperatures below 40 K are obtained in W-Band. Moreover, [34] presents noise temperatures below 28 K in the whole ALMA Band-2+3. In Q band, the LNAs for ALMA are based on InP HEMTs obtaining a noise temperature below 18 K [35]. For both bands, commercial cryogenic LNAs with noise temperatures similar to those mentioned above can be obtained with Low Noise Factory LNAs. The only drawback of these LNAs is that they are already packaged so they can not be integrated in a single module with the mixers.

At the beginning of the PhD study there were no commercial availability of InP HEMTs (as single transistors chips) or MMIC LNAs based on InP HEMTs. GaAs HEMTs from UMS were evaluated but they suffer from degradation at cryogenic temperatures (personal work). HRL InP HEMTs were discontinued some years ago, fortunately, W band LNAs from HRL were obtained previously at the laboratory. The only option available was the OMMIC MMICs based on m-HEMTs with high indium contain. In [36] an analysis of the m-HEMTs from OMMIC are studied showing a very good performance up to 50 GHz.

1.6 Hypothesis

Based on: the Chilean community interest to develop astronomical instrumentation, the global interest for compact receivers for multibeam system, the commercial availability of MMICs LNAs with m-HEMTs that can work at Q and W and finally, the interest of the scientific community in study astrochemistry at these frequencies it was decided to build

components for radio receivers at millimeter wavelengths. It is expected that the development of these components is the first step towards the construction of small, highly integrated receivers for focal plane arrays at Universidad de Chile during the next years.

1.7 Objectives

The main objective of this thesis is the design, construction and measurement of components for the astronomical receivers for the Q and W Bands. Q-band component could be used, for example, in Band-1 of the Large Latin American Array (LLAMA). W-band components, on the other hand, could be used in LLAMA band-3 or in a possible upgrade of the Southern Millimetre Wave Telescope (SMWT) located at Cerro Calan, Chile. In particular, the specific objectives are described below.

- Construction of a Low Noise Amplifier (LNA) for the Q-Band based on Indium Phosphide (InP) High Electron Mobility Transistor (HEMT) and Metamorphic HEMT (mHEMT). The amplifier will be based on a hybrid integration of a single transistor and a commercial Microwave Monolithic Integrated Circuit (MMIC) to achieve high performance.
- Packaging a MMIC LNA for W-Band based on InP HEMTs from HRL and OMMIC foundries.
- Construction of a mixer based on a Schottky diode for the W-band to down-convert the incoming signal to a proper and useful intermediate frequency (IF).
- Integration of the previous W-Band components (LNA and mixer) in a compact module as possible solution for future "radio cameras".
- Design and construction of a Tapered Slot Antenna that can be integrated with the LNA and the mixer in a compact design.

1.8 Outline of this thesis

Chapter 2 of this thesis presents the development of the optimized tapered slot antennas. Chapter 3 presents a review of mixers design and the development of sub-harmonic mixers at U. de Chile. In chapter 4, first a review of LNA design is presented. Then an overview of the work in LNAs for bands Q and W is presented. Chapter 5 presents the results of a prototype of down-converting module for W-band. Each of the chapters has its own conclusion. Finally, chapter 6 presents the conclusions and future work related to this thesis.

Chapter 2

Tapered Slot Antennas

At millimetre-wave frequencies and above, the usual antenna element is a horn antenna and the connection with the rest of the circuit is usually achieved using waveguides and planar transmission lines. These characteristics limit compactness and further integration with integrated circuits. In certain applications a Tapered Slot Antenna (TSA) could be more suitable.

In this chapter we present a TSA which profile and corrugations have been optimized to maximize it's performance over the W-band. The aim is to construct an antenna smaller than a horn that could be suitable for millimeter wave applications.

2.1 Introduction

In 1979 Gibson introduced the "Vivaldi aerial", [37] a planar antenna capable of producing a symmetrical end-fire radiation pattern. Several studies have introduced variations to the original design to increase their performance [38] [39]. These antennas have been extensively studied at frequencies below 15 GHz because they present several advantages:

- Broad bandwidth.
- Narrow beam widths (down to 15° at −3 dB).
- Symmetrical radiation patterns.
- Greater compactness than horn antennas.
- Easier integration with integrated circuits.

These characteristics make them very interesting for applications such as satellite communications, radio telescopes and millimeter-wave imaging systems [40] [41]. In these applications there is an increasing interest in high-density multibeam systems and it is in this topic where Tapered Slot Antenna (TSA) arrays with integrated technology could be very useful.

TSAs have been extensively studied at lower frequencies. However, few studies have been carried out at millimetre wavelengths, since their construction is more complicated due to the

Table 2.1: Comparison of W-Band Tapered-Slot Antennas

Ref.	Profile	Corrugations	Manufacture Tech.	Bandwidth GHz	Sidelobe level dB	Cross Pol. level dB	S11 dB
[42]	Exponential	Constant	SM [a]	65-115	−8	N.A.	−9
[43]	Exponential	No	LPKF [b]	75-110	−10	N.A.	−7
[44]	Exponential	Constant	LTCC [c]	75-82	−8	N.A.	−15
This work	Optimized	Optimized	LPKF	75-110	−16	−25	−10

need for thin substrates with low dielectric constant. Some efforts to construct a TSA that covers the W-band have been carried out, but with limited success. Table 2.1 summarizes these efforts and presents a comparison of the beam properties and their manufacturing process. In [42] a TSA built with a surface micromachined process was measured but the E-plane was found to be asymmetric due to the slot-line feed. The TSA measured in [43] was manufactured in a simpler way (Laser PCB Prototyping) but the simulated E and H planes were asymmetrical respect to their maximums. The Vivaldi antenna presented in [44] was built in Low Temperature Cofired Ceramic (LTCC) showing good properties but operates in a reduced bandwidth. In all the aforementioned work and that reported in other frequency bands, the antennas are constructed with well-known profiles (linear, constant width, exponential and Fermi) and the depth of the corrugations along the antenna is fixed but there is no further analysis on new profiles or variable corrugations. The works mentioned previously include beam pattern measurements. In [39] simulations of a W band TSA are presented. In [45] simulations and also S_{11} measurements are presented. Both of these antennas show good beam patterns and return losses better than −12 dB.

2.2 Design

The design of the TSA was performed using a custom-made optimization program and HFSS [46]. The design process was divided into two stages. First, only the radiating part was simulated and optimized. Symmetries in the electromagnetic field were used whenever possible in order to reduce computation times. In a second stage a microstrip-to-slot-line transition was included in the simulation.

2.2.1 Antenna Design

The TSA is a class of end-fire travelling-wave antenna known as a surface-wave antenna [38]. It consists of a tapered slot which has been etched within the metallic surface on a dielectric substrate. The E-plane is parallel to the substrate since the field is attached to the horizontally-separated tapers prior to being radiated along the direction of the substrate. The electromagnetic wave moves through the metal tapers until a separation of about half a wavelength has been reached [38]. At this point the electromagnetic wave uncouples from the metallic taper and the antenna structure radiates into free space from the substrate end.

In order for the TSA to radiate properly it has to behave as a surface-wave antenna. To achieve this, according to studies presented in [40], the effective dielectric thickness $t_{eff} =$

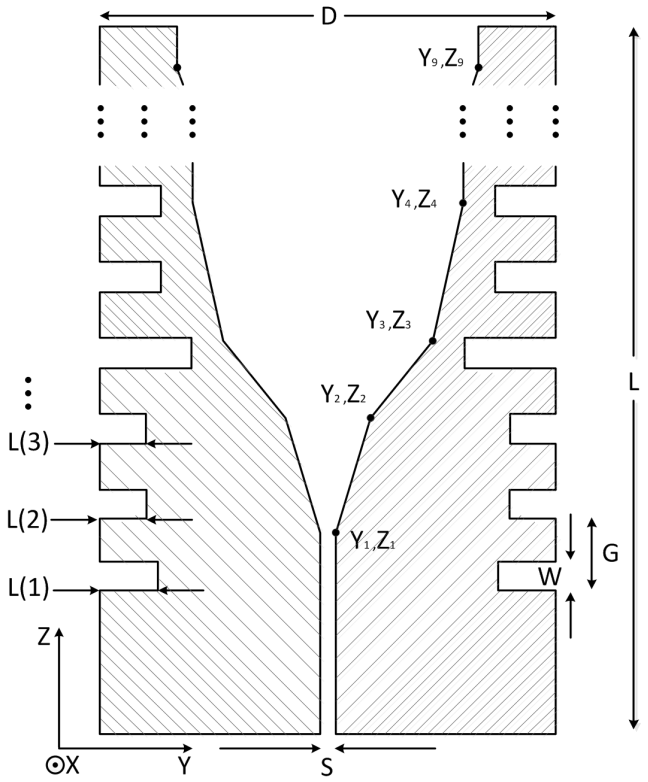

Figure 2.1: Geometry of the ten-segment corrugated TSA. During the optimization the total length L, slot width S, aperture of the antenna, number of segments of the profile and number of corrugations were fixed.

$(\sqrt{\varepsilon_r} - 1)t$ (t being the actual substrate thickness) must meet, approximately, the following requirement ,

$$0.005\lambda_0 < t_{eff} < 0.03\lambda_0, \tag{2.1}$$

where λ_0 is the free space wavelength at the center frequency. For substrates with thinner effective thickness the beam width will be wider, while for thicker substrates the main beam will break up producing asymmetric beams [40]. Due to the condition stated in (2.1) a TSA at millimeter wavelengths have to be built in a very thin substrate with low dielectric constant. The selected substrate for the present design was Rogers Duroid 5880 ($\varepsilon_r = 2.2$, $\tan\delta = 0.0009$) with a thickness of 127 μm.

Since the profile defines the radiation pattern of the TSA, an initial design was selected by dividing the antenna into ten linear segments. Then, corrugations were added to reduce sidelobe levels [47] and cross polarization. The geometry of the proposed radiating part of the design is shown in Figure 2.1. The length of the antenna (L) was fixed to 19 mm (about 5.75λ at 90 GHz) to produce a half-power-bandwidth (HPBW) of approximately 23°, according to [38]. To ensure radiation down to 60 GHz the aperture of the antenna was fixed at 6 mm.

One of the main difficulties in building a high-frequency TSA is obtaining a low input impedance. The antenna input impedance is defined by the slot line separation (S). Small

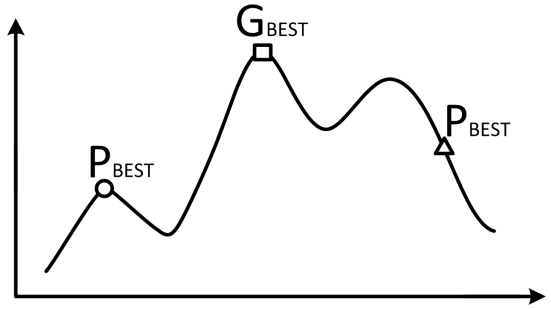

Figure 2.2: Graphical 1D representation of the PSO Algorithm. Three particles move in the solution space searching for the maximum of a function with some velocities. Each one of the particles keeps track of its own best value (p_{best}) of the objective function and the best value of the group of particles (g_{best}). The velocities of the particles are updated according to the relative positions of p_{best} and g_{best}.

values enable an impedance closer to 50 Ω. A comfortable construction value of $S = 75$ μm was selected which corresponds to an impedance of 146 Ω.

The rest of the tunable parameters are the start position of nine segments (Y and Z coordinates), the total width of the antenna (D), the length of each of the 40 corrugations, and two variable to describe the width and separation used in all the corrugations. The total number of variables is 61.

Particle Swarm Optimization

The variables presented above were optimized to reduce return loss, side lobes and cross polarization below −18 dB and to also obtain a symmetric circular beam.

The optimization was carried out using Particle Swarm Optimization (PSO) [48] due to the high dimensionality and discontinuity of the problem. Under these conditions PSO yields fast convergence, simplicity and effectiveness [49]. Furthermore, in some cases, PSO can outperform other methods of optimization such as genetic algorithms [50]. A graphical representation of the algorithm can be seen in Figure 2.2.

The values of the variables are limited such that they have physical meaning and do not unnecessarily increase the number of iterations to achieve the optimum. The restrictions added to the optimization problem were:

- Corrugations need to be small enough not to break the TSA conductor in two.
- The added length of all the segments (in the radiation direction) must be equal to the total length of the antenna.
- The Y_{i} coordinate of the segments must always be bigger than the previous Y_j coordinate to ensure the aperture increases as the wave is radiated.
- An absorbing wall condition was used when a variable reaches the boundary of the solution space [49].

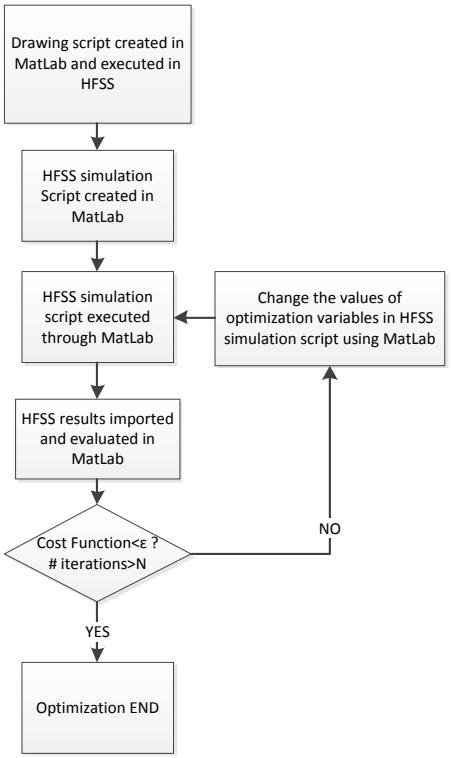

Figure 2.3: Flow diagram used to implement HFSS simulations optimized with PSO. An extra condition in the number of iteration was added to stop the algorithm.

Antenna Optimization using PSO

The electromagnetic simulation was performed with HFSS and the optimization using MatLab. A flow diagram of the optimization process is presented in Figure 2.3. This method can be of great help to minimize computational resources since each EM simulation only takes a few minutes. Once one simulation is finished, HFSS is closed and MatLab manages the simulation data. HFSS simulates the far-field pattern and return loss of the antenna at 80, 90, 100 and 110 GHz. For each frequency, the following values are exported;

- Reflections (S_{11}).
- Sidelobe level (SL).
- Maximum cross polarization between $\pm 100^{\circ}$ (X_{pol}).
- Standard deviation of the difference of the full width between half-maximum between H and E plane (STD_{FWHM}).

It is desired that the designed antenna has cross polarization, sidelobes and reflections below -18 dB. In order to have a circular beam the standard deviation between the FWHM at E and H plane should be smaller than 0.01°. Non-linear weights, $W(\mathrm{i})$, were added to set the weight to zero when the quantity is below the target value. At each frequency point, f, the cost function is defined by

a)

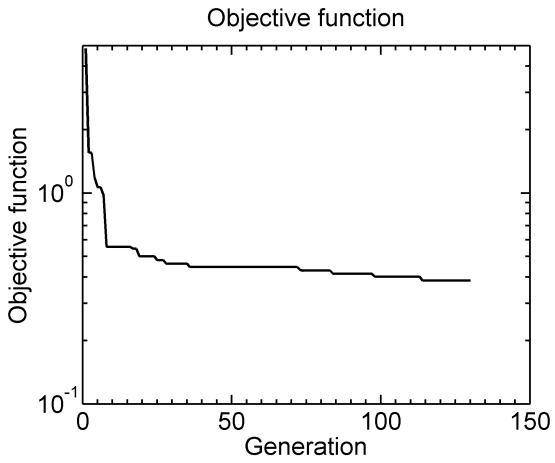

b)

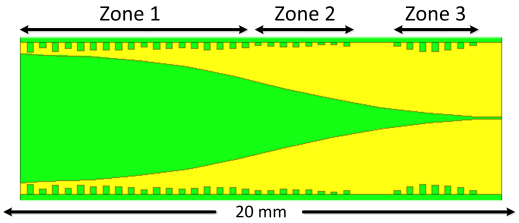

Figure 2.4: (a) Minimum cost value for each generation. (b) Final design of the corrugated ten-segment tapered slot antenna design (drawn to scale).

$$\begin{aligned} Cost(f) &= W(1)(S_{11}(f) - S_{11}^{target})^2 \\ &+ W(2)(X_{pol}(f) - X_{pol}^{target})^2 \\ &+ W(3)(SL(f) - SL^{target})^2 \\ &+ W(4)(STD_{FWHM}(f) - STD_{FWHM}^{target})^2. \end{aligned} \tag{2.2}$$

Finally, the objective function to minimize, using the PSO algorithm, is:

$$F_{obj} = \sum_{f} Cost(f). \tag{2.3}$$

After approximately twenty days of continuous simulation using a standard workstation with 16 G of RAM and a 3 GHz processor, and due to no further reduction in the cost function, the optimization was stopped. In total, 130 generations were simulated with 30 iterations per generation giving a total of 3900 iterations. The minimization of the cost function after each generation and the optimized design can be seen in Figure 2.4.

The optimization of a non-specific profile and the corrugations allows to combine several characteristics that improve the overall performance of the antenna. Regarding the profile, the optimized TSA presented here has three distinctive sections. A small launch angle to

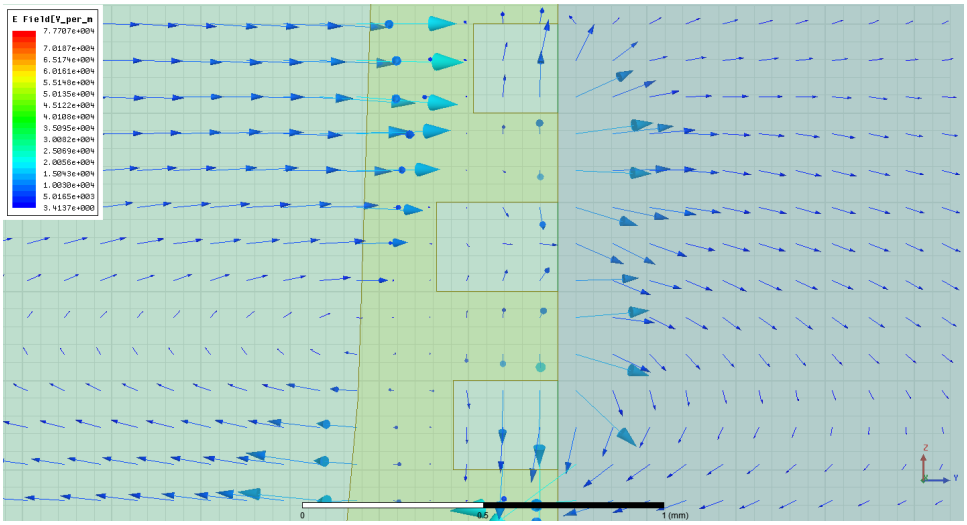

Figure 2.5: Electric field lines in the upper side of the substrate near the radiating border in zone 1. It can be seen that an electric field is established between the corrugations.

obtain a directive beam [40] resembling a small angle LTSA, an intermediate shape similar to a Fermi or Vivaldi that reduces sidelobes [51], and a linear feed to obtain a frequency-independent impedance [38].

Three corrugated sections can also be distinguished in the final TSA (Figure 2.4b). To investigate their effect quantitatively we performed simulations comparing results for the same antenna with and without corrugations. Table 2.2 presents maximum sidelobe, cross polar level and return losses when different corrugated sections are added or taken out from the final profile. This was analysed calculating the mean values from 75, 90 and 110 GHz simulations. In zone 1, near the radiating part, an electric field is established between the corrugations at the edges of the antenna [47]. The electric field inside the corrugations is parallel to the radiation direction and the magnetic field is perpendicular to the electric field. A picture of the electric field lines can be seen in figure 2.5. Similar to the effect of corrugations in aperture antennas [52], this field distribution affects the boundary condition of the tangential electric and magnetic fields at the edge of the antenna. Without corrugations the electric field in the edge of the antennas is opposite to the electric field inside the aperture. With corrugations, the electric field at the edges is in the same direction as the electric field in the aperture resulting in a radiation pattern with low cross polarization and sidelobes, and allowing a better matching of the TSA to the free space. This effect is induced by the electric field inside the corrugations whose intensity becomes stronger when the length of the corrugations is less than $0.15\lambda_0$ and greater than $0.04\lambda_0$ [47]. In the optimized TSA presented here the mean length of the corrugations in the zone 1 is 0.31 mm $\approx 0.1\lambda_0$.

In zone 2 there are almost no corrugations and the effect of adding them in this section is almost negligible. Finally, zone 3 serves to match the impedance of the slot line input to the radiating section of the TSA. These corrugations have a second-order effect on the shape of the beam. By adding only corrugations in zone 1 the beam characteristics improve substantially but only when the corrugations in zone 3 are added, the reflections are diminished.

Table 2.2: Corrugation effect

Zones with corrugations	Sidelobe [dB]	Cross Pol. [dB]	S_{11} [dB]
None	−12.1	−17.0	−12.5
1	−17.2	−22.9	−13.1
3	−12.6	−16.1	−12.9
1 & 3	−18.6	−25.7	−14.9
1 & 2	−17.9	−21.0	−13.0
1 & 2 & 3	−18.9	−25.0	−15.2

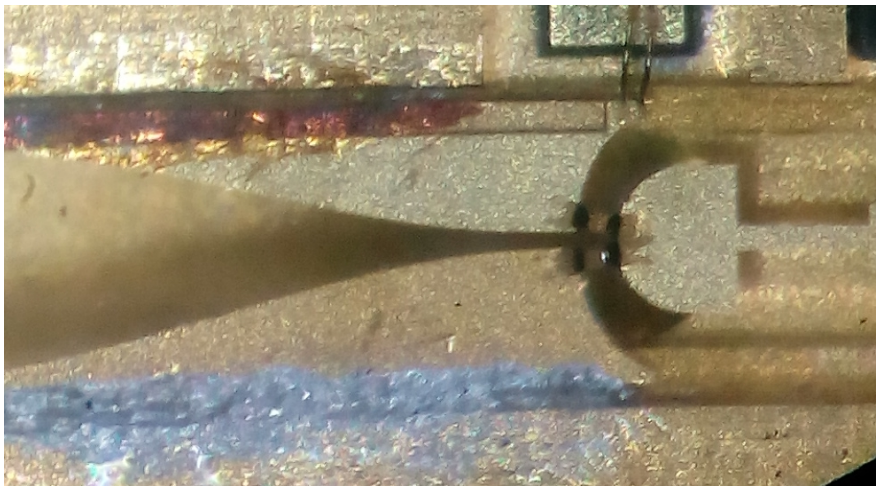

Figure 2.6: Balanced mixer with a fin-line transition to form a 180 degrees hybrid.

2.2.2 Transition from Slot Line to Waveguide

TSA are very easy to integrate with circuits, a simple way to achieve this is by using a slot line to microstrip or coplanar transition. If a 180 degree hybrid is needed, the branches of the TSA can be used as a hybrid: a microwave circuit has to be connected to each of the conductive lines of the TSA. This type of connection has already been used in commercial devices with fin-line transitions, for example, figure 2.6 presents the diode connection of a commercial balanced mixer [53].

The beam-pattern measurement setup, as described in Section 2.3, has a waveguide feed to test antennas. Therefore, the TSA was designed to be mounted in a metallic split block containing a rectangular waveguide. Although the antenna could have been tested using a direct transition from slot line to waveguide [54], for active-antenna applications with MMIC integration, a transition from slot line to either microstrip or coplanar lines is preferred. For the purpose of this work we have selected the former transition, previous to launch the signal into the waveguide. This transition is based on the design presented in [55], where non-planar transitions with different stub configurations are analyzed. The transition was designed using a slot line with the same width that the input slot line has in the corrugated ten-segment antenna. The microstrip-line impedance was selected to be 109 Ω.

a)

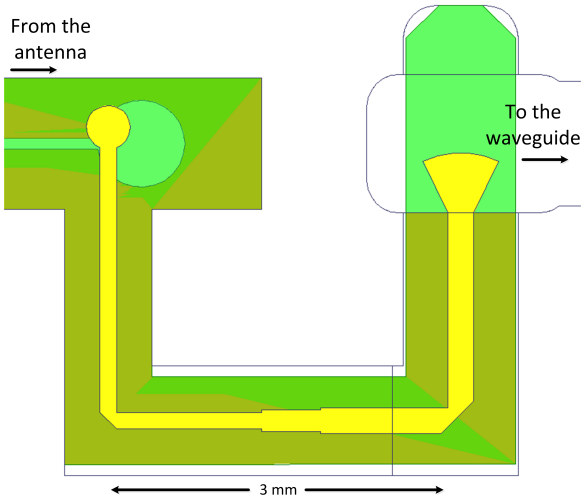

b)

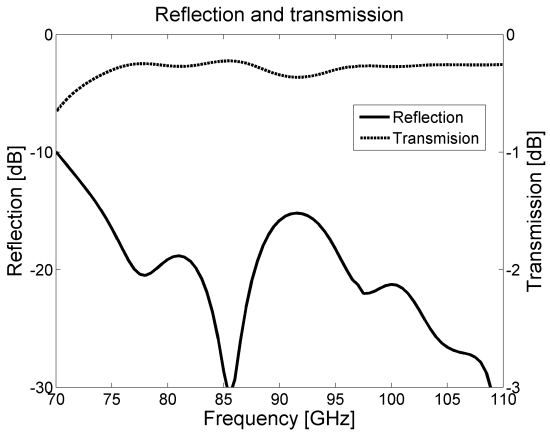

Figure 2.7: (a) Design of the transition from slot line to waveguide (drawn to scale). (b) Simulated reflection and transmission of the full transition.

In order to launch the signal into the waveguide, a transition from a 50 Ω microstrip line to a rectangular waveguide was designed, based on the work of [56]. This transition has return losses better than 20 dB in the W-band. The final element of the full transition is a matching line that connects the 109 and 50 Ω lines. In order to have the TSA aligned with the waveguide, two mitered microstrip bends were added to the line. The full transition, as described above, was designed to be placed over the same substrate where the antenna was constructed. Furthermore, this transition was also designed to be enclosed in a metallic cavity to avoid that its radiation affects the radiation pattern of the antenna. We were particularly careful in selecting the size of the cavity such that the cut-off frequency of waveguide modes inside them is above 120 GHz. The final design and simulations of its reflection and transmission are presented in Figure 2.7. The full transition has return losses better than 15 dB.

2.2.3 Clamping of the Antenna

Due to the flexibility of the substrate and its length, the TSA can easily bend and affect the radiation pattern. To overcome this, the substrate was extended sideways and two metallic clamps were added. After some simulations the substrate width and the dimensions of the clamps were chosen to minimize its effect on the TSA performance. The total width of the substrate was selected to be 20 mm so that the antenna width is the same as a WR-10 flange. All the comparisons between simulations and measurements presented in the following sections include the effects of the metallic clamps.

2.3 Construction and Measurements

The TSA and its transition to the output waveguide were constructed using a Protolaser S from LPKF over Duroid 5880 with a thickness of 127 μm and a copper layer of 17 μm. First, they were etched over different sides of the same substrate. Then, the resulting circuit was placed in an aluminium split block containing the clamps for holding the antenna, and a groove and a cavity to place and align the transition. The block also contains the output waveguide. Figure 2.8 shows the resulting construction.

Measured and simulated reflections, including the waveguide to microstrip transition, are shown in Figure 2.9. Reflections are below -12 dB in the complete W-band. In the first part of the W-band good agreement with simulations is obtained. The discrepancy above 101 GHz is attributed to construction problems in the waveguide-to-microstrip transition not being fully aligned in the waveguide. It has to be noted that below 75 GHz reflections increase because the transitions were designed to operate only above this frequency.

To characterize the antenna, a near-field pattern setup covering the frequency range from 75-110 GHz was constructed. A picture of the anechoic chamber can be seen in figure 2.10. An open-ended waveguide was selected as probe antenna. The distance between the TSA and the probe was larger than $3\lambda_0$ at 75 GHz, to be outside the reactive region. For each frequency a sampling factor of $0.48\lambda_0$ was used to scan the near field and avoid aliasing. To have a proper measurement of the antenna sidelobes, a half angle of 60° was selected to define the scanning area. The near field measurement is transformed to the far field using a custom-made algorithm. Before measuring the TSA, the near field set-up and far-field transformation were tested using a standard pyramidal horn. The measurements were in excellent agreement with HFSS simulations.

Figure 2.11 presents the co-polar and cross-polar near-field measurement and the transformed far field radiation pattern of the TSA at 90 GHz. According to the coordinate axes defined in Figure 2.1, the E and H planes are obtained by varying θ at $\phi = \pi/2$ and $\phi = 0$ respectively. Figure 2.12 and 2.13 show the measured and simulated E and H planes at different frequencies. The far-field pattern agrees very well with simulations. At 90 GHz the E and H plane beamwidths are 19° and 29° respectively, as expected. Sidelobes are below -19 dB at the beginning and middle part of the band but increase slightly to -16 dB at 110 GHz. Cross polarization measurements at 75 and 90 GHz are below -26 dB for $\phi = \pm\pi/4$ with

varying θ. At 110 GHz the cross polarization could not be measured but the simulation predicted values below -25 dB. The H-plane is not completely symmetrical, probably due to an alignment problem in the anechoic chamber. In fact, it can be seen in Figure 2.11 that the beam is not completely centred.

Finally, figure 2.14 presents simulations performed to test the performance of the antenna at 60 GHz. They still predict a reasonable performance (sidelobes and cross polarization at -14 and -18 dB, respectively) despite the fact that the antenna was not optimized below 75 GHz. Further optimization promises ultra-broadband operation with excellent properties.

2.4 Conclusion

A millimeter-wave tapered-slot antenna has been presented. Using Particle Swarm Optimization and an adaptable design for the TSA it has been possible to enhance its radiation properties enabling its use in demanding applications, such as radioastronomy or telecommunications, as active antennas. By adding optimizable corrugations and a ten-segment profile, a VSWR < 1.6 and side lobes below -16 dB were obtained. Far field co-polar and cross-polar measurements are in good agreement with simulations performed in HFSS. The optimized corrugated TSA presented here is suitable for use in applications where small antenna separations are required such as in millimeter-wave imaging or focal-plane arrays.

a)

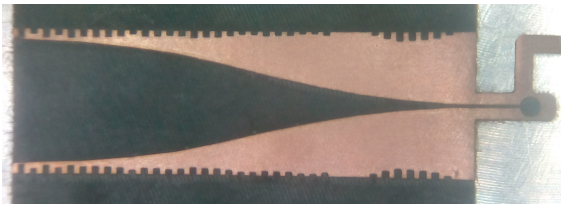

b)

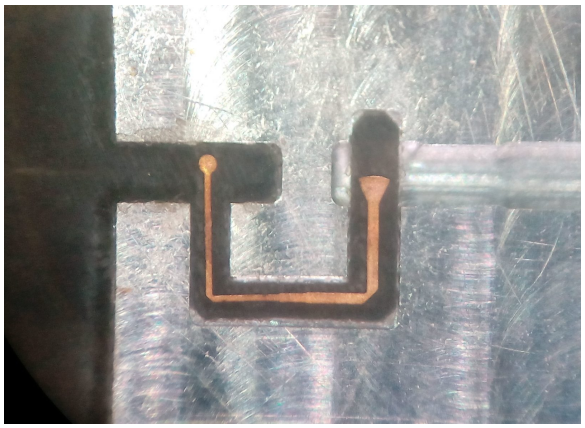

c)

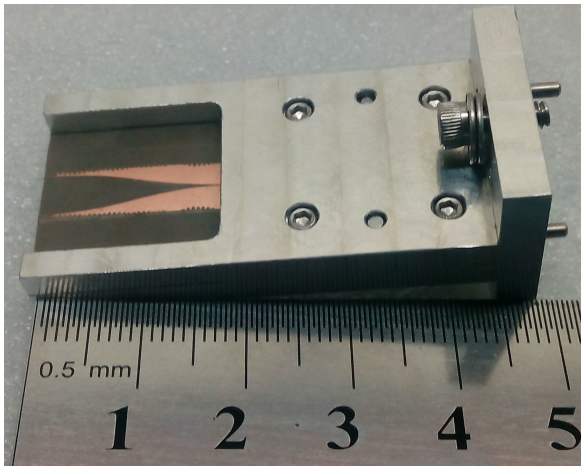

Figure 2.8: Constructed TSA. (a) Bottom side of the substrate. (b) Transition from the antenna to the waveguide. It was mounted in the bottom block inside a groove to ensure proper alignment. (c) Complete block with the mounted antenna.

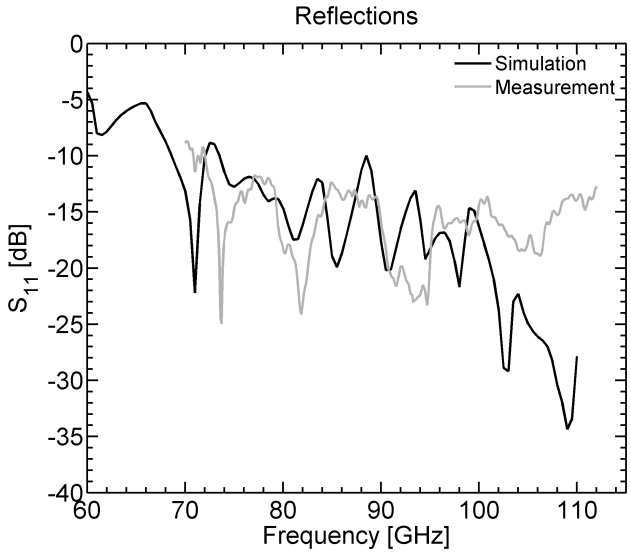

Figure 2.9: Antenna reflection measurement (solid gray) and simulations (solid black). A small standing wave can be noticed in the measurement.

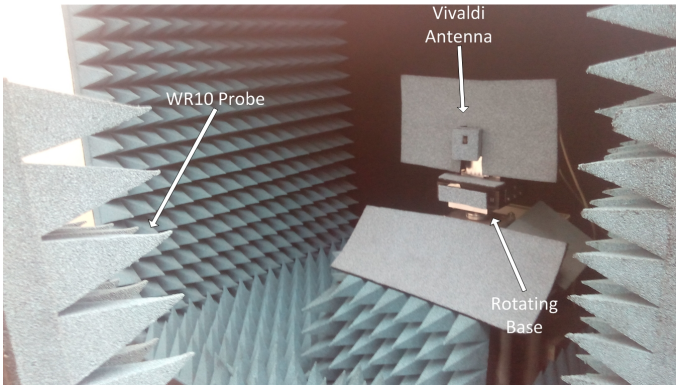

Figure 2.10: Anechoich chamber for W-band near field measurements

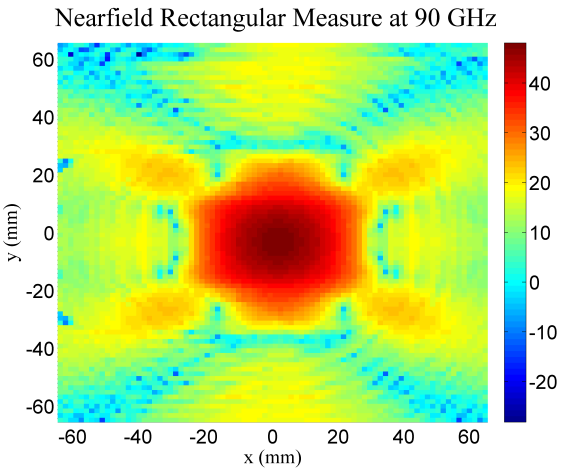

(a) Measured co-polar near field radiation pattern at 90 GHz

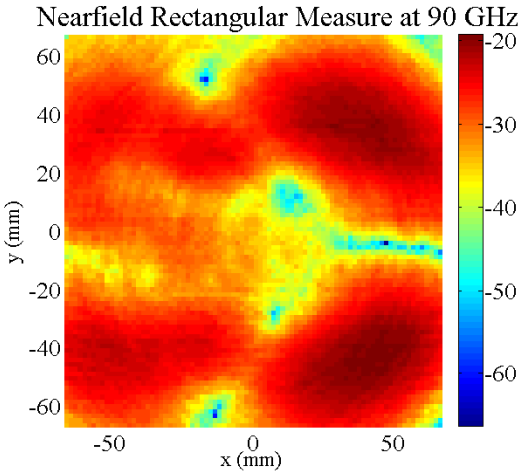

(b) Measured cross-polar near field radiation pattern at 90 GHz

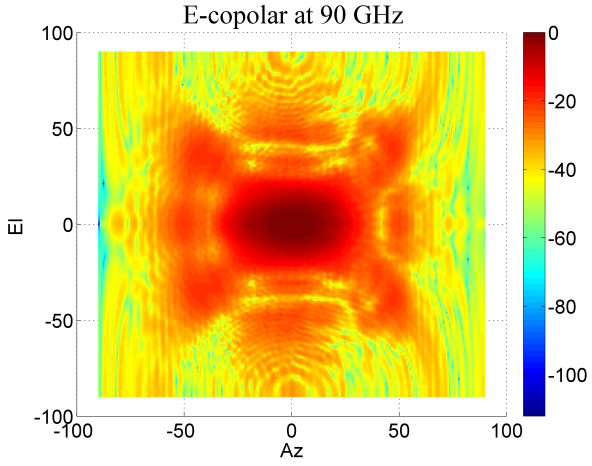

(c) Transformed co-polar far field radiation pattern at 90 GHz

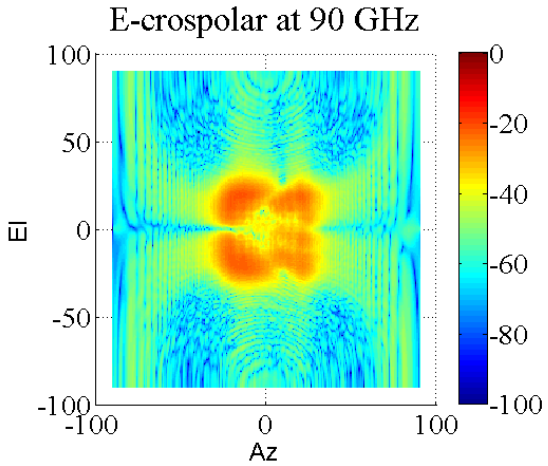

(d) Transformed cross-polar far field radiation pattern at 90 GHz

Figure 2.11: Example of the characterization of the TSA. (a) Near-field co-polar measurement. (b) Far-field transformed radiation pattern at 90 GHz

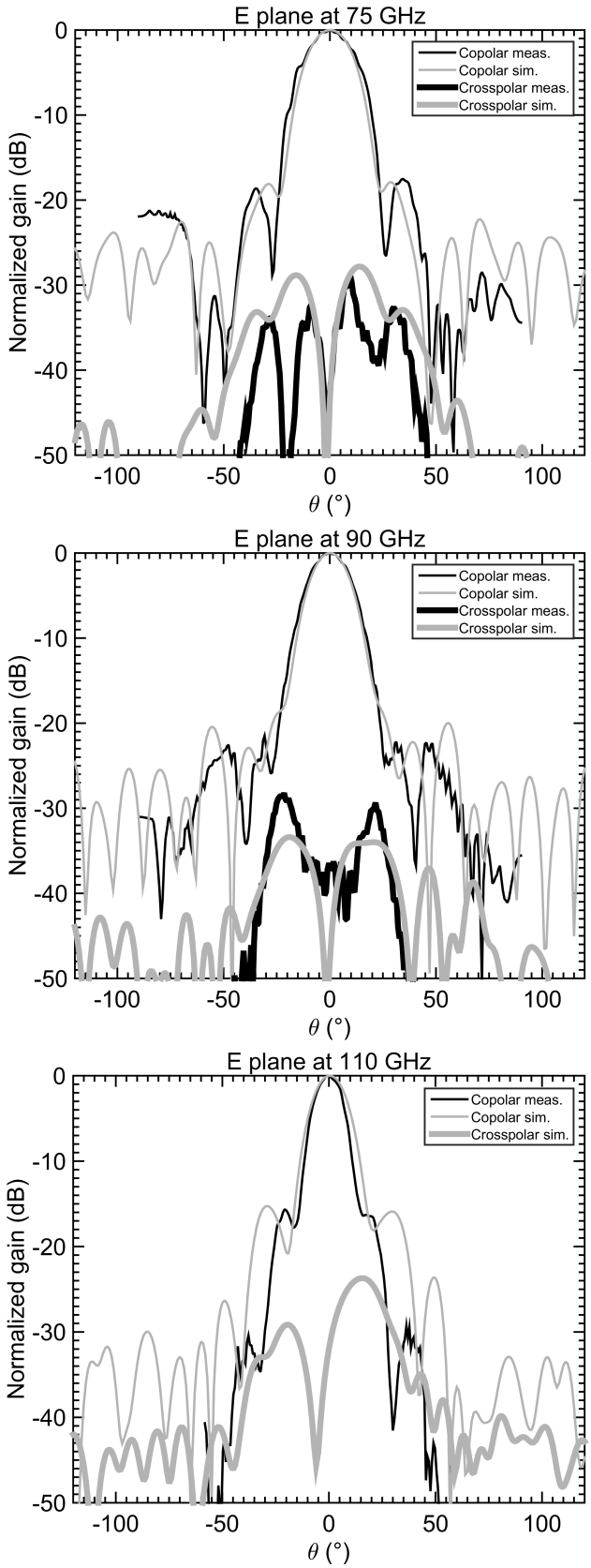

Figure 2.12: E plane radiation patterns at 75, 90 and 110 GHz. Measured co-polar (thin black line) and cross-polar (thick black line), and simulated co-polar (thin gray line) and cross-polar (thick gray line).

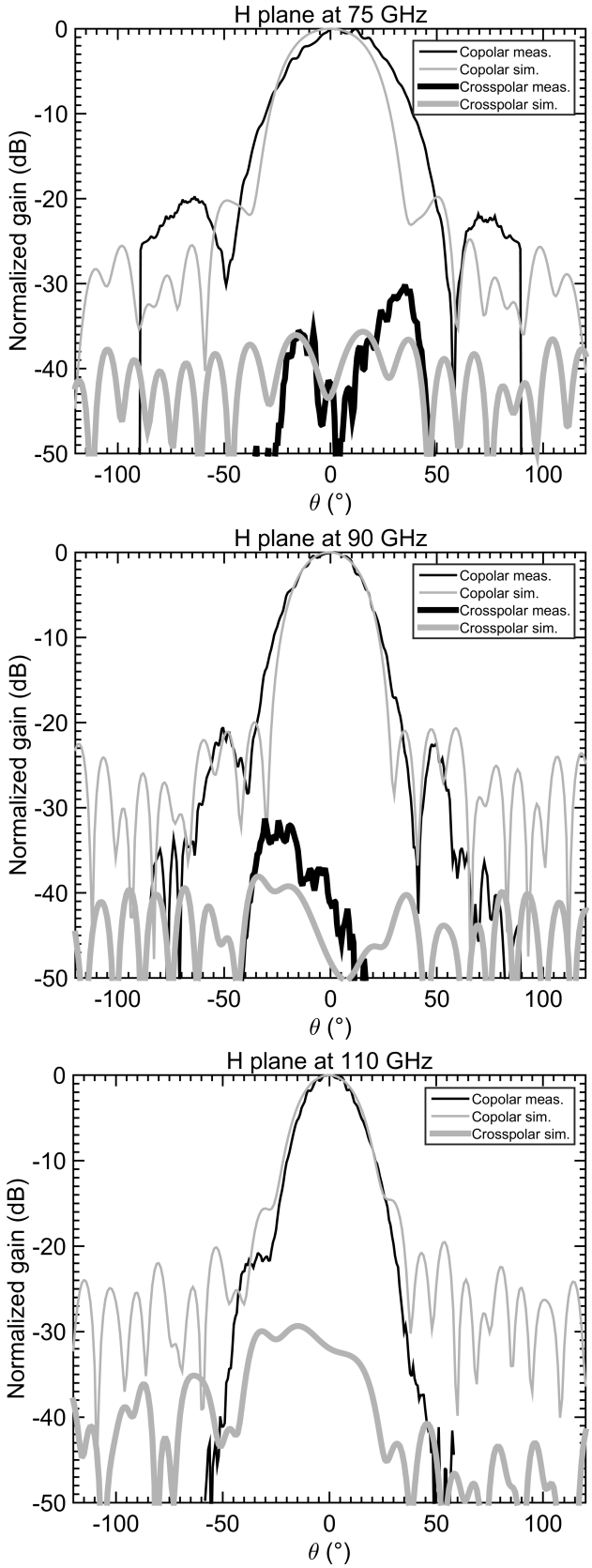

Figure 2.13: H plane radiation patterns at 75, 90 and 110 GHz. Measured co-polar (thin black line) and cross-polar (thick black line), and simulated co-polar (thin gray line) and cross-polar (thick gray line).

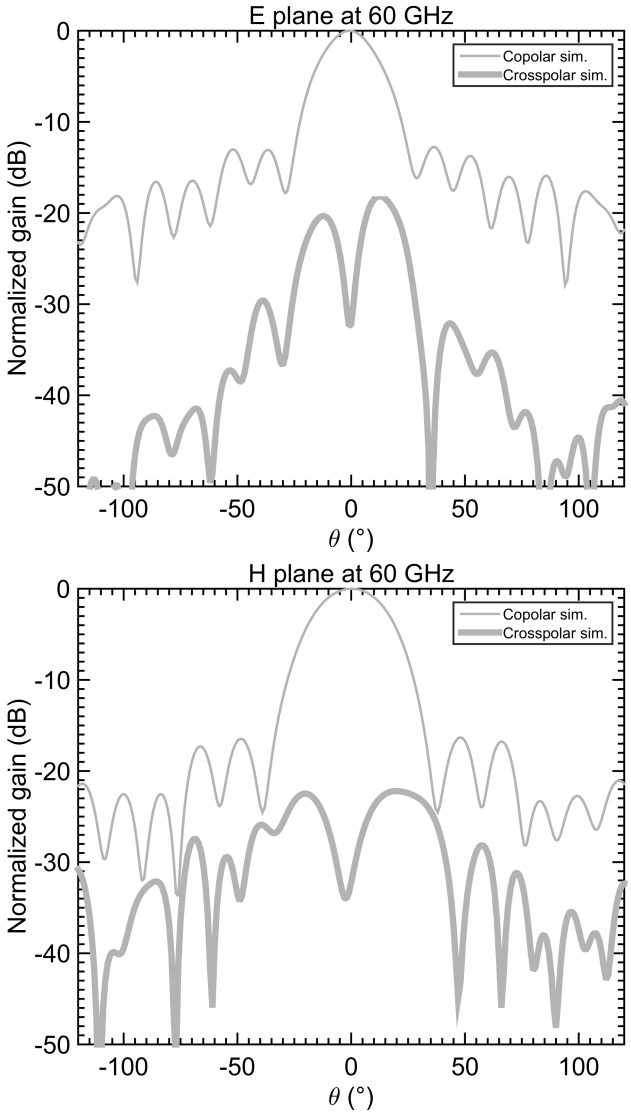

Figure 2.14: Simulated co-polar (thin gray line) and cross-polar (thick gray line) radiation patterns at 60 GHz

Chapter 3

Mixers

In this chapter, first the basics concepts of mixers operation are reviewed, then the designs and measurements of mixers built at Universidad de Chile using discrete components are presented.

3.1 Introduction

A mixer is a three-port device that has two input ports and one output port. It uses a non-linear element to achieve frequency conversion. In a mixer the output-signal frequency is given by the difference (or sum) of the frequencies of the inputs signals. When the desired output frequency is lower than the input frequencies, the process is called down conversion and the relationship between the inputs and outputs is given by

$$f_{IF} = |f_{RF} - f_{LO}| \tag{3.1}$$

where f_{RF} is the high frequency signal, f_{LO} is the local oscillator frequency that is used as reference, and f_{IF} is the low frequency signal.

In an ideal mixer the output signal is the product of the two incoming signals. Let us consider the RF input signal written as

$$v_{RF}(t) = \cos(2\pi f_{RF} t) \tag{3.2}$$

and applied to the mixer along with the local oscillator signal that can be represented as

$$v_{LO}(t) = \cos(2\pi f_{LO} t). \tag{3.3}$$

Then, the output signal is

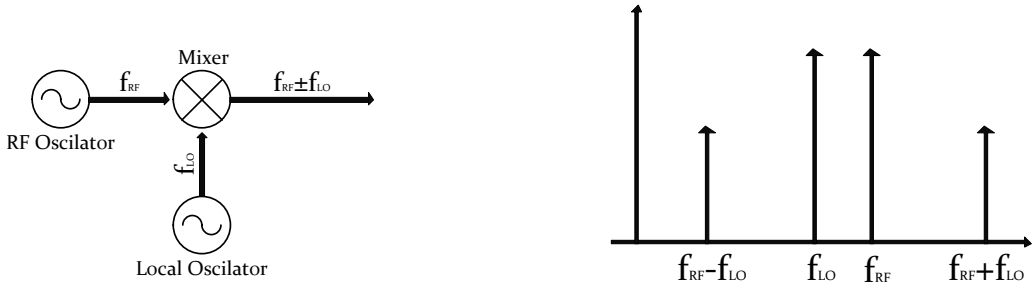

(a) Downconverting mixer schematic.

(b) Spectra of the input and output signals of the mixer.

Figure 3.1: Frequency downconversion using a mixer.

$$v_{IF}(t) = K v_{RF} v_{LO} = K \cos(2\pi f_{LO} t) \cos(2\pi f_{RF} t) \tag{3.4}$$

$$v_{IF}(t) = \frac{K}{2} \left[\cos(2\pi(f_{RF} - f_{LO})) + \cos(2\pi(f_{RF} + f_{LO}))\right] \tag{3.5}$$

where K is a constant accounting for the voltage conversion loss of the mixer. According to equation 3.5 the mixer output consists of the sum and difference of the input signal frequencies. The desired frequency in a receiver is $f_{RF} - f_{LO}$ which can be selected using a low pass filter. In a realistic mixer many more unwanted products will be generated due to the non-linear characteristic of the diode. A simple downconversion process in frequency domain is illustrated on figure 3.1. To understand how a mixer works, a single ended diode mixer will be reviewed.

3.2 Single-Ended diode mixer

This section is mainly based in the reference [11]. A basic diode mixer is shown in figure 3.2. The RF and LO signals are combined using a diplexer to feed the diode. A DC voltage must also be added to bias the diode. This line must be decoupled from RF and LO signal paths, which is achieved using decoupling capacitors and a RF choke. The output signal of the diode is passed through a low-pass filter to obtain the desired low frequency signal.

The LO and RF input voltages are applied across the diodes junction. For small signals the total diode current can be approximated using a Taylor expansion,

$$\mathrm{i}(t) = I_0 + G_\mathrm{d}(v_{RF}(t) + v_{LO}(t)) + \frac{G'_\mathrm{d}}{2}(v_{RF}(t) + v_{LO}(t))^2 + ... \tag{3.6}$$

The first term in 3.6 is a DC bias current which is blocked at the output by the DC decouplers. The second term will be filtered by the low pass IF filter. Finally, if the RF and LO input voltages are given by

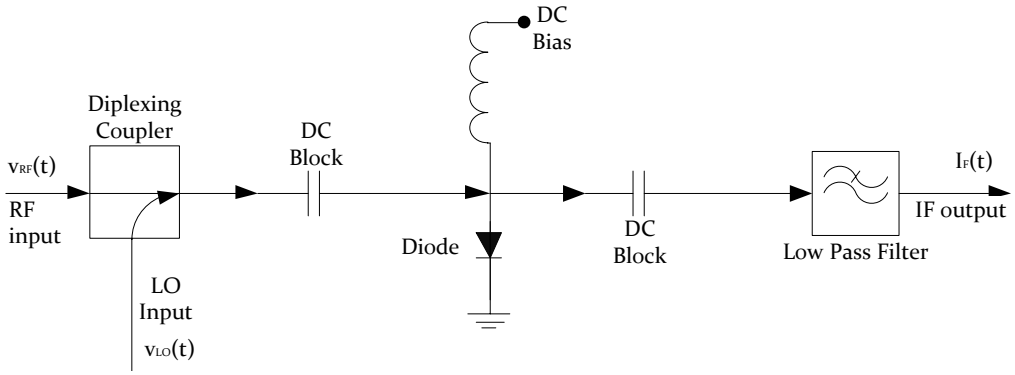

Figure 3.2: Single-ended diode mixer

$$v_{RF}(t) = V_{RF}\cos\omega_{RF}t \tag{3.7}$$
$$v_{LO}(t) = V_{LO}\cos\omega_{LO}t. \tag{3.8}$$

the third term can be rewritten using trigonometric identities as

$$\mathrm{i}(t) = \frac{G'_\mathrm{d}}{2}(V_{RF}\cos\omega_{RF} + V_{LO}\cos\omega_{LO})^2 \tag{3.9}$$
$$\begin{aligned}\mathrm{i}(t) = &\frac{G'_\mathrm{d}}{4}\left[V_{RF}^2(1+\cos 2\omega_{RF}t) + V_{LO}^2(1+\cos 2\omega_{LO}t)\right.\\ &\left.+2V_{RF}V_{LO}\cos(\omega_{RF}-\omega_{LO})t + 2V_{RF}V_{LO}\cos(\omega_{RF}+\omega_{LO})t\right].\end{aligned} \tag{3.10}$$

Equation 3.10 shows signals with more frequency components and two DC terms. If all but the lowest frequency term are blocked we have

$$\mathrm{i}_{IF}(t) = \frac{G'_\mathrm{d}}{2}V_{RF}V_{LO}\cos(\omega_{RF}-\omega_{LO})t. \tag{3.11}$$

3.3 Sub-harmonic Mixers

Sub-harmonic mixers are used in receivers to downconvert the incoming RF signal to an intermediate frequency. The difference with a fundamental mixer is the frequency required for the LO input port to achieve frequency conversion. A fundamental mixers used as down-converter produces an IF frequency given by equation 3.1. Sub-harmonic mixers can achieve the same frequency conversion as the fundamental mixer but the frequency of the LO signal is a fraction of the frequency required in a fundamental mixer. The analogous equation to 3.1 for an N^{th} order sub-harmonic mixer is given by:

$$f_{IF} = |f_{RF} - Nf_{LO}|. \tag{3.12}$$

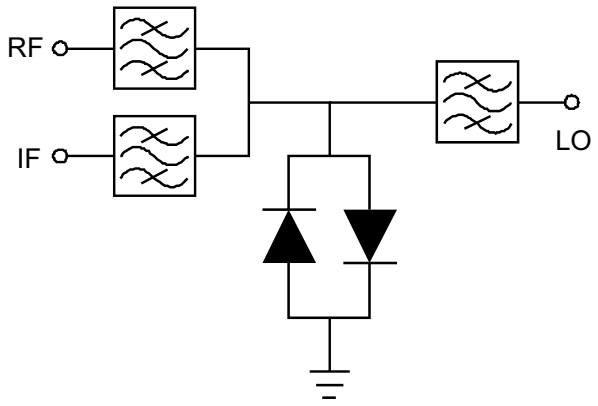

Figure 3.3: Subharmonic mixer schematic

The frequency reduction in the applied LO signal is the main advantage of the sub-harmonic mixers. The operation of these mixers is not equivalent to using a lower frequency LO signal and adding a multiplier on the LO line. In a sub-harmonic mixer there is a greater frequency separation between LO and RF signals making easier to obtain higher isolations between these ports. The main disadvantages of using sub-harmonic mixers is the higher conversion loss due to the use of a higher harmonic.

A schematic of a subharmonic mixer is shown in figure 3.3. This configuration allows conduction in both positive and negative cycles of the LO voltage resulting in two identical conduction pulses for each cycle. Therefore, the lowest frequency component is twice the LO frequency. Because of the opposite polarity, the current at the output terminals of the diode pair contains only odd frequencies [57] . The current with even frequency components circulate inside the diode loop. The current flowing to the diode pair is given by:

$$\begin{aligned} \mathrm{i}(t) =& \mathrm{i}_1(t) + \mathrm{i}_2(t) \\ \mathrm{i}(t) =& I_s \mathrm{e}^{\alpha V} - I_s \mathrm{e}^{-\alpha V} \\ \mathrm{i}(t) =& I_s sinh(\alpha V) \end{aligned} \tag{3.13}$$

the hyperbolic sine can be expanded in odd powers of its argument thus, for the ideal case of identical diodes, there is no DC current flowing into or out of the loop. Furthermore, the current only contains mixing products with the frequencies $mf_{LO} + nf_{RF}$ where $m + n$ is an odd integer. Al the even components, including DC, flow inside the loop.

3.4 Schottky Diodes

Schottky diodes are non-linear devices widely using in microwave applications. The main reason of for the use of Schottky diodes in millimeter wavelengths is that it is a majority carrier device and therefore it does not suffer from charge-storage effects that limits the switching speed of typical P-N junction diodes.

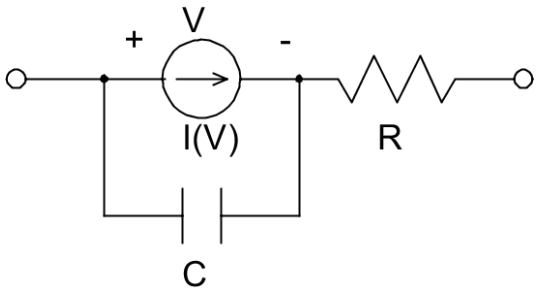

Figure 3.4: Schottky diode circuit model

Schottky diodes are composed by a junction of a semiconductor and a metal. Although P-type or N-type semiconductors can be used, the carrier mobility for N-type is greater, so diodes using this type of semiconductors have lower series resistances and higher cut-off frequencies. Hence, N-type semiconductors are used for microwave mixer diodes. In general, diodes can be constructed on silicon or gallium arsenide (GaAs). For GaAs typical metals to form the junction are platinum, titanium and gold.

One of the most important characteristics of a diode is the IV curve. The electron conduction occurs mainly by thermionic emissions over the barrier. In equilibrium (under zero bias) the net current is zero because emissions occurs equally in both directions. When forward bias is applied, an increased electron emission occurs from the semiconductor to the metal. The current flowing through the diode is:

$$I(V) = I_{sat}\,(\mathrm{e}xp(qV/\eta KT) - 1) \tag{3.14}$$

where the ideality factor η is added to compensate for non-ideal behaviour and is always greater than 1 [58].

Equivalent Circuit

In order to design a mixer, it is necessary to have a model of the diode. Due to the semiconductor nature of the device the width of the depletion layer and the depletion charge changes when a forward bias voltage is applied to the junction. Therefore, the junction operates as a capacitance which varies non-linearly with the applied voltage. For mixers, with low input LO power, the mixer operates as a variable-resistor diode therefore the non-linearity of the junction resistance is the main contributor to the mixing operation of Schottky diodes. Figure 3.4 presents a circuit model for the Schottky diode. It is comprised of a capacitor and a resistance that can vary with voltage and a fixed series resistance. Other circuit elements can be added to account for bond-wires or packaging parasites. The parameters for the model are given by

$$C(V) = \frac{C_{j0}}{(1 - V/\phi)^{\gamma}} \tag{3.15}$$

where C_{j0} is the zero bias junction capacitance, ϕ the built-in potential and the current source is given by eq. 3.14. If the junction is uniformly doped γ is equal to 0.5 [58]. Based on the parameters of the circuit model for the Schottky diode, the cut-off frequency f_c can be estimated by

$$f_c = 1/2\pi R_s C_{j0}. \tag{3.16}$$

It is important to notice that the frequency estimated by the previous equation may be considerably higher if R_s and C_{j0} are not determined at higher frequencies where, for example, the skin effect would increase R_s.

3.5 W-Band Mixer

3.5.1 UMS Diodes

One of the most important parts of the mixer is the selection of diodes with a high cut-off frequency to assure proper operation at W band. The Schottky diode selected to construct the mixer was BES45 from UMS company. These are commercial diodes fabricated using the BES process from UMS company. These diodes have a very low junction capacitance that allows them to work, according to the datasheet, up to 2.4 THz. A picture of the diode and its equivalent circuit are presented in figure 3.5. The equivalent circuit parameters, provided by UMS, are the following:

- Ideality factor $\eta = 1.2$
- Gate width $W_u = 5\mu$m
- Saturation current $I_{sat} = 35f$A
- Zero voltage junction capacitance C_{j0}= $9.5f$F
- Parasitic capacitance $C_{par} = 5.8f$F
- Series resistance R_s= 4.4Ω

It is important to notice that the chip already has two junctions connected in series. Considering the chip layout, a shunt connection is more suitable for the mixer design.

3.5.2 Design

The general schematic of a harmonic mixer presented in figure 3.3 does not contain phase information of the filters. A detailed schematic of the diode connection is presented in figure 3.6. The opens are needed to ensure that the reflected waves do not cancel part of the incomings signal towards the diodes and thus reducing the mixer performance. Under the condition of small LO power and in the absence of filters, the impedance seen from the RF and LO ports to the diodes alone did not change too much with frequency, but when the

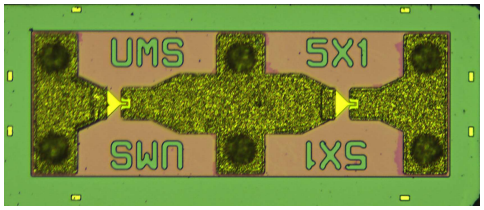

(a) Picture of the diode.

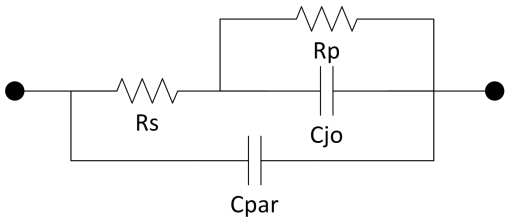

(b) Equivalent circuit of a single junction of the diode provided by UMS.

Figure 3.5: Commercial UMS diode.

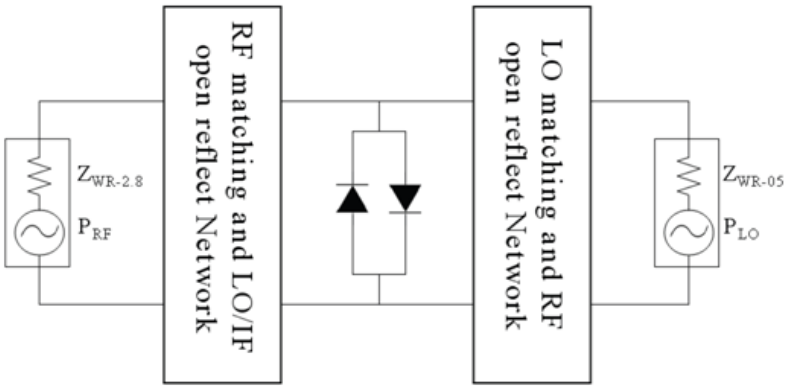

Figure 3.6: Sub harmonic mixer schematic with anti-parallel diodes in shunt configuration.

filters were added, it was necessary to adjust the type of filter and the width and length of the lines to properly match the impedances seen from the filters to the diodes in the proper bands.

All the active parts of the design were simulated using AWR Microwave Office. Initial designs of passives were also made with AWR but an improved simulation was done latter using HFSS. These simulations were then exported to AWR. The mixer was designed to work in the W-band using a LO signal from 37.5 to 50 GHz and IF from DC to 15 GHz. Due to its manufacturing properties, microstrip technology was selected for the transmission lines. The substrate used for the microstrip lines was Duroid 5880 ($\varepsilon_r = 2.2$) with a thickness of 127 μm.

An schematic of the design of the mixer is presented in figure 3.7. It comprises the design of three filters. First, a low pass filter based on conical open stubs is used to receive the IF signal. This filter has a cut frequency of 15 GHz and act as an open reflector for the LO. Second, for the LO signal, a pass band filter based on coupled lines with a design frequency between 35 and 52 GHz was added. Both of these filter works as an open reflector at the RF frequency by adding a 1950 μm line. Third, a band pass filter for the RF signal is needed to make an open for the LO and the IF. All the filters were simulated together using HFSS. The cavities for the filters and microstrip lines have widths small enough not to allow a rectangular waveguide propagation in the structures.

The LO and RF signals are feed using a rectangular waveguides. Transitions from rectangular waveguide to microstrip were constructed to inject the LO and RF signal. The

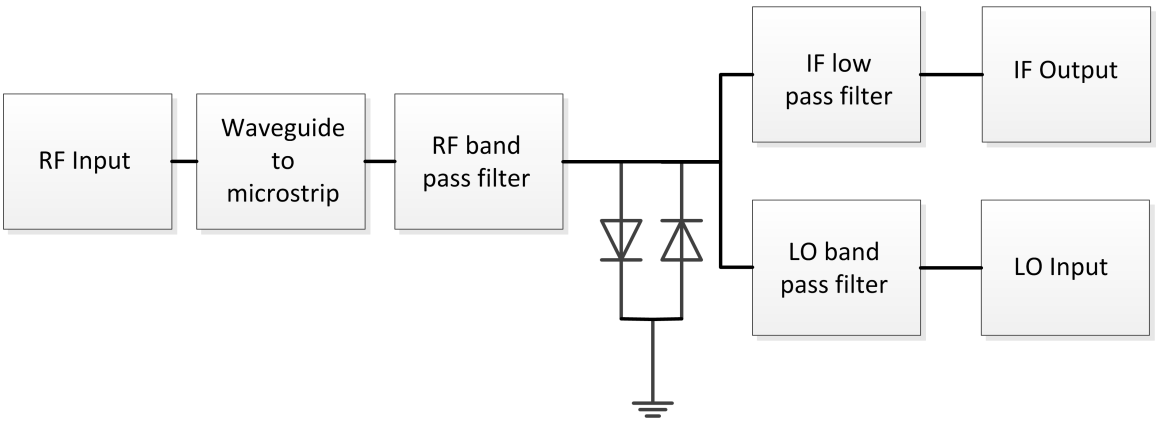

Figure 3.7: Mixer design of the sub-harmonic mixer using the diodes connected to ground.

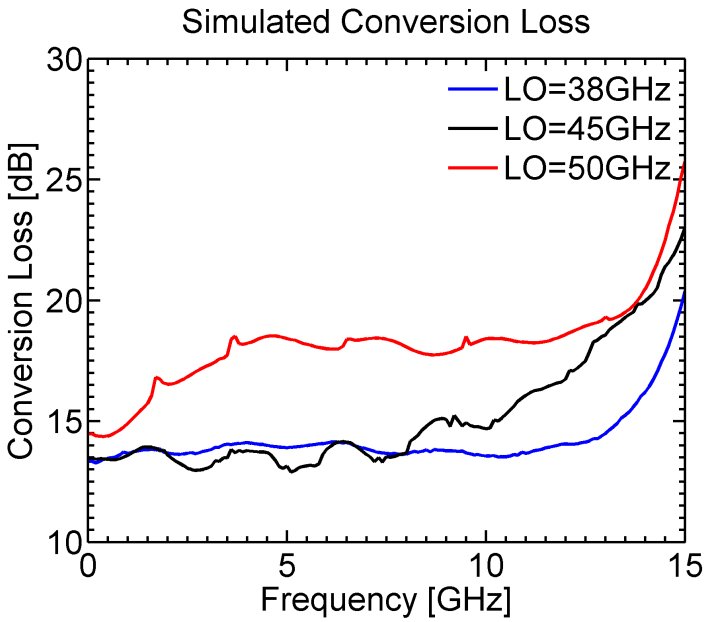

Figure 3.8: Conversion loss simulations at different LO frequencies for the W-band mixer. The effect of the conductive glue to connect the diodes to ground has also been considered.

connection between the microstrip lines and the diodes were done using bond wires. For the ground connection of the diodes an epoxy conductive glue was used. The resistance of the glue measured at DC was 4Ω.

Simulations were performed with different LO powers. The minimum power needed to allow current to flow in the diodes is 9 dBm. Its value is strictly related to the attenuation of the LO band pass filter at its frequency edges. Simulation results are presented in figure 3.8. Conversion losses are below 20 dB in the whole band using an IF frequency up to 10 GHz. It is important to notice that these simulations include a resistance to simulate the conductive glue used to connect the diodes to ground, the effect of this has in conversion losses is to increase them specially at high frequencies by approximately 5 dB.

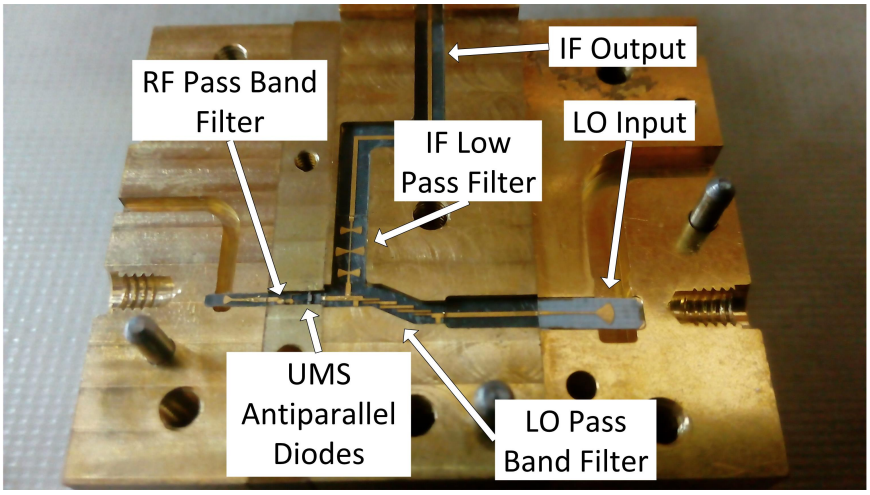

(a) Complete mixer assembled.

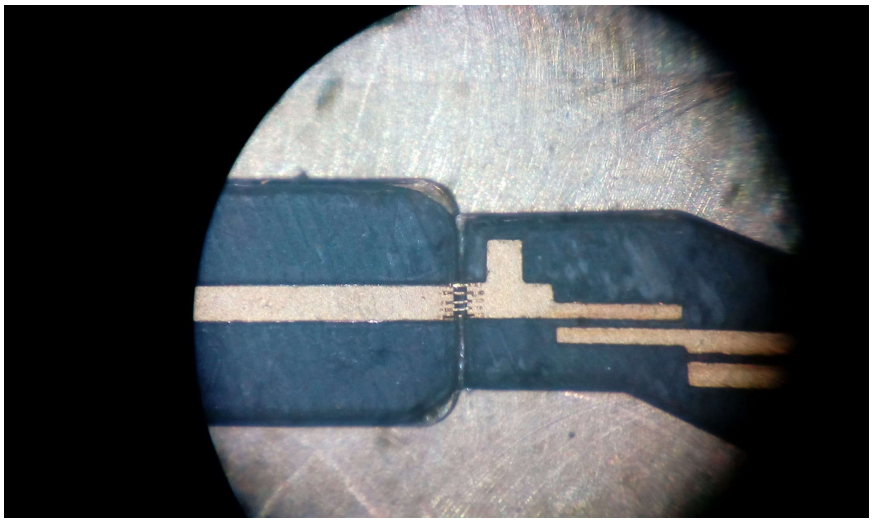

(b) Detail of the connection between microstrips using bondwires.

Figure 3.9: Pictures of the constructed mixer for W-band.

3.5.3 Construction and Measurement

The mixer was built using different blocks that interconnects between them. In this manner, individual parts of the mixer can be tested. The LO and IF filters were tested independently from the rest of the mixer. Moreover, the transitions from microstrip to rectangular waveguide and from microstrip to coaxial were measured using this method. One of the blocks is also used to mount the diodes and the LO-IF open. This block was tested as a tripler to check if the diode has been mounted properly.

The blocks were connected using bondwires. The effect of the bondwires was added during simulations. Five bondings in parallel were used reduce the equivalent inductance they add to the circuit. Figure 3.9 presents a picture of the constructed mixer with all the blocks ensambled and a picture of the bondwires connecting two microstrips.

Conversion-loss measurements were carried out using two spectrum analysers for deter-

Table 3.1: Available power for the LO

Output Frequency GHz	Anritsu Power dBm	Measured Power dBm
34	13	14.03
34	14	15.11
42	13	14.12
42	14	15.26
50	13	12.51
50	14	13.10

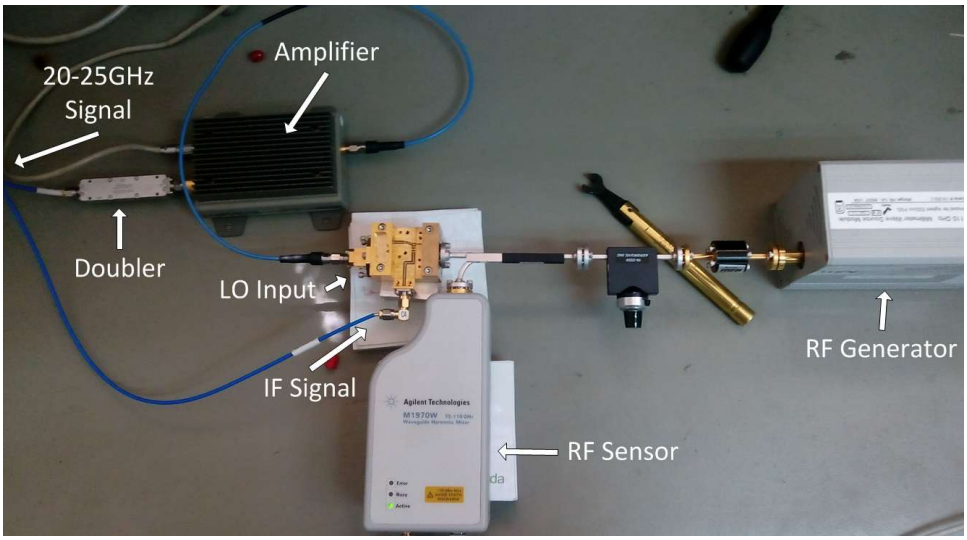

Figure 3.10: Conversion loss measurement set-up

mining the RF power and the converted IF signal. The RF signal goes through a 10 dB coupler before being measured. The LO was generated using a MARKI $\times$ 2 multiplier and an Anritsu generator from 17 to 25 GHz. An instrumental amplifier was also added to increase the LO power. A picture of the experimental set-up can be seen in figure 3.10. The LO chain was measured to ensure that enough power is available for the mixer. Table 3.1 presents the available power of the LO at different output frequencies for different set-up powers of the Anritsu generator, above 14 dBm the instrumental amplifier gets saturated.

The conversion losses were measured with different LO power but the minimal power needed was 12 dBm. The measurement of the conversion losses at different LO frequencies with a power of 12 dBm are presented in figure 3.11. Results are in accordance with simulations, but more LO power is needed. This is probably due to extra losses in the 2.9 mm cable before the doubler. The noise temperature of the mixer was not measured because due to the high level of conversion losses the Y-factor method using liquid nitrogen as cold load did not show a significant difference when measuring the output power.

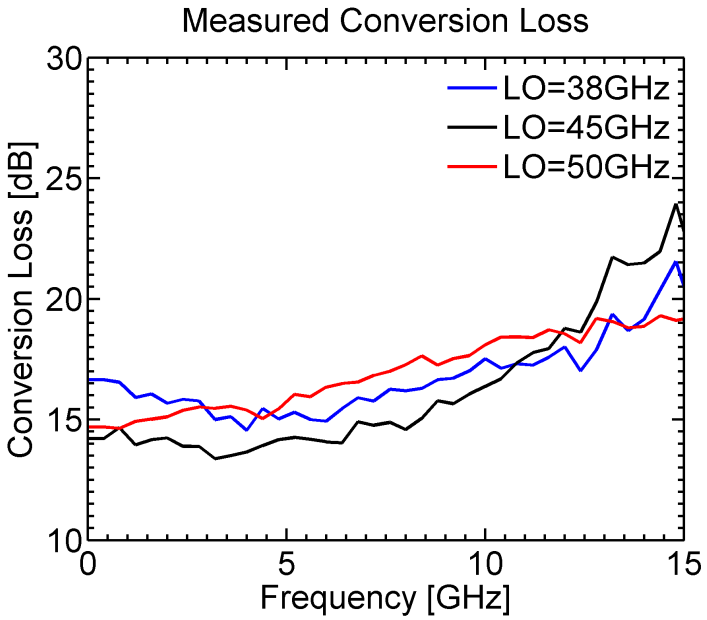

Figure 3.11: Conversion loss measurement at different LO frequencies for the W-band mixer

3.6 Band-2+3 Mixers

3.6.1 Design

Based on the results obtained in the first version of the mixer and inspired by the development of a single receiver that can detect Bands 2 and 3 of ALMA (67 to 116 GHz), a new version of the mixer was designed to work in this band. The mixer was designed using the same diodes from UMS used in the previous mixer. The frequency of the LO signal is from 33 to 58 GHz and of the IF signal from DC to 15 GHz. Due to the size of the fractional bandwidth, one of the most difficult features of this mixer is the design of the LO filter. A band-pass coupled-line filter was selected. Thin lines with small gaps are needed to increase the bandwith of this type of filters. Furthermore, the mixer was designed using a 1.85 mm coaxial input for the LO signal. This allow to reduces its size considerably. A schematic of the designed mixer is presented in figure 3.12

Figure 3.13 shows the simulated conversion losses at the IF frequency for different LO frequencies using a pump signal of 12 dBm. It is important to notice that the cyan curve for an LO of 55 GHz is only presented up to 7 GHz of IF frequency which corresponds to an RF frequency of 117 GHz, the limit of the Band 2+3.

Return loss simulations at LO and RF ports are presented in figure 3.14 to check that these signals are not being completely reflected. The reflections at the RF port are the lowest near the middle part of the band indicating a good match between the diodes and the RF port, but below 80 GHz they increase and more than half of the power is reflected.

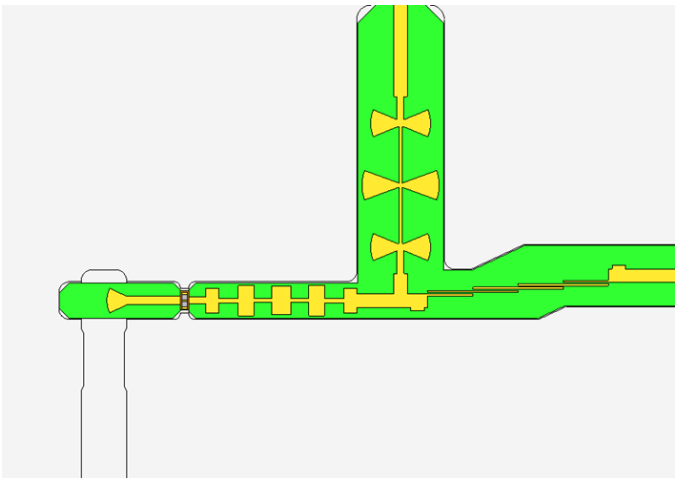

Figure 3.12: Band 2+3 mixer layout.

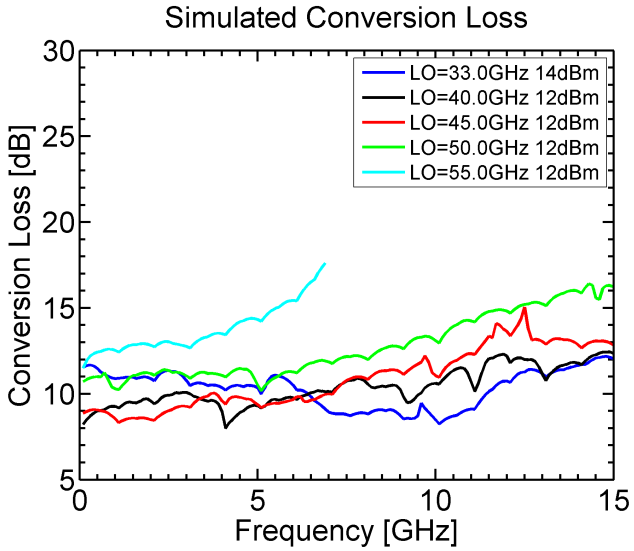

Figure 3.13: Simulated conversion losses of the Band 2+3 mixer.

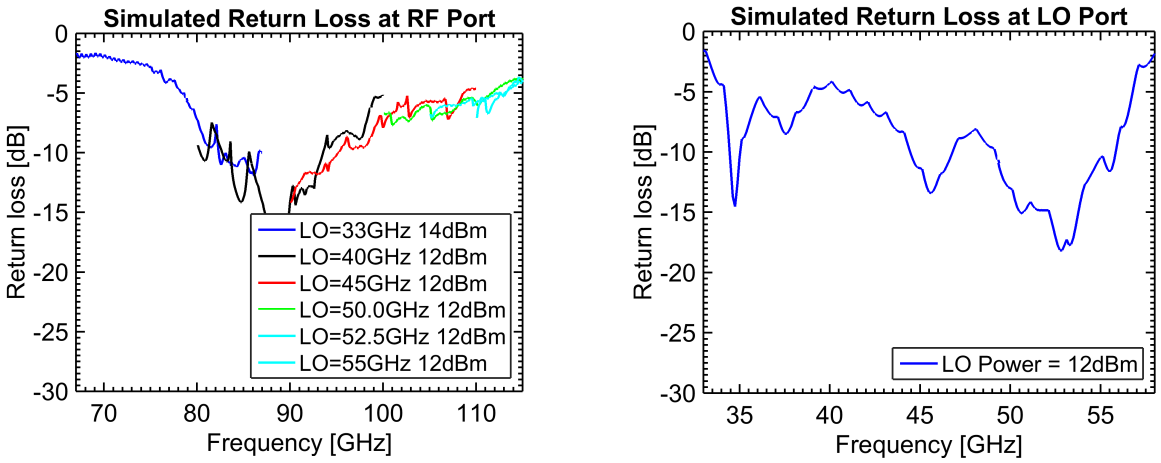

(a) Return loss at RF port.

(b) Return loss at LO port.

Figure 3.14: Return losses at LO and RF ports.

3.6.2 Construction and measurement

The designed mixer was built in bronze and then gold plated. It is comprised of two blocks: the first one is the main frame of the mixer which includes the diodes, transitions and filter, the second one is a transition from a 1.85 mm coaxial input to microstrip. The objective of this block is to test this type of transitions. Figure 3.15 shows a picture of the two transitions connected using bond wires and the measurement of the transmission in the band of interest. Transmissions are better than 4 dB below 55 GHz but they are still very low for this kind of transitions. Due to time constrains there were not enough time to improve them but the pin alignment and the solder had a big impact on transmission.

Once the transitions were measured one of them was connected to the mixer main block. The ground connection for the diodes was done using conductive glue. The mixer was tested using the same set-up used in section 3.5 . The assembled mixer and the measurements of conversion losses at different LO frequencies varying the IF are presented in 3.16. Conversion losses are better than 18 dB in the whole band. At lower frequencies, the mixer requires 14 dBm of LO power; above 104 GHz more power is needed. At 108 GHz the mixer cannot be turned on. This is probably by a construction problem of the LO band pass filter in the upper band limit.

3.7 MMIC Mixer

3.7.1 Design

Based on the community interest for multi-beam systems and therefore, the need of compact receivers, a subharmonic mixer was designed in MMIC technology. It was designed using the DBES process from UMS foundry and have already been built but not measured yet. Unlike the mixers presented above, which combined simulations from AWR and HFSS, this MMIC

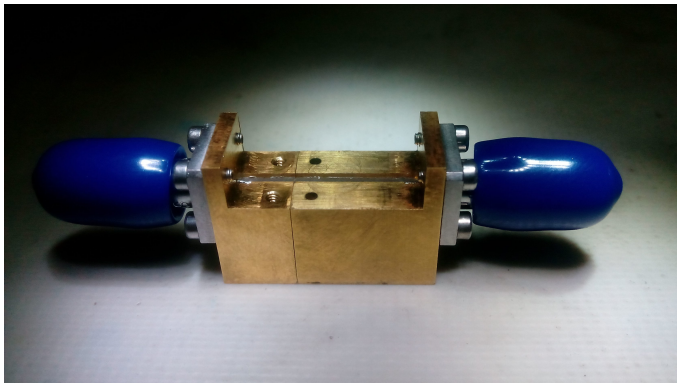

(a) Two coaxial to microstrip transitions connected back to back using bondwires.

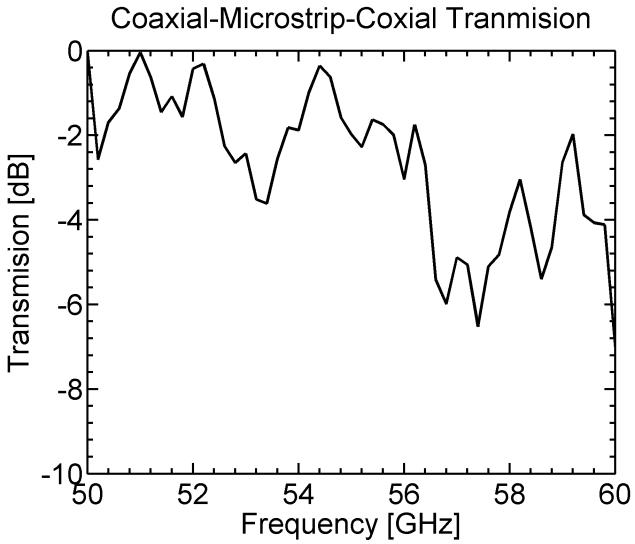

(b) Measured transmission of the connected transitions measured above 50 GHz.

Figure 3.15: Measured transmission of the two microstrip to coaxial transitions.

was designed using only AWR and using AXIEM simulator for EM simulation. The main objective of this design is the construction of a downconverter module for focal plane arrays. Considering that the final idea is to have a high number of mixers they should require low LO power. To achieve this, the design is based in a biased sub harmonic mixer [59].

The layout of the MMIC is presented in figure 3.17. A taper at the RF inputs matches the mixer to the 50 Ω RF input, after passing through the diodes the RF signal is reflected in an open using a radial open stub. The LO signal comes through a DC blocking capacitor and after pumping the diodes it gets reflected using a third order resonator composed of two small capacitors and an open stub. The IF low pass filter is built using an LCL network. An extra capacitor is needed outside the MMIC to block the DC in the IF path.

To obtain a shunt connection that can also bias the diodes two capacitors connected to ground were added. These capacitors limit the low part of the IF frequency, a high capacitance ensure operation at lower frequencies but affect the overall performance of the mixer. The selected frequency for the IF goes from 2 to 15 GHz. To increase the symmetry

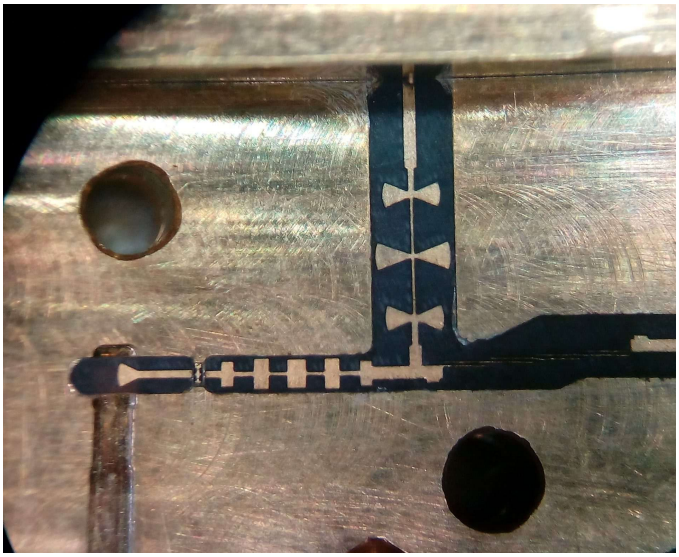

(a) Picture of the constructed mixer.

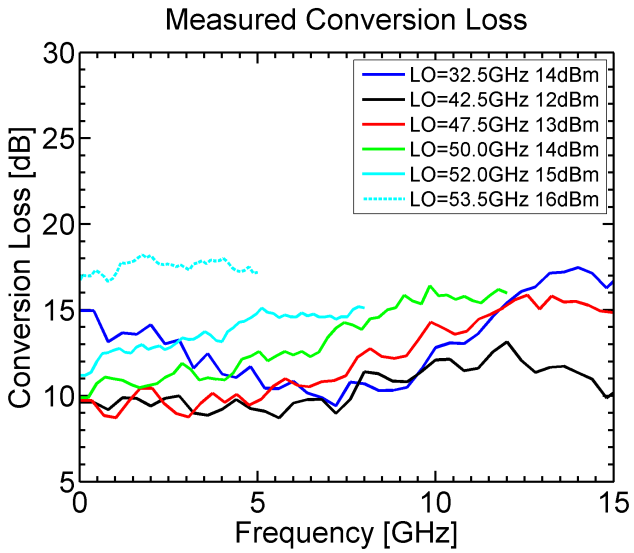

(b) Measurement of conversion loss for different LOs.

Figure 3.16: Constructed Band 2+3 mixer and measured conversion losses.

of the diodes connection, the MMIC is biased using a positive voltage for the first diode and a negative voltage for the second.

Figure 3.18a shows the simulation results. In the band of interest (67 to 116 GHz) conversion losses are below 16 dB but the mixer can operate above the upper limit. The optimal bias current is 0.4 mA. The reflections seen at the RF and LO ports are presented in figure 3.19. Although the matching filters could be improved to have the resonances near the middle of the band, reflections are below -5 dB.

Left side of figure 3.20 shows the response at fixed IF of 5 Ghz with an LO of 55 GHz varying the LO power and also the linear response at the same frequency point varying the input RF power. Conversion losses decreases as more LO power is injected to the mixers but 0 dBm is enough to pump the mixers. This behaviour is similar in other frequency points.

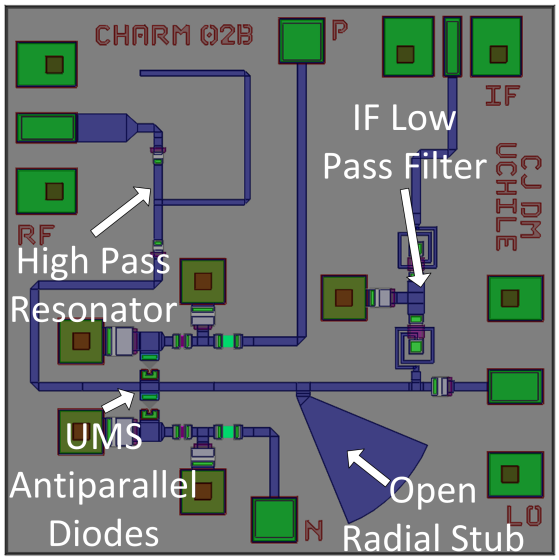

Figure 3.17: MMIC Layout.

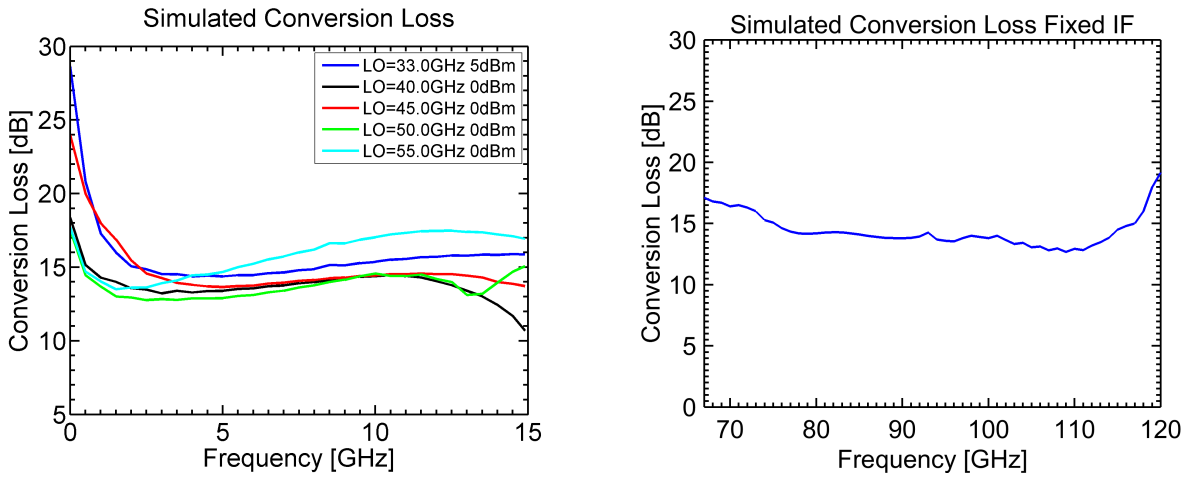

(a) Conversion losses varying LO and IF.

(b) Conversion losses at fixed IF of 2 GHz.

Figure 3.18: Simulation results for the biased mixer for Band-2+3.

On the right side of figure 3.20 the linearity of the mixer is presented. For powers below −10 dBm the mixer behaves linearly, above this value the mixer starts to get saturated.

Removing Bias

The same mixer described in the previous section was also simulated removing the bias lines and connecting directly the diodes to ground. The third order resonator is based in an open stub and two small capacitors, this capacitors are in the limit of what can be constructed with the UMS foundry process. The resonator at the input of the RF line can be tested by constructing a simple version of the previous mixer without the bias lines. The layout and simulation result of this mixer can be seen in figures 3.21a and 3.21b. The required power for the LO is 13 dBm and conversion losses are below 14 dB. This mixer requires more LO power because the impedance seen from the LO and RF port to the diode changed when the

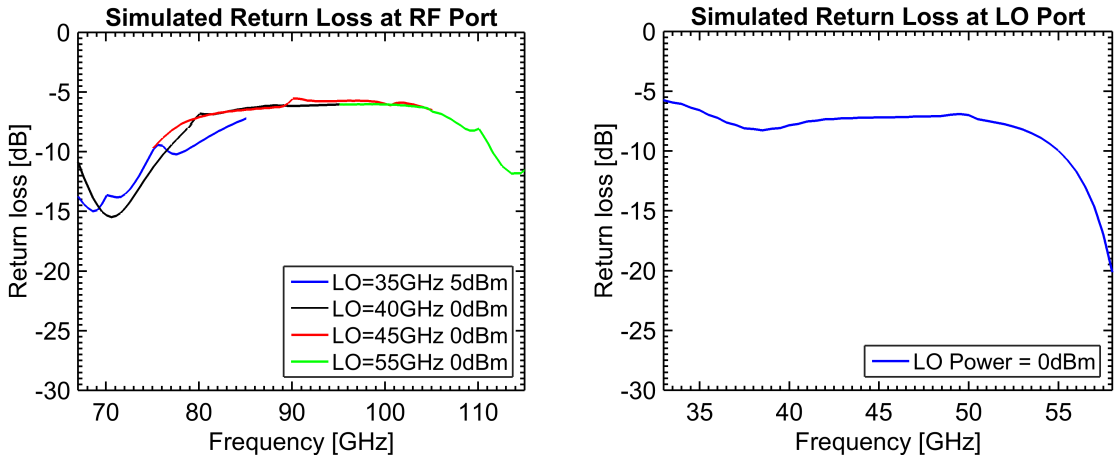

Figure 3.19: Return losses at the RF (left) and LO (right) ports.

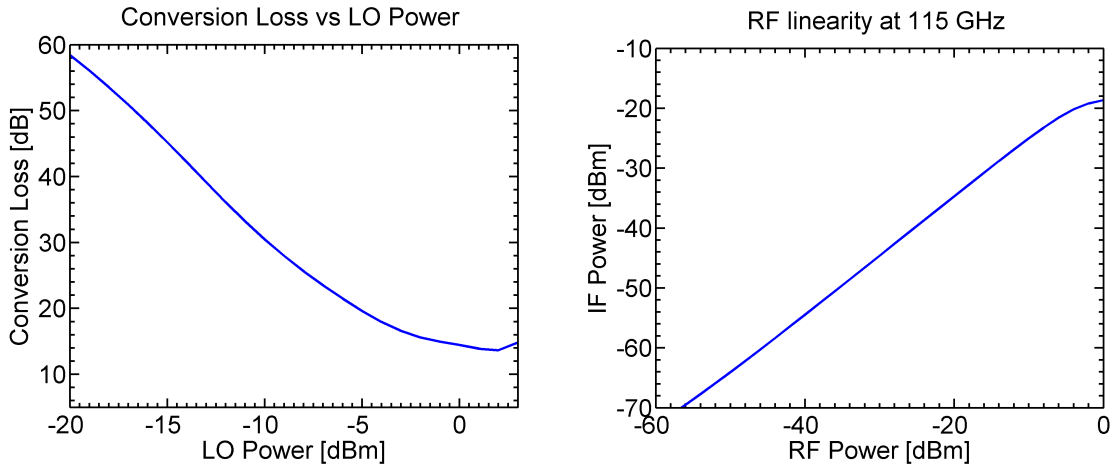

Figure 3.20: Biased mixer MMIC for band 2+3 simulated at 115 GHz with an IF of 5 GHz . Left: Conversion loss for different LO power. Right: IF output power for different RF input power.

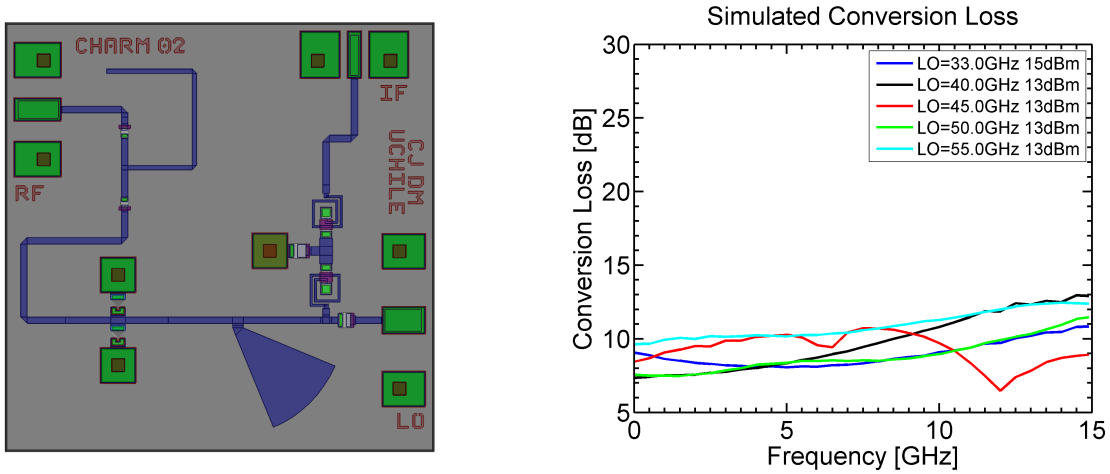

(a) MMIC Layout. (b) Simulated conversion losses.

Figure 3.21: Layout and simulation results for the unbiased mixer for ALMA Band-2+3.

bias lines were removed.

Both of these mixers have already been built by UMS foundry. Figure 3.22 presents a picture of both MMICs. They will be measured during 2018.

Series Mixer

A third mixer was designed using diodes connected in series. Figure 3.23a presents the layout of the mixer . The IF and LO filters have the same frequency behaviour but an RF short that also match the LO line to the diodes was added. From the RF port the LO and IF are grounded and the RF line is matched to the diodes. The simulated conversion losses are shown in figure 3.23b It can be seen that conversion losses are below 15 dB in the whole band.

A block to mount the MMIC was designed and constructed. Transitions from waveguide to microstrip for the RF and LO were manufactured. THe LO and IF line use Rogers Duriod 6010 substrate because it has a high dielectric constant. This is necessary to reduce the size of the cavities for the microstrips by reducing the size of the microstrip copper lines. A picture of the assembled mixer and the measurement results are presented in figure 3.24. In the measurements the LO power was optimized to obtain the lowest conversion losses.

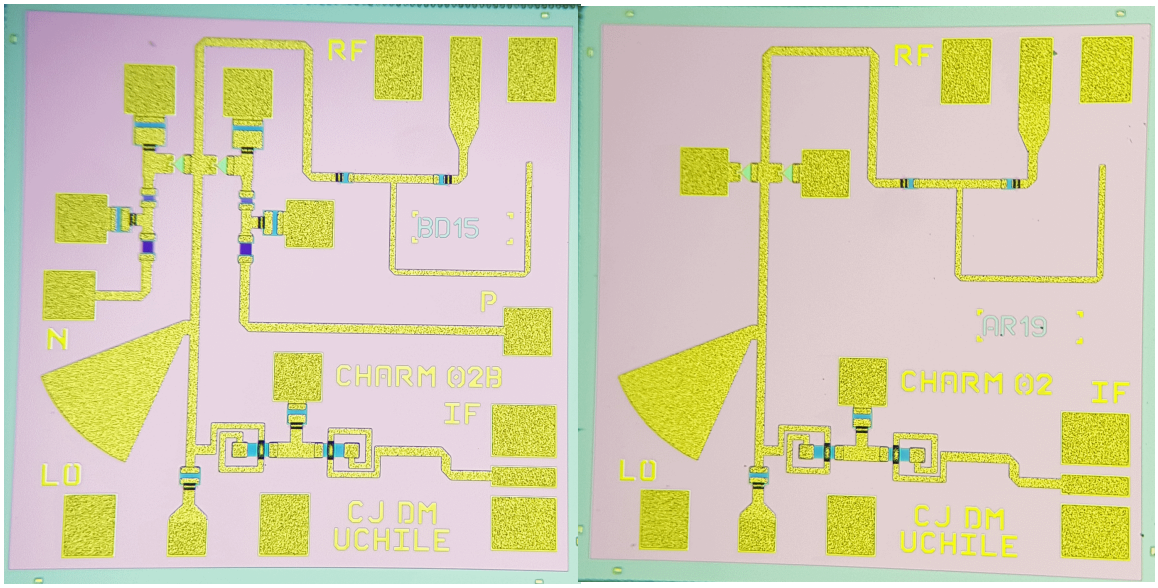

(a) Picture of the constructed MMIC mixer CHARM02B.

(b) Picture of the constructed MMIC mixer CHARM02.

Figure 3.22: Constructed MMIC mixers for ALMA Band 2+3.

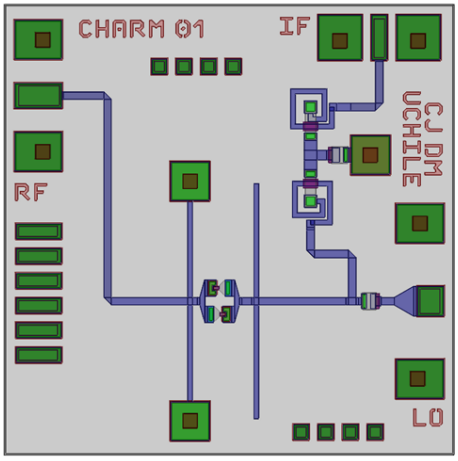

(a) Layout of the designed MMIC with diodes in series configuration.

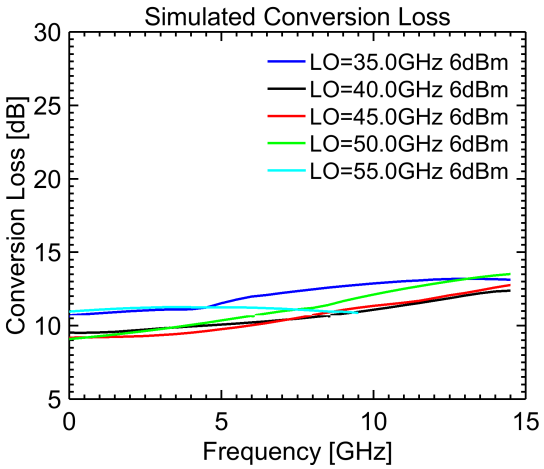

(b) Simulated conversion losses.

Figure 3.23: Layout and simulation results for the unbiased mixer for ALMA Band-2+3.

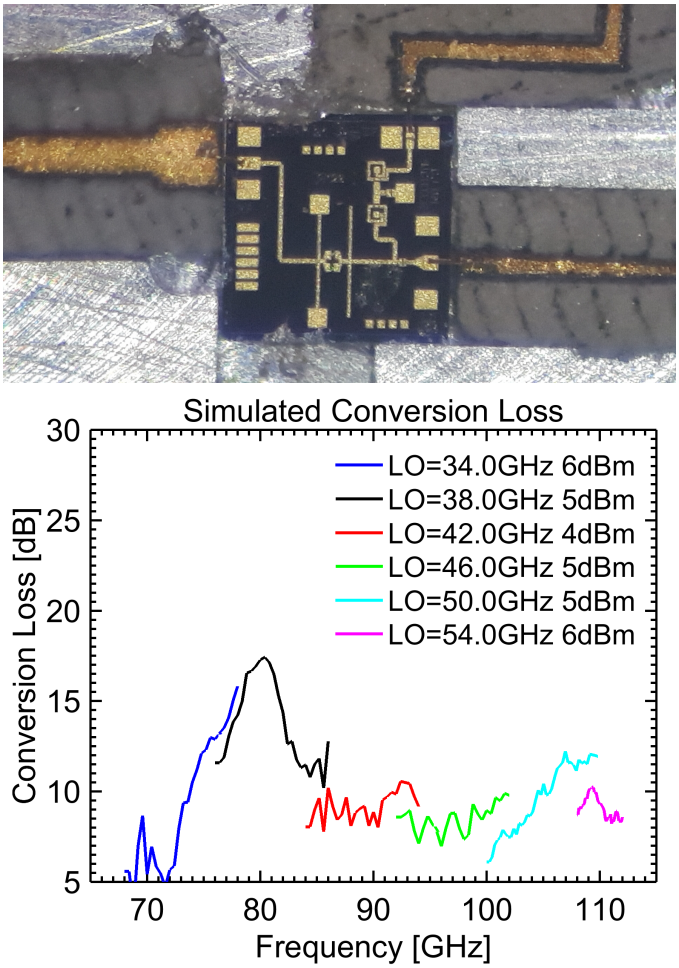

Figure 3.24: On top: Picture of the mounted MMIC. On bottom: Measurements of mixer

3.8 Conclusions

The work presented here corresponds to the first generation of mixers completely designed and built at Universidad de Chile. It is expected that these results will encourage future local developments in this area.

Four sub-harmonic mixers were designed. The first two mixers were constructed and characterized. The first prototype covers W-band and the second version can work in an extended W-band from 67 to 115 GHz being much more compact. Both of these mixers show excellent bandwidth. Conversion losses are high compared to state of the art mixers based on Schottky diodes, this is probably due to an incomplete diode model, the difficulty to implement a broadband match and tolerances in the circuit fabrication. Although the mixer for the extended W-band is very noisy it has been used in a downconversion set-up after a low noise amplifier to measure low noise amplifiers in band 2+3.

The other two sub-harmonic mixer were designed using MMIC technology. These designs are part of the efforts to build a small compact heterodyne camera at the extended W-band by placing these mixers after a low noise amplifier in a 2SB architecture. The main characteristics of these mixers are the bandwidth of operation and the low LO power their require. To reduce even more the LO power needed the first MMIC designs is biased. The second MMIC design has already been packaged and measured presenting good agreement with simulation between 85 and 112 GHz and requiring less than 6 dBm of LO power.

Chapter 4

Low Noise Amplifiers

In this chapter, first the basics of LNA design will be reviewed: HEMTs, noise and stability. Then, the design of an amplifier for the Q-band and the measurement of commercial MMIC LNAs at W-band are presented.

4.1 High Electron-Mobility Transistors (HEMTs)

The high electron-mobility transistor (HEMT) is a type of transistor able to achieve high operation frequencies. Its operation is based on the Field Effect Transistor (FET), being the conduction channel the main difference.

The first HEMT was fabricated using an AlGaAs/GaAs junction [60] with AlGaAs having a wider band-gap than GaAs. When a n-doped AlGaAs is placed in contact with a non-doped GaAs layer, electrons will diffuse from AlGaAs to GaAs generating a depleted AlGaAs layer. The heterojunction created by the difference in bandgap between the two materials forms a quantum well in the conduction band of the GaAs layer where the electrons can move with high mobility because there are no impurities on the GaAs side and the electrons are confined by the quantum well. This creates a two dimensional electron gas (2DEG) with high electron concentration and mobility. Figure 4.1 shows a HEMT band diagram.

HEMTs high mobility allows them to operate at frequencies above 100 GHz. Currently, the lowest noise temperatures have been achieved using Indium Phosphide (InP) HEMTs [61] which can go below 20 K in the Q Band and below 30 K in W Band [34]. One of the most important requirements to design a LNA is to have an accurate transistor model that ideally includes cryogenic behaviour.

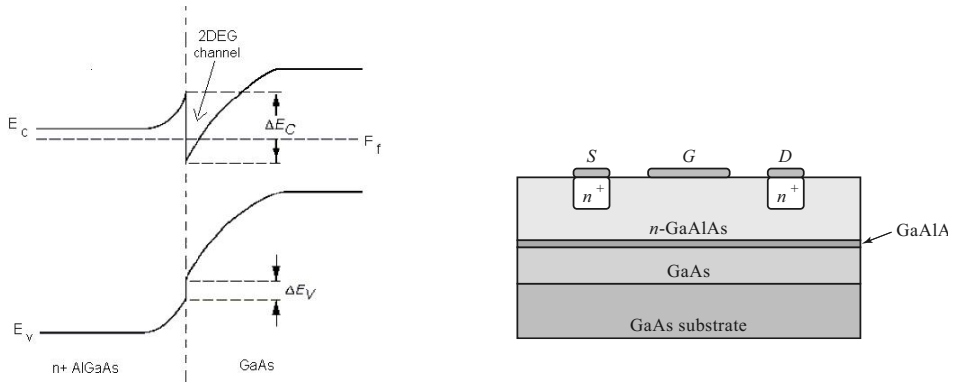

Figure 4.1: HEMT energy bands diagram and internal structure

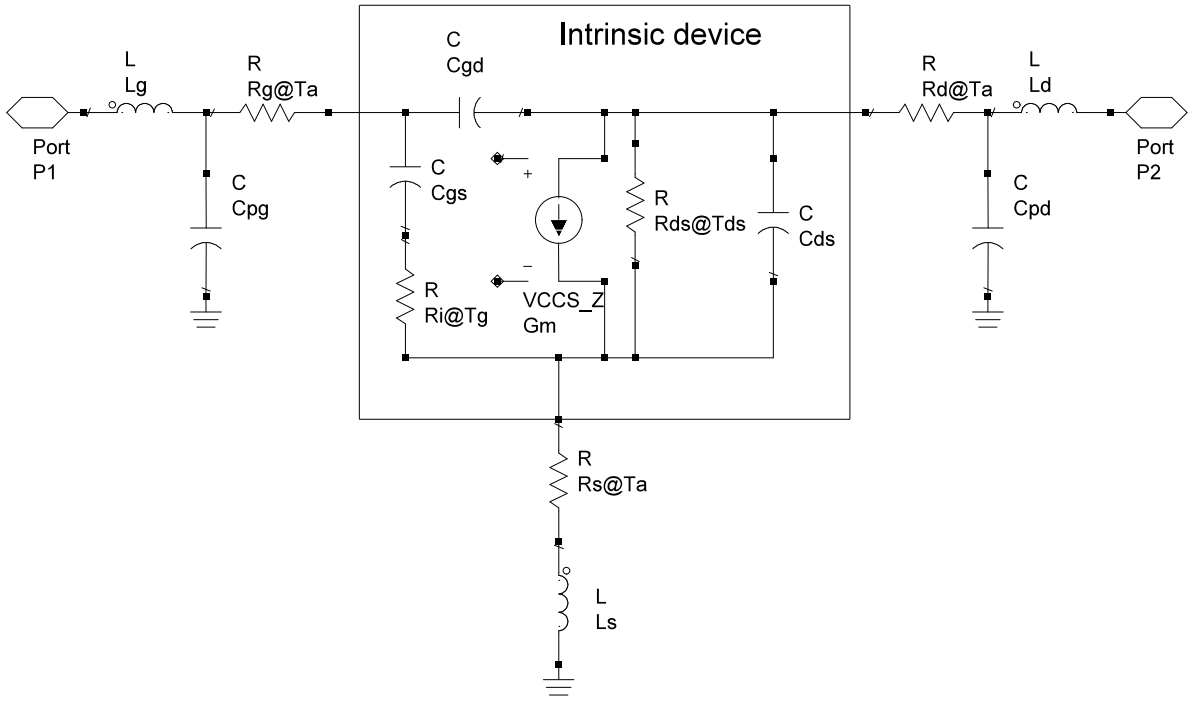

Figure 4.2: HEMT equivalent model for small signal

4.1.1 HEMT Modelling

The linear model for HEMT devices is presented in figure 4.2. The active part is modeled by a current source controlled by voltage with a transconductance G_m and a time delay τ. C_{ds} and C_{gs} represent the geometrical capacitances between gate, drain and source, respectively. R_{i} represents the gate resistance and R_{ds} the channel resistances. All these components define the intrinsic device model. The model also includes parasitic effects of each pad modeled using resistors, capacitors and inductances, which are called extrinsic components [61]. The parameters, shown in figure 4.2, can be extracted by performing two measurements with the VNA as explained below.

1. The extrinsic parameters are obtained by doing a measurement of the transistor S parameters at pinch-off voltage. At this operation point the current source is switched

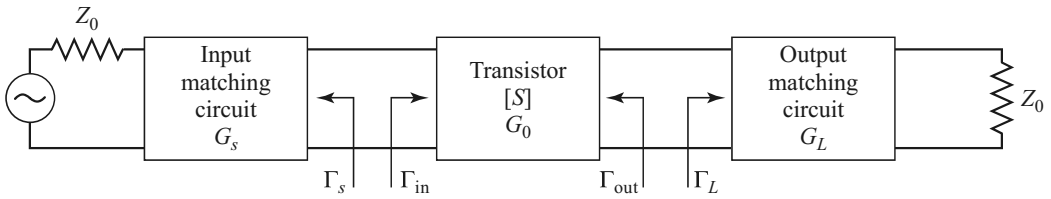

Figure 4.3: General transistor amplifier [11].

off and the transistor model simplifies.

2. The second measurement is performed with the transistor switched on at the operation point. S parameters are measured and the extrinsic parameters (previously calculated) are de-embedded to obtain the intrinsic components.

Since the amplifier has less noise temperature at cryogenic temperatures it is important to consider that the small-signal parameters change with temperature. To determine the cryogenic behaviour it is necessary to perform a measurement of S parameters using a cryogenic probe station.

4.2 Design of Low Noise Amplifiers

The first stage of a receiver, according to equation 1.3, has the dominant effect on the noise performance of the system. Therefore, it is required to use a LNA with the lowest possible noise figure and higher gain. A LNA is composed of several transistor stages connected in cascade. Each stage has its own bias network and input and output matching lines. The biggest limitation of this architecture is the maximum input power. However, this is not an issue for radio-astronomical applications. The main task in the design of a LNA is the design of the input and output matching lines to achieve the required gain and noise level. In order to understand an amplifier design, a single-stage transistor amplifier will be reviewed. A more extended treatment of microwave transistor amplifiers can be found in [12].

4.2.1 Design of a Single Stage Amplifier

A single-stage microwave transistor amplifier can be modelled by the circuit of figure 4.3. Matching networks are used on both sides of the transistor to transform the input and output impedance Z_0 to the source impedance Z_S and load impedance Z_L, respectively, at the transistor ports.

Separate gains for the input matching network, the transistor and the output matching network [11] can be defined as

$$G_S = \frac{1-|\Gamma_S|^2}{|1-\Gamma_{in}\Gamma_S|^2} \tag{4.1}$$

$$G_0 = |S_{21}|^2 \tag{4.2}$$

$$G_L = \frac{1-|\Gamma_L|^2}{|1-S_{22}\Gamma_L|^2}. \tag{4.3}$$

The overall transducer gain of the amplifier is $G_T = G_S G_0 G_L$. The maximum transducer power gain occurs when the source and load are conjugately matched to the transistor. The maximum gain will be given by

$$G_{T_{MAX}} = \frac{1}{1-|\Gamma_S|^2}\,|S_{21}|^2\,\frac{1-|\Gamma_L|^2}{|1-S_{22}\Gamma_L|^2}. \tag{4.4}$$

In many cases it is preferable to design the amplifier for less gain than the maximum obtainable to improve the bandwidth or reduce the noise level. Mismatches are added on purpose to obtain the desired amplifier performance.

4.2.2 Noise

The noise figure of a two port amplifier is given by:

$$F = F_{min} + \frac{4R_N}{Z_0}\frac{|\Gamma_S - \Gamma_{opt}|^2}{(1-|\Gamma_S|^2)(1+|\Gamma_{opt}|^2)} \tag{4.5}$$

where:

- Γ_S is the source reflection coefficient.
- F_{min} is the minimum noise figure of the transistor obtained when $\Gamma_S = \Gamma_{opt}$.
- R_N is the equivalent noise resistance of the transistor.
- Γ_{opt} is the reflection coefficient that results in minimum noise figure.

The quantities F_{min}, Γ_{opt} and R_N are known as noise parameters and are characteristics of each transistor. F_{min} depends on the operation point and frequency and there is one value of Γ_{opt} for each value of F_{min}. Measuring these noise parameters is an extremely difficult task because it is needed to measure the output noise with different input impedances. A linear model of the HEMT can be used to simulate the behaviour of the transistor.

According to eq. 4.5 the minimum noise figure of an amplifier is F_{min} and it is obtained when $\Gamma_S = \Gamma_{opt}$. In principle the source impedance is different from the impedance needed to achieve high gain so there is a trade-off between gain, noise and input reflection in low-noise design.

4.2.3 Stability

The schematic shown in figure 4.3 can oscilate if either the input or output impedance has a negative real part. This occurs when $|\Gamma_{in}| > 1$ or $|\Gamma_{out}| > 1$. There are two types of stabilities.

- Unconditional Stability: The network is unconditionally stable if $|\Gamma_{in}| < 1$ and $|\Gamma_{out}| < 1$ for all passive source and load impedances.
- Conditional stability: The network is conditionally stable if $|\Gamma_{in}| < 1$ and $|\Gamma_{out}| < 1$ only for a certain range of passive source and load impedances. This case is also referred to as potentially unstable.

The majority of transistors are conditionally stable. Therefore, in an amplifier the input and output matching network, $|\Gamma_S|$ and $|\Gamma_L|$, have to be carefully designed to consider the amplifier stability. One of the easiest ways to check the amplifier stability is the $K - \Delta$ test. It can be shown that an amplifier will be unconditionally stable if satisfies the Rollet's condition, defined by [11]:

$$K = \frac{1 - |S_{11}|^2 - |S_{22}|^2 + |\Delta|^2}{2\,|S_{12}S_{21}|} > 1 \tag{4.6}$$

and

$$|\Delta| = |S_{11}S_{22} - S_{12}S_{21}| < 1. \tag{4.7}$$

If the Rollet's condition is not satisfied, $|\Gamma_S|$ and $|\Gamma_L|$ must be chosen such that the amplifier is conditionally stable. Other stability sources caused by feedback must also be considered as bias de-coupling, waveguide modes in microstrip cavities or ground coupling.

4.3 Q-Band LNA

A Q-band LNA has been designed based on a hybrid concept. It is composed of a single transistor followed by a commercial Microwave Monolithic Integrated Circuit (MMIC) from the OMMIC foundry. The single transistor and the MMIC are to be mounted on different mechanical blocks that can be connected through microstrip lines using three bondwires in parallel to reduce the inductance. In this way it is possible to measure the MMIC and the HEMT. This allows the ability to measure the improvement when adding the transistor.

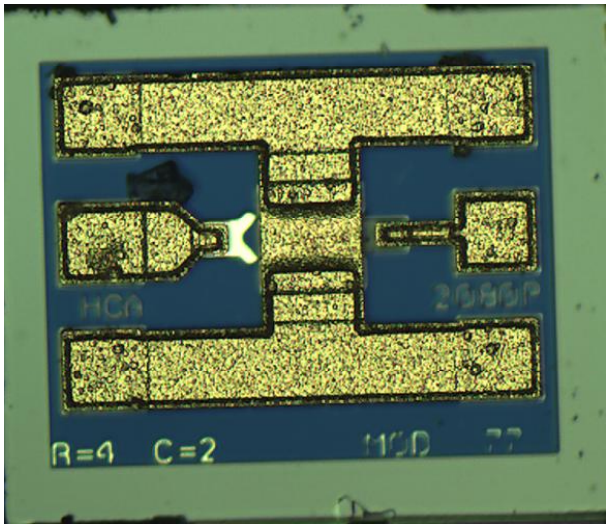

Figure 4.4: Two fingers 80 μm gate width cryo3 HEMT from wafer 4099-040

4.3.1 Single Transistor

The HEMTs used in the LNA design are TRW's (now Northrop Grumman Space Technology NGST) Cryo3 fabricated in 1999 for operation between 1 and 100 GHz. The transistors are two fingers devices with gate width of 80 micrometers from wafer 4099-040. They are among the HEMTs with the lowest noise ever produced. A picture of one transistor can be seen on figure 4.4 .

The transistor model was obtained from [62] and has been checked in a collaboration with the Yebes Astronomical Center in Spain. The Figure 4.5 shows the equivalent circuit and the values of the equivalent-circuit components.

4.3.2 MMIC

Chosing the MMIC is one of the most complicated task because it requires stringent restrictions:

- Working frequency between 30 and 50 GHz.
- Noise temperatures of 200 K at room temperature.
- Low power consumption (below 400 mW for laboratory test purposes).
- The HEMT's conduction channel in the MMIC should not be made from GaAs.

The selected MMIC is from the OMMIC foundry, CGY2122XUH. It is based on Metamorphic HEMTs (mHEMT) with high Indium contain to achieve low noise temperatures. The S parameters provided by the manufacturer are plotted on figure 4.6.

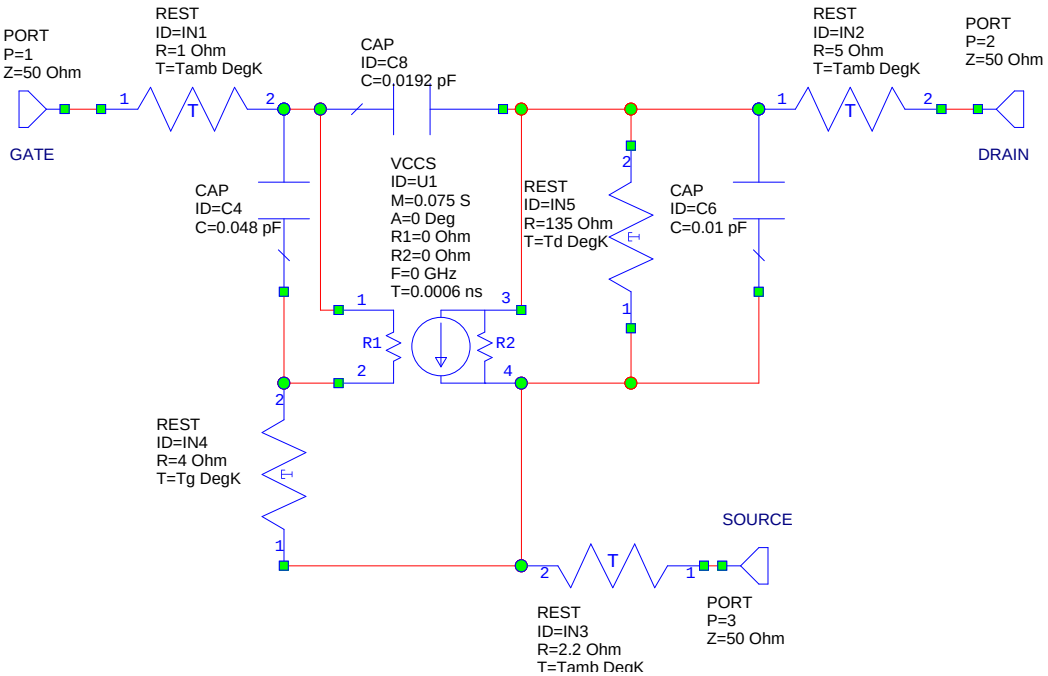

Figure 4.5: Cryo3 small signal equivalent circuit

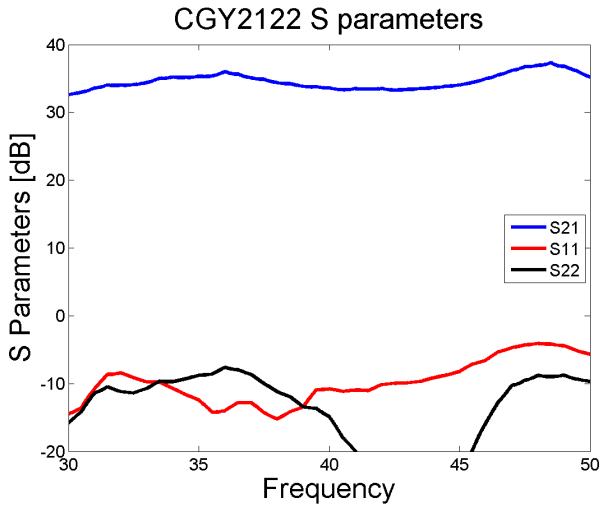

Figure 4.6: CGY2122XUH S parameters from manufacturer.

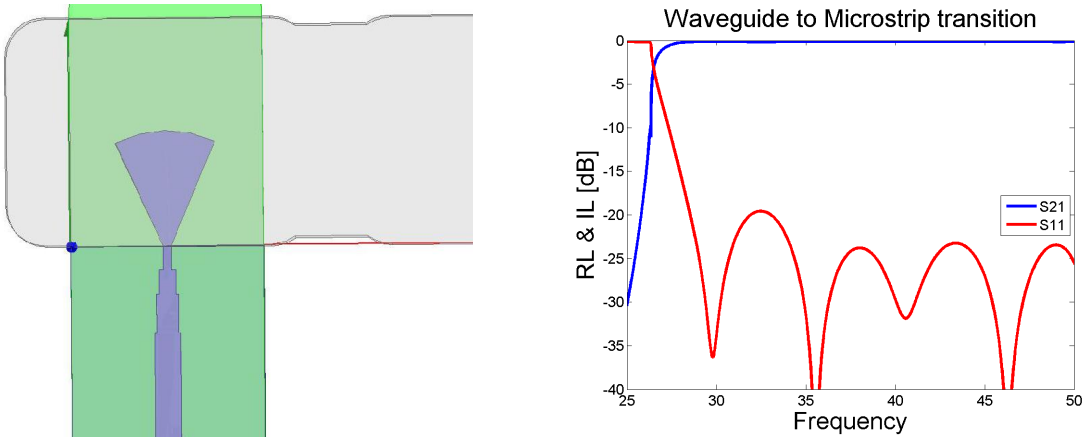

Figure 4.7: Left: waveguide to microstrip transition design. Right: HFSS simulation results of the transition. The probes were fabricated at the LOM using Duriod6002 with 127 μ m thickness

4.3.3 Input and Output Lines

The inputs and outputs of the amplifier are built in waveguide for an easy couple with the horn and the other components of the receiver. HFSS was used to design a rectangular waveguide to microstrip transition that can transmite the main mode of a rectangular waveguide to a 50 Ω microstrip with reflexions below -20 dB in the Q Band [63] . The size of the cavity for the microstrip was chosen so as not to allow propagation of rectangular waveguide modes in the desired band. The substrate used in the design is Rogers Corporation Duroid6002 with 127μm thickness. An schematic of the transition and the results of the simulations can be seen on figure 4.7.

4.3.4 Matching Lines

The electric schematic of the amplifier requires the design of input microstrip lines to match the 50 Ω input line and the transistor optimum noise impedance to reduce the LNA noise. The output is a 50 Ω microstrip line to match the MMIC input impedance reducing possible reflections between the transistor and the MMIC. Furthermore, each of these microstrips must consider lines necessary to bias the transistor's gate and drain pads. The input matching line was optimized using microsoft AWR simulator. The design of the transistor input line can be seen in figure 4.8. It consists of a line to match the 50 Ω microstrip (P1) to the input impedance of the transistor. There is also a line of high impedance with an open stub that prevents the transmission of high frequencies to port 3. The dimensions allow to fully reject the band of interest.

The cryogenic noise temperature of the MMIC is not specified by the manufacturer so the noise simulations were done using the noise information provided in the datasheet. It is expected that the noise temperature drops when the MMIC is cooled. The simulations of the LNA are presented in figure 4.9. It can be seen that the original noise from the MMIC decreases to one third of its original value when adding the Cryo3 HEMT.

4.3.5 Mechanical Design

The mechanical design was made in TopSolid considering all the requirements to interconnect each block: alignment pins and the threads to unite in different combinations the blocks. A single bias connector is located in the MMIC block and the transistor bias is connected to the cryo3 block using bondwires. The cavities in the MMIC block are to locate PCBs that can carry the DC signals towards the MMIC drain and gate pads and also to protect the chip from over-voltages. The mechanical design is shown on figure 4.10.

4.3.6 Measurements

Waveguide to MicroStrip transition

The first measurement that took place is the measurement of transitions, it was done connecting two transitions and then using the VNA. In figure 4.11 the S parameters of the two transitions connected with three bond wires are presented, the reflections are below -13 dB in the range of 37 to 50 GHz.

OMMIC Amplifiers

Once the transitions were characterized, the MMIC gain was measured at room temperature. The transitions were connected to the MMIC block using three small bondwires to reduce the series inductance. A picture of the amplifier with the MMIC block open can be seen in figure 4.12.

The S parameters of the amplifier can be seen in figure 4.13. The gain is above 25 dB from 26.5 to 50 GHz and can be improved by injecting more power trough the MMIC bias

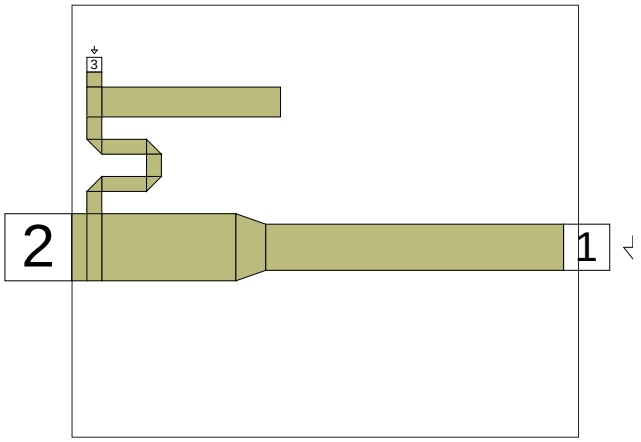

Figure 4.8: Transistor input line to achieve minimum noise temperature. Port 1 is a 50 Ω line, port 2 is the gate connection point and port 3 is the gate bias connection

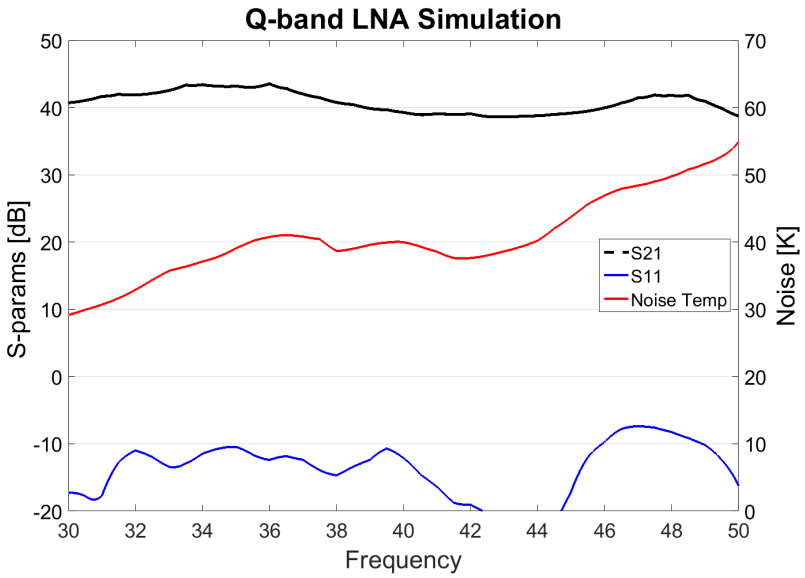

Figure 4.9: LNA simulation results using AWR.

as stated in the MMIC datasheet. The only issue is the high reflection the MMIC has at 47 GHz. This could be produced by the input transition block but has to be more carefully studied.

OMMIC Noise Measurement

The noise of the amplifier was measured using the Y-factor method. This method consists of measuring the output power of the device under test when the input power comes from a load at two different known temperatures. In this case the temperatures of the loads are ambient temperature and liquid nitrogen. Further details on the Y-factor method calculations can be found in [75]. A downconverting setup with a high-gain low-frequency amplifier was built to increase the power of the signal. This downconverter is based in a Quinstar mixer pumped by a LO up to 40 GHz. The LO signal is provided by a high-power output signal synthesizer.

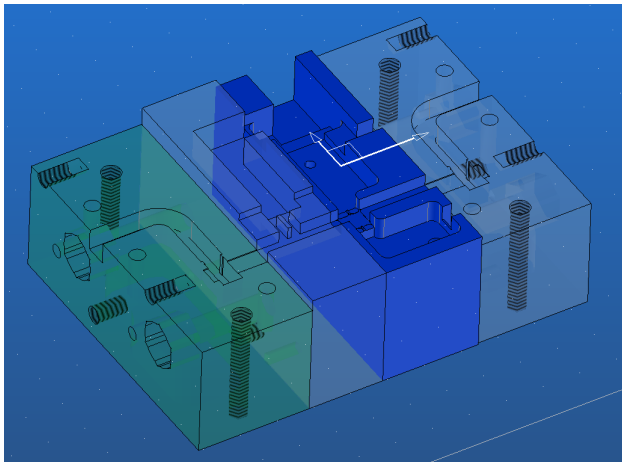
Figure 4.10: LNA mechanic design, the outter blocks are the waveguide to microstrip transitions, in the middle the cryo3 and MMIC blocks are located.

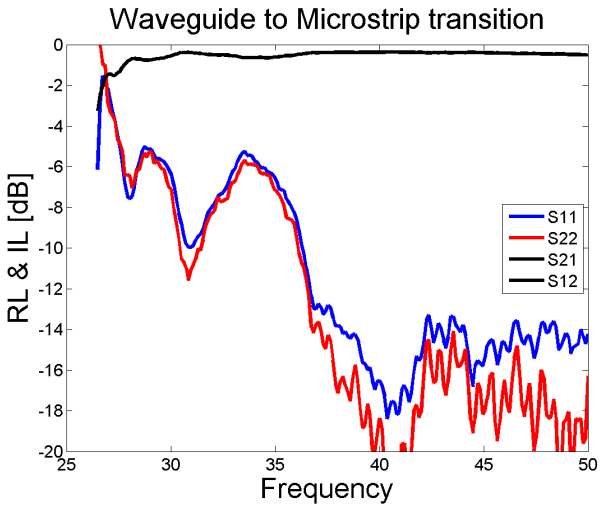

Figure 4.11: Measurement of back to back waveguide to microstrip transitions.

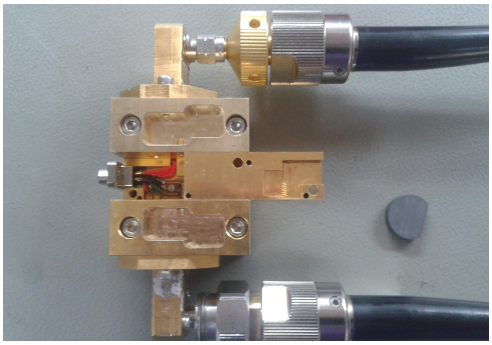

Figure 4.12: Picture of the LNA with the OMMIC block open and the VNA connected for gain measurement.

A waveguide high-pass filter with cut-off frequency of 30 GHz was used to ensure a proper measurement of the noise in the upper-side band. The noise figure of the downconverter was too high and did not allow a proper calibration, therefore an extra LNA was used as first element in the downconverting stage. This amplifier is based in the MMIC from HITTITE company ALH376. A picture of the downconverting stage is presented in figure 4.14. A pyramidal horn was used as input signal for the hot and cold loads.

The noise measurement of the amplifier at room temperature can be seen in figure 4.15. The measurement was performed varying the IF frequency from 4 to 12 GHz for different LO values. In figure 4.15 colors correspond to different LO frequencies. The gain obtained from the noise measurement is also plotted. The amplifier shows a gain above 27 dB and a noise temperature of 220 K in the whole band of interest. Due to measurements errors, a gain above 35 dB was measured at 46 GHz that does not correlate accordingly with the measurements with other LO. The bias point of the measurement is presented in table 4.1. It is important to notice that the noise temperature of this device at room temperature is comparable with a packaged LNA from Fraunhofer Institute for Applied Solid State Physics (IAF) whose noise at room temperature is approximately 200 K (J. D. Gallego, personal communication, April, 2013).

To measure the noise at cryogenic temperatures a vacuum window was built in HDPE.

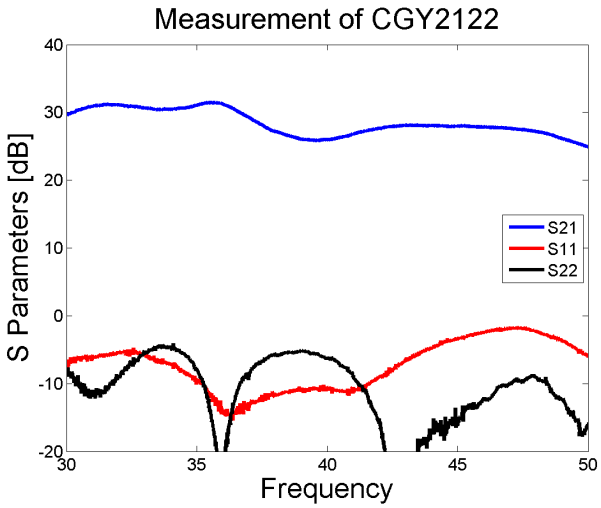

Figure 4.13: Measurment of S parameters of the MMIC.

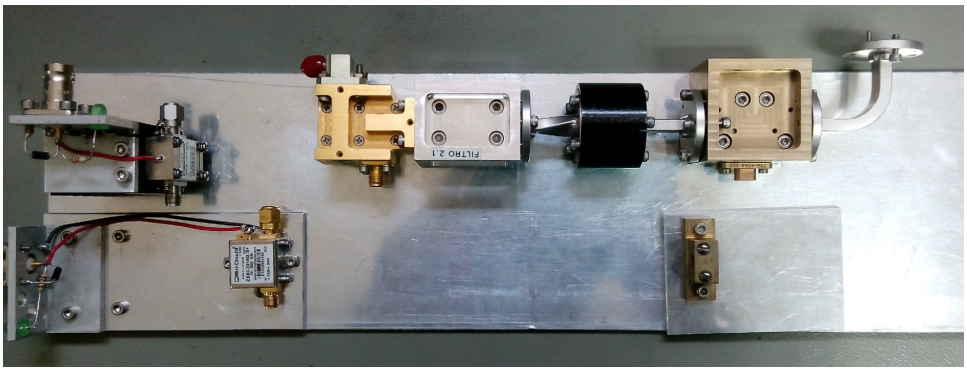

Figure 4.14: Picture of the down-converter plate for Q band measurements.

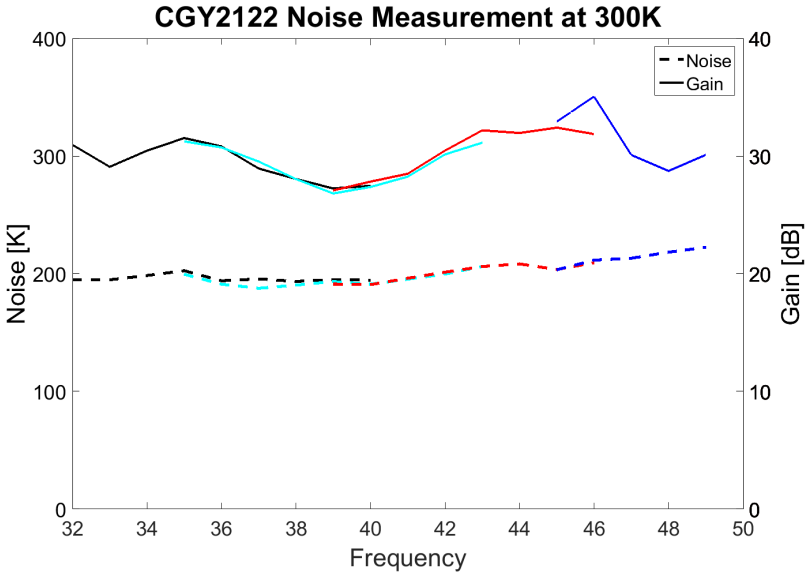

Figure 4.15: Noise measurement of the packaged CGY2122 MMIC at room temperature. Solid lines represents the gain (right axis) and dashed lines the noise (left axis). Different colors corresponds to different frequencies of the LO signal.

Table 4.1: CGY2122 bias point for room temperature noise measurement

Stage	V_{d} [V]	I_{d} [mA]	V_g [V]
1	1	9.5	-0.1
2	1	7	-0.16
3 & 4	0.9	14	-0.1

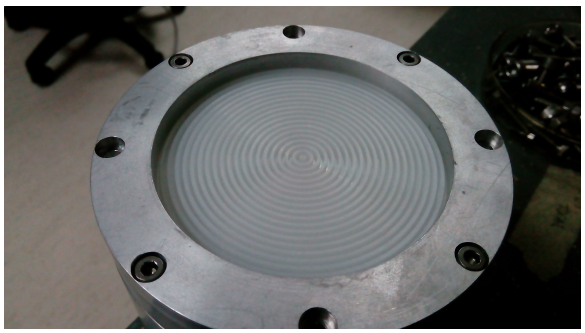

Figure 4.16: Picture of the grooved vacuum window built in HDPE.

Circular grooves were added to minimize the losses of the window, see picture 4.16. After the LNA a thin layer (12 μm) of Mylar was used between the waveguides in the cryostat output. Temperature sensors were used to check that the LNA was at the proper temperature.

Finally, several noise measurements at different bias points were performed. Figure 4.17 presents the best results obtained at 15 K subtracting the effects of the vacuum window. The noise temperature decreases and is below 40 K, the gain increases being above 33 dB in the whole band. The total power consumed by this LNA is below 20 mW. These characteristics makes this commercial MMIC very suitable to be part of a cryogenic down-converting stage.

4.3.7 Cryo3 + MMIC Amplifier

After the MMIC was completely measured the final amplifier (comprised by the cryo3 transistor and the OMMIC MMIC) was re-simulated using the measured noise temperature. The final simulations can be seen in figure 4.18. The simulated noise temperature of the amplifier is below 18 K in the whole band with a minimum of 12.5 K in the lower part of the band. The simulated gain is above 40 dB. Figure 4.19 shows two pictures of the cryo3 transistor mounted in front of the MMIC. Although the transistor in figure 4.19 seems to be mounted correctly, a problem with the bound wires occurred. During the bonding process the met-

Table 4.2: CGY2122 bias point for cryogenic measurement

Stage	V_{d} [V]	I_{d} [mA]	V_g [V]
1	0.7	4	-0.04
2	0.7	4	-0.03
3 & 4	1.1	12	-0.04

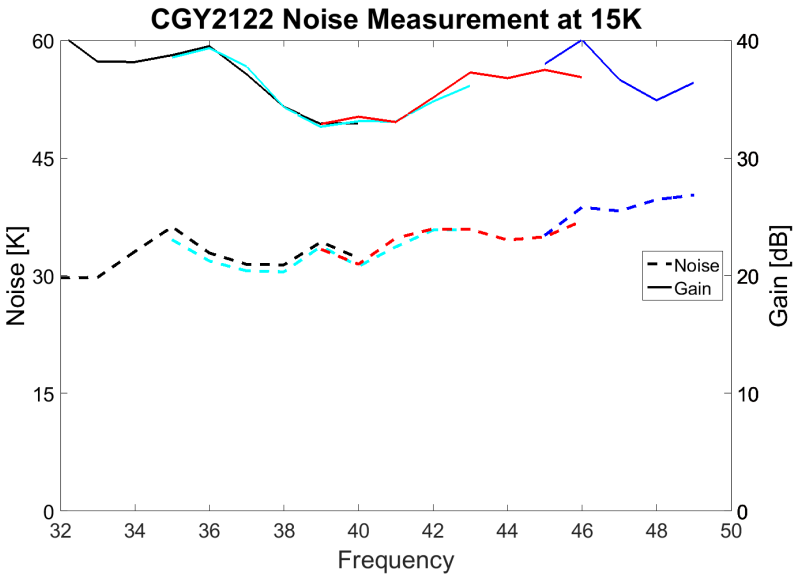

Figure 4.17: Noise measurement of the packaged CGY2122 MMIC at cryogenic temperature. Solid lines represents the gain (right axis) and dashed lines the noise (left axis). Different colors corresponds to different frequencies of the LO signal.

allization of the drain pad was removed. This could only be seen with the microscope in the probe station which has more zoom than the one installed in the bonding machine. A detail of the mounted transistor can be seen in figure 4.20. Unfortunately, the removal of the metallization makes the transistor unusable. Two more attempts to bond the transistor were made with lower ultrasonic power but the results were the same. Therefore it was not possible to measure this LNA.

4.4 W-Band LNA

In this section we packaged and measured two commercial LNA MMICs. The aim is to use these MMICs as a first stage of a downconverter compact module to reduce the equivalent noise temperature added by the mixers. To build a complete receiver with state-of-the-art noise temperature an extra amplifier will be needed. At the time of developing this thesis, only two alternatives were available:

- HRL: LN4-110: The LN4-110 HRL MMIC is a four stage amplifier based on InP HEMTs. It has a single drain supply and is typically used with an independent gate bias for the first stage and a common gate bias for the remaining stages. The behaviour given by the manufacturer can be seen in figure 4.21. The MMIC has a gain above 22 dB and a noise figure below 3.2 dB on the whole frequency band.
- OMMIC CGY2190: The CGY2190 is four stage LNA based on GaAS mHEMT with a high indium contain. The behaviour given by the manufacturer can be seen in figure 4.22. The MMIC has a gain above 20 dB and a noise figure below 3 dB on the whole frequency band.

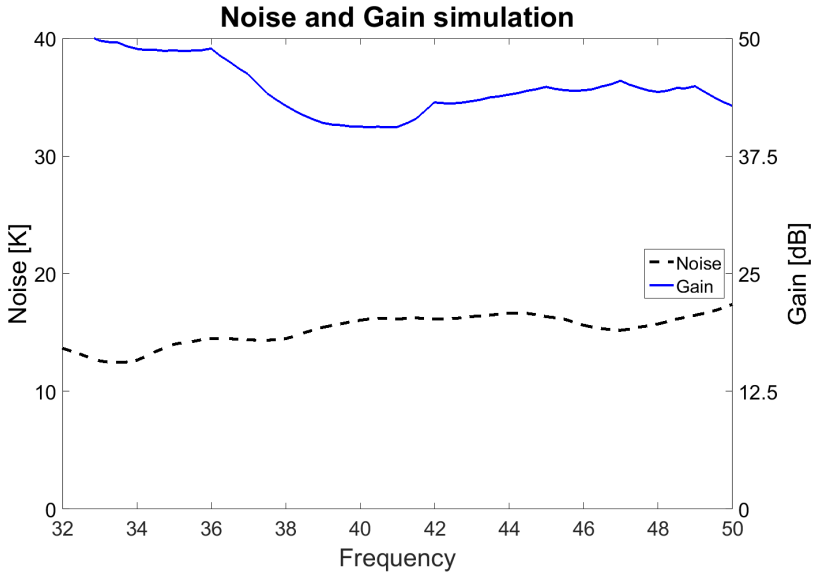

Figure 4.18: Complete LNA simulations using the gain and noise measurements of the MMIC in the model. Solid lines represents the gain (right axis) and dashed lines the noise (left axis). Compared with simulation based only with data in figure 4.9 the noise temperature improves substantially

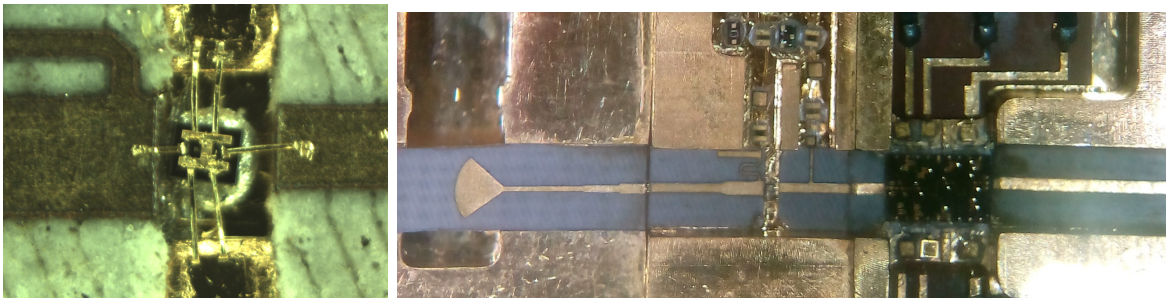

Figure 4.19: Cryo3 transistor mounted in front of the OMMIC MMIC. Left: detail of the bondwires connecting the cryo3. Right: Picture of the transition, transistor and MMIC block assembled.

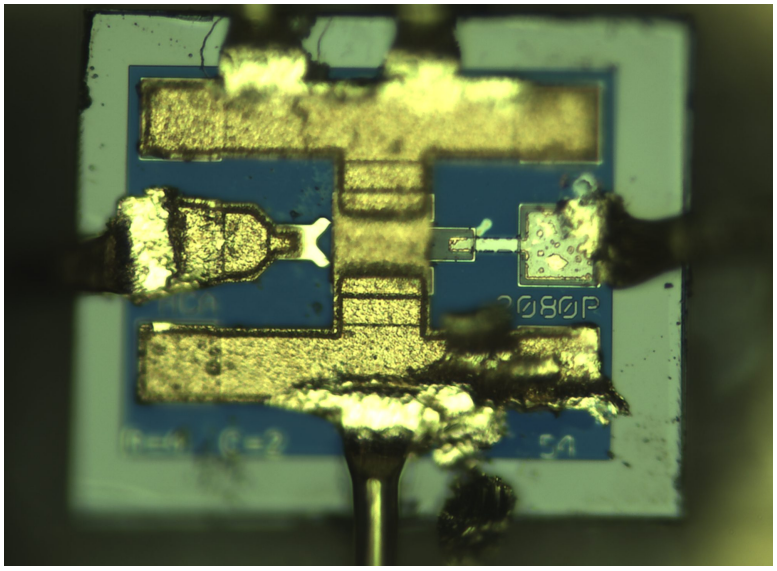

Figure 4.20: Cryo3 transistor mounted with the drain pad metallization removed. Compare with figure 4.4 which has it's full metallization.

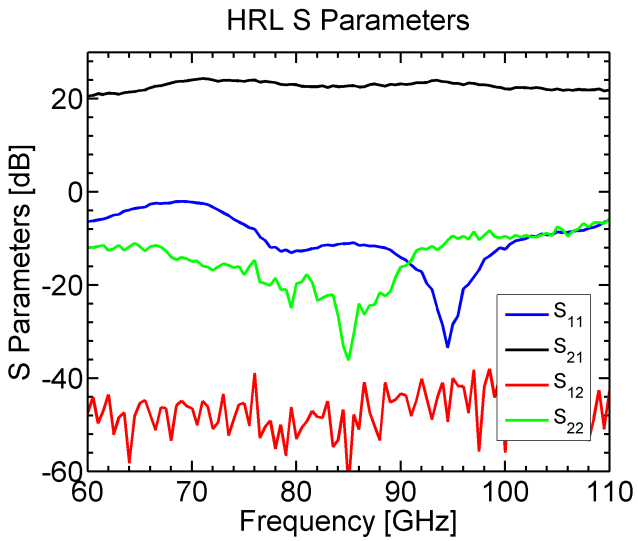

Figure 4.21: S parameters for LN4-110 MMIC obtained from the datasheet

Finally, for comparison, a LNA built in CalTech for the same frequency band was also tested in the laboratory. This LNA is biased using a single value for V_{d} and V_g.

4.4.1 Waveguide to microstrip transition:

A low-reflection antenna was designed in HFSS to transmit the principal mode of a rectangular WR-10 waveguide to a 50 Ω impedance microstrip line. This line can be modified to compensate the input bondwire of the MMIC. The simulation was done in Duroid 5880 substrate ($\varepsilon_r = 2.2$) of 127 μm thickness and showed reflections lower than -20 dB between 75 and 110 GHz. The size of the cavity for the microstrip line was chosen to not allow the propagation of rectangular waveguide modes on the desired band. With the dimension of the

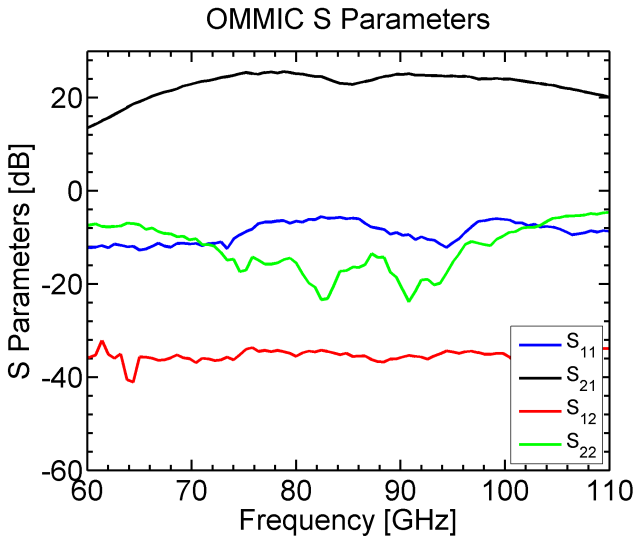

Figure 4.22: S parameters for CGY2190 MMIC obtained from the datasheet

final design the cut-off frequency of these modes is above 160 GHz.

Figure 4.23 shows the measured insertion and return losses of two waveguide to microstrip transitions connected back-to-back. Return losses are below -14 dB and insertion losses lower than 1.9 dB in almost all the band. To estimate the real insertion losses of the transition from figure 4.23 several items have to be taken into account:

- The waveguide inside the bronze split block is approximately 20 mm long, the simulated value of the insertion loss is 0.19 dB at 90 GHz for each transition.
- The transmission loss of the microstrip was estimated using AWR. For the 2.5 mm long substrate the loss is 0.1 dB for each transition at 90 GHz.
- Insertion loss at 90 GHz is approximately 1.4 dB

It is important to notice that the previously detailed transmission losses are only theoretical and the real value is higher. The estimated transmission losses of each transition is 0.45 dB. This estimation is very inaccurate but from their values it is possible to deduce that the transition losses are not too high and that a big contribution to the total losses are the losses in the waveguides and in the substrate. Considering these losses the noise temperature of the MMIC will drop by approximately a 20%

4.4.2 Noise measurement

The noise of the amplifier was measured using the Y-factor method. A downconverting setup with a high gain amplifier for low frequencies was built to increase the noise floor of the power meter. The donwconverter is based on the sub-harmonic mixers built and designed in the laboratory for band 2+3 3.6. The LO is generated using an Anritsu Generator that works up to 40 GHz followed by a Marki doubler, this enables us to generate a signal up to 65 GHz. To increase the LO output power an instrumental amplifier was used. To decrease the noise added by the mixers two RF LNAs were used as first element in the downconverting stage.

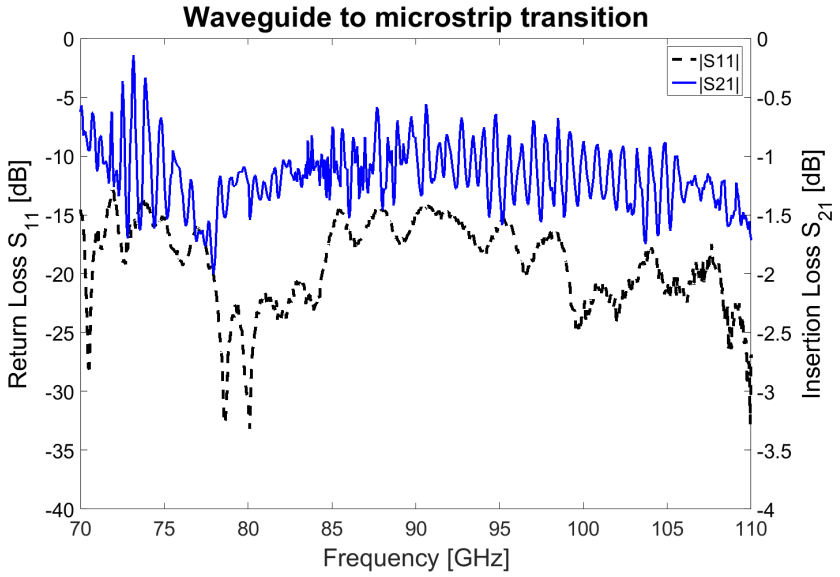

Figure 4.23: Measurement of two rectangular waveguide to microstrip transitions.

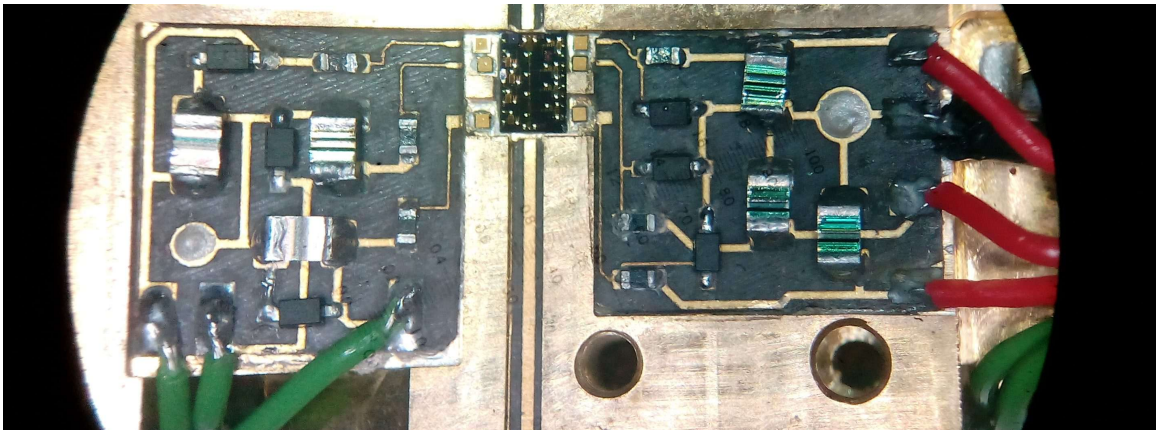
Figure 4.24: Picture of the MMIC CGY2190 from the OMMIC foundry packaged with microstrip input and output.

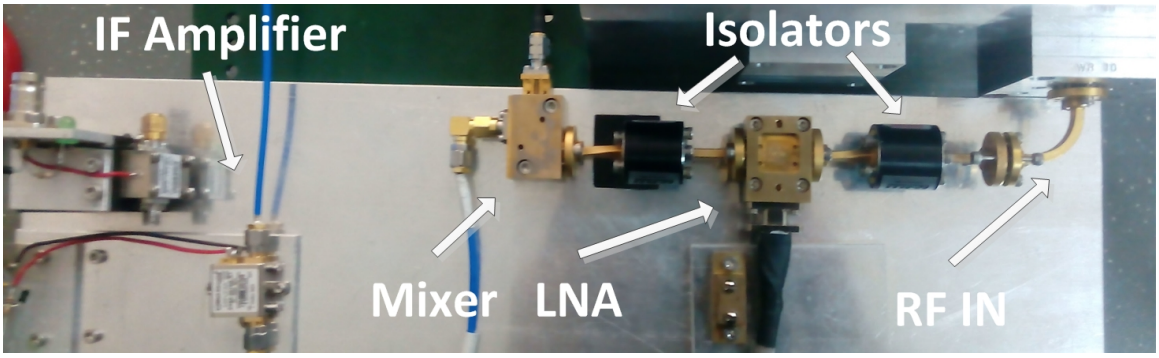

Figure 4.25: W-band down-converter for noise measurements

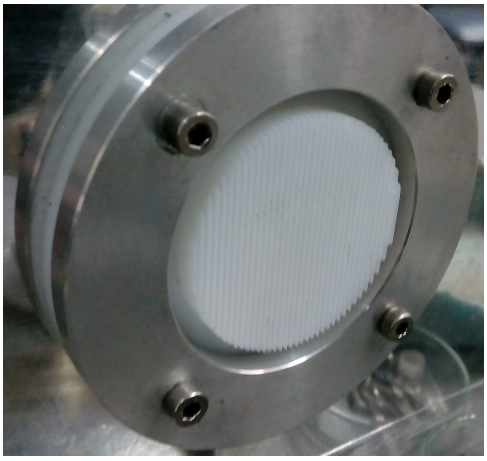
Figure 4.26: Vacuum window built in HDPE for W-Band

The amplifiers used are CalTech W10 and an amplifier based in the HRL MMIC. The mixer, as described in section 3.6, cannot work with an LO above 53 GHz. The measure was done using a fixed IF at 150 MHz varying the LO signal. A picture of the downconverting stage is presented in figure 4.25.

To measure the noise temperature at cryogenic temperature a vacuum window in HDPE was built. This vacuum window ensures good transmission in the band of interest by using triangular grooves. A picture of the vacuum window built is presented in figure 4.26

Figures 4.27 and 4.13 present the noise temperature and gain measurement at 15 K from LN4-110 and CGY2190 respectively subtracting the effects of the vacuum window. For the HRL MMIC (LN4-110), the noise is below 85 K and the gain above 17 dB in the band from 75 to 105 GHz. The noise of CGY2190 is about 10 K higher than LN4-110 and the gain is similar. Both LNAs are suitable to be used in a down-converter unit due their noise temperature, gain, low power consumption and commercial availability.

Finally the packaged LNA "CalTech 48" was measured. The gain and noise temperature measured at 15 K are presented in figure 4.29. The noise is below 74 K and the gain above 16 dB. A great performance is shown in the whole band. The bias point used for the measurement is: $V_g : 0.085V$, $I_g : 3nA$, $V_\mathrm{d} : 0.4V$ and $I_\mathrm{d} : 7.6mA$.

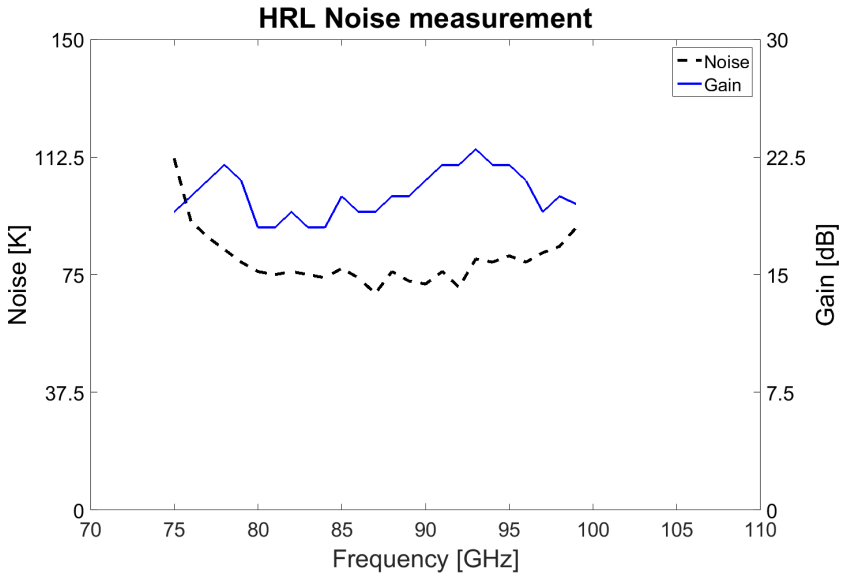

Figure 4.27: Noise measurement of LN4-110 MMIC. Noise and gain are presented in black dashed line and solid blue line respectively.

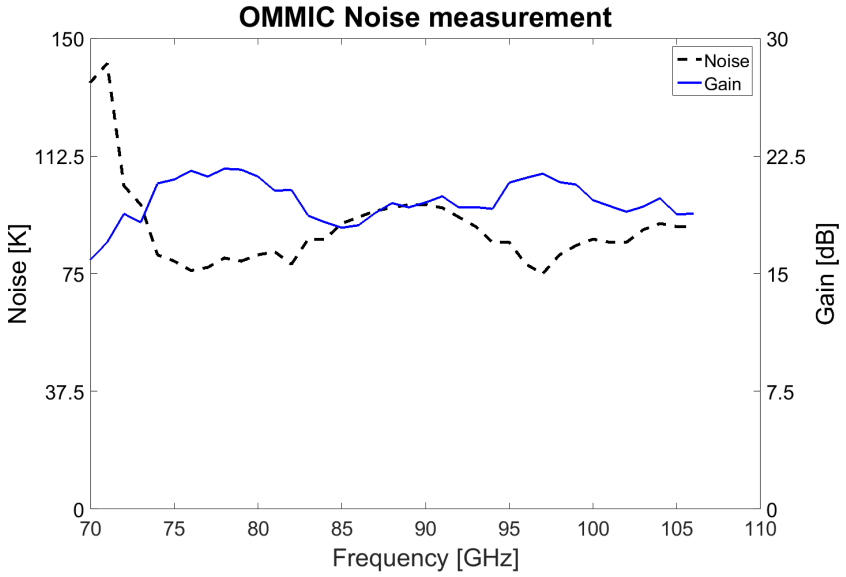

Figure 4.28: Noise measurement of CGY2190 MMIC. Noise and gain are presented in black dashed line and solid blue line respectively.

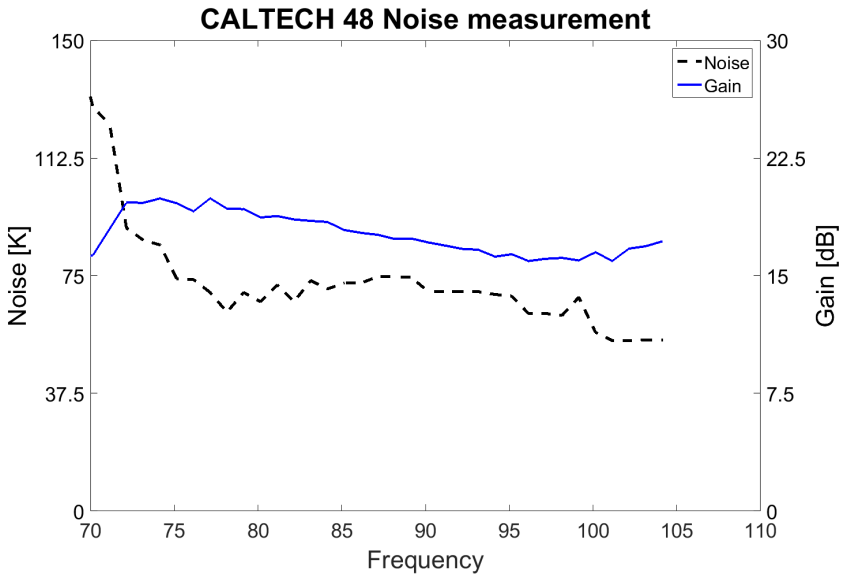

Figure 4.29: Noise measurement of CALTECH-48 LNA. Noise and gain are presented in black dashed line and solid blue line respectively.

4.5 Conclusions

In this chapter the efforts to build LNAs for the Q and W bands have been presented. In both bands, cryogenic setups were built to measure the noise temperature accurately.

For Q-band, a hybrid LNA was designed . It is comprised of a cryo3 transistor placed in front of a commercial MMIC from OMMIC foundry. The chosen MMIC shows a measured noise below 40 K and a gain above 32 dB at cryogenic temperature. The simulations of the complete LNA, including the measurements of the MMIC, shows promising results: a noise temperature below 18 K and a gain above 40 dB in the whole band. In the future, the complete LNA will be measured once the packaging of the transistor is finished.

For the W-band two different commercial MMICs were packaged and measured. Both of them have very low power consumption and, although not tested by their manufacturer, can work at cryogenic temperatures. The first, from HRL is based in InP HEMTs, the noise is below 85 K and a gain above 17 dB from 75 to 105 GHz. The second is from OMMIC foundry, and it is based on GaAs mHEMTs with 70 indium content. Measurements show a noise temperature 10 K above the HRL MMIC and a similar gain. Considering these MMICs are commercially available they are very suitable for a down-converting stage of a heterodyne receiver at these frequencies. Finally, for comparison, a LNA from CALTECH was measured at the laboratory. It shows a great performance from 80 to 105 GHz with a noise temperature below 70 K and a gain above 15 dB.

Chapter 5

Compact down-converter module

5.1 Introduction

In this chapter we present the measurements of a simple prototype of a downconverter module. This is the first step in the laboratory towards a more compact downconverter to be used in multibeams systems at ALMA Band-2+3 frequencies. This module could also be used as an upgrade for the downconverting stage of the SMWT radiotelescope located at Cerro Calan.

5.2 Construction

The components presented in chapters 4 and 5 were interconnected using bond wires to assemble a simple prototype of a compact receiver for W-band. Due to the unavailability of a good LNA MMIC, the first stage of this prototype is based in the OMMIC MMIC described previously. The aim of this receiver is to be used as small downconversion unit placed after the main LNA. For this prototype, the mixer designed in section 3.5 was used. A diagram of the components present inside the module is shown in figure 5.1

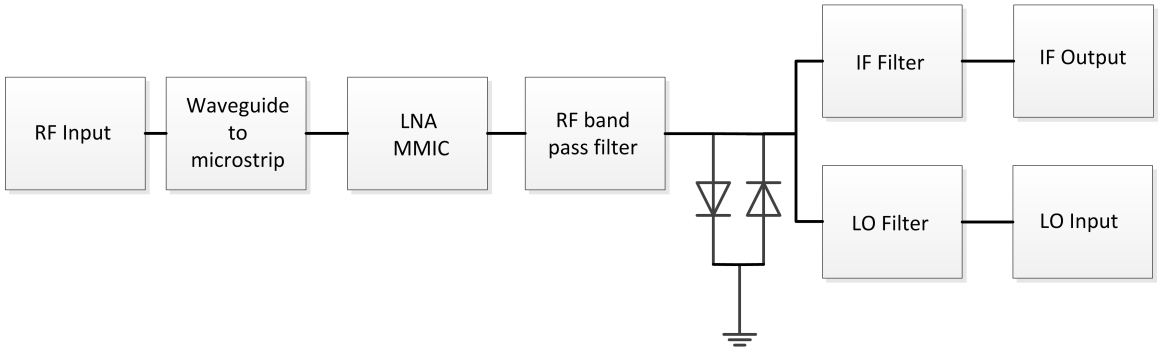

Figure 5.1: Downconverting prototype design.

All the blocks were interconnected using bond wires. A picture of the assembled single pixel prototype is presented in figure 5.2.

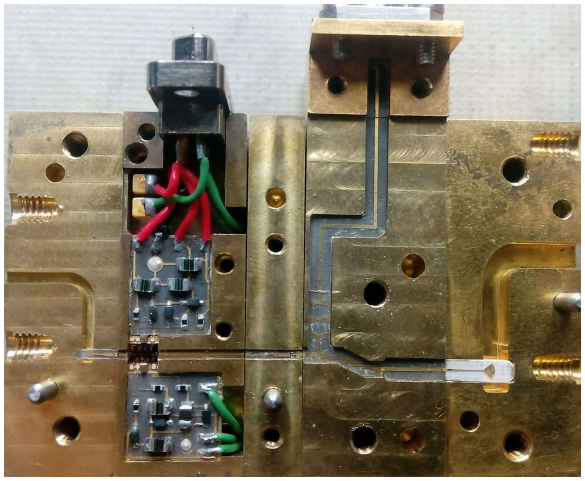

Figure 5.2: Downconverting prototype module assembled with the components previously designed.

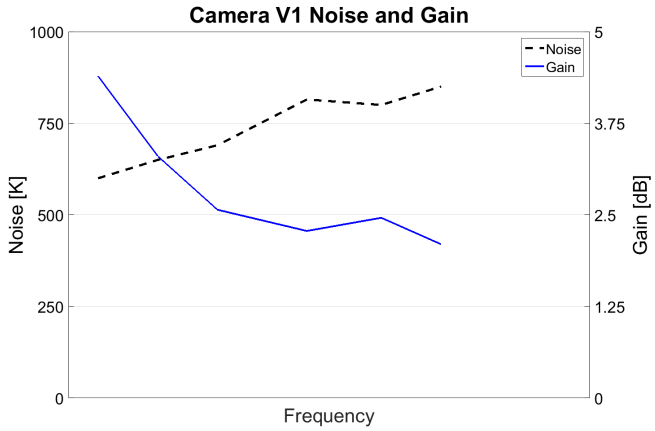

Figure 5.3: Measured noise and gain of the downconverting module.

5.3 Measurements

Noise temperature and gain at room temperature were measured encouraged by the idea of using this module outside the cryostat. Both measurements can be seen in figure 5.3. To increase the output power level for the noise measurement an IF amplifier was used which effect was discounted.

Noise temperature is below 850 K and conversion gain is above 2 dB. This module can be used as a downconversion unit behind a state of the art LNA [33] [34] [64] with, for example, a gain of 20 dB, thus contributing to the total noise of the receiver chain by just 8 K. It is important to notice that this result can probably be improved by adding more bondwires at the input of the MMIC or by designing a different microstrip input. The effect of adding more bondwires have already been measured, in effect, at room temperature measurements with just one bondwire and three bondwires were performed when measuring just the OMMIC LNA. Figure 5.4 shows the change in the noise temperature of the LNA when adding more bondwires. In the measurements presented in figure 5.4 the effect of the downconverting stage has not been discounted, for this reason, the noise increases at frequencies above 95 GHz.

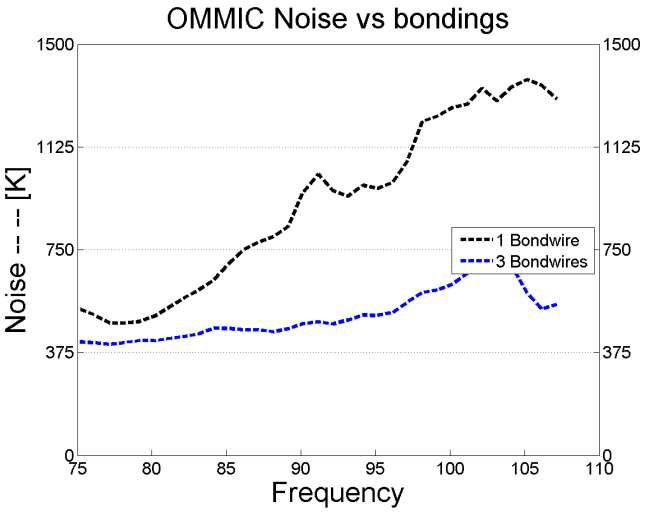

Figure 5.4: Noise measurements of the CGY2190 MMIC alone at room temperature changing the number of bondwires at the input.

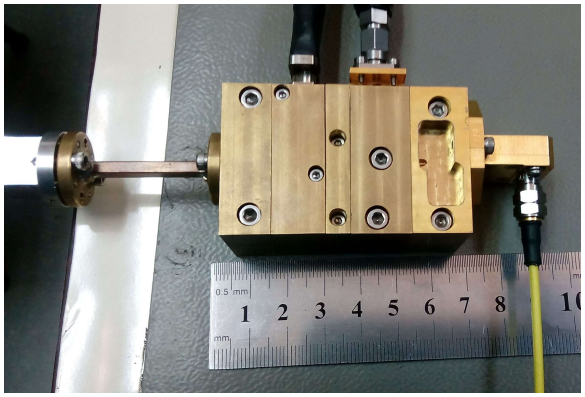

Figure 5.5: Single pixer prototype module assembled with the components previously designed.

A picture of the enclosed module can be seen in figure 5.5. It can be seen from this figure that the size of this prototype is at least two times greater than a WR-10 circular flange, making it unsuitable for a high density focal plane array. The main reason why this prototype is too bulky is because of the bolts needed to interconnect the different blocks. To reduce its size the following strategies can be used:

- Remove interconnecting bolts and construct the module in one split block.
- Replace the WR22 flange and waveguide distribution for the LO and use GPPO or 1.85 mm connectors.
- Replace the mixer circuit built using discrete components by the mixer designed in MMIC technology described in section 3.7.

The last strategy also allows to increase the possible bandwidth to ALMA Band-2+3 and reduce the required LO power.

5.4 Conclusions

A simple prototype of a compact downconverter module has been presented. It is based in an OMMIC MMIC low noise amplifier and in the first version of the mixer built at U. de Chile. Although it has not been optimized, the module has conversion gain above 2 dB and a noise below 850 K. This noise probably can be reduced by adding more bondwires or modifying the microstrip input.

We expect to build a compact and more efficient down-converting module using the designed MMICs. Moreover, by changing the LO input from waveguide to 1.85 mm or GPPO connectors the module can reduce its size. Moreover, we aim to use two MMIC mixers to use a 2SB scheme in the module. Moreover, considering the low LO power the mixer MMICs requires they, are suitable for downconverting modules in a multibeam system.

Chapter 6

Conclusions and Future Work

The main goal of this thesis has been the development of technologies to design, build and measure high-quality components for receivers for bands Q and W that could be used in astronomical receivers. In both of these bands there are several scientific cases that give rise to the development of radio receivers.

The cryogenic low noise amplifier for ALMA Band 1 (Q-band) has been of interest in the last years due to its demanding noise goals. Amplifiers based only on commercial microwave monolithic integrated circuits (MMICs) had noise temperatures too high to meet ALMA specifications. In this work we designed an amplifier based on a hybrid scheme, composed by a cryo3 transistor and a commercial MMIC from the OMMIC foundry. The MMIC was measured at cryogenic temperatures showing a great performance and promising results for the complete LNA. The complete amplifier has a noise temperature below 18 K and gain above 40 dB which makes this LNA very suitable to be used as first LNA in a receiver. In the future the complete LNA will be measured once the packaging of the transistor is finished.

Several components were designed for W-band. There are two main reasons to develop components in this band. First, there has been international interest in the development on multi beam systems in this band. Then to create compact receivers it is necessary to develop all the components in the laboratory to integrate them as needed. Furthermore, an effort was done to extend the frequency range of the components to include the upper part of band V, thus the components could be suitable for ALMA Band 2+3. Second, the components could be used to upgrade the Southern Millimeter Wave Telescope (SMWT) located at Cerro Calan, Chile.

Special emphasis during this thesis project was the development of mixers based on Schottky diodes. This was the first attempt in the laboratory at U. de Chile to design and build this type of devices. In particular, four versions of mixers were fabricated. The first two of them were built using discrete components using diodes from UMS. The first prototype covers band W and is very bulky. The second version had many improvements that made the mixer smaller and also with more bandwidth. Both of these mixers behave accordingly with simulations and show conversion losses below 15 dB in their working band. Although these mixers have an exceptional bandwidth their noise temperature is too high and therefore they

need to be used with a LNA in front. There is still a lot of work to be done to diminish the conversion losses and the noise temperature, including the possibility to use other diodes has to be considered.

The last two mixers were designed using MMIC technology from the UMS foundry. This will allow us to package our mixers easily and in less area. The first MMIC uses a shunt configuration and has a bias configuration that allows the mixer to work with less LO power. The second MMIC uses a series configuration and has already been measured presenting a good behavior from 85 to 112 GHz. The promising results of this first generation of mixers developed completely at U. de Chile allow us to think about continuing to develop this area in the future.

During the study of new ways to integrate the antenna element and the integrated circuit, a tapered slot antenna (TSA) was developed. This is a planar antenna built in a substrate that allows an easy integration with MMICs. Moreover, they are very small compared to horn antennas. TSAs have been extensively studied at low frequencies in the past but there were few studies at millimeter wavelengths. During this thesis a corrugated TSA was optimized. The optimization included the profile and the corrugations to obtain a high performance antenna. The results shows stable beam patterns and working frequency from 75 to 110 GHz.

Low noise amplifiers for W-band were packaged and tested. These amplifiers are based on commercial MMICs from OMMIC and HRL foundries. Both of these amplifiers work at cryogenic temperature and show a good performance at 15 K. Their noise temperature is higher than a state of the art LNA but they can be very useful as a first stage amplifier in a downconverting module working at cryogenic or room temperature.

Finally, all the components developed for W-band allowed us to start the design and construction of a downconverting module for an array receiver. In a collaboration with the Shanghai Observatory for the next two years we plan to build a 2SB small and compact dowconverting module with low LO power consumption and a conversion loss of 0 dB. The designed MMIC mixer and the OMMIC LNA are key components for this project.

Bibliography

[1] F. J. Lovas, "Nist recommended rest frequencies for observed interstellar molecular microwave transitions 2002 revision," *Journal of Physical and Chemical Reference Data*, vol. 33, no. 1, pp. 177–355, 2004.

[2] B. F. Burke and F. Graham-Smith, *An introduction to radio astronomy*. Cambridge University Press, 2010.

[3] F. Walter, F. Bertoldi, C. Carilli, P. Cox, K. Lo, R. Neri, X. Fan, A. Omont, M. A. Strauss, and K. M. Menten, "Molecular gas in the host galaxy of a quasar at redshift z = 6.42," *Nature*, vol. 424, no. 6947, pp. 406–408, 2003.

[4] N. Fourikis, *Advanced array systems, applications and RF technologies*. Academic Press, 2000.

[5] R. Rudersdorfer, *Radio Receiver Technology: Principles, Architectures and Applications*. John Wiley & Sons, 2013.

[6] J. Zmuidzinas, A. Karpov, D. Miller, F. Rice, H. G. Leduc, J. Pearson, and J. A. Stern, "Coherent detection and sis mixers," in *Far-IR, Sub-mm and MM Detector Technology Workshop*, 2002.

[7] G. Gol'tsman and D. Loudkov, "Terahertz superconducting hot-electron bolometer mixers and their application in radio astronomy," *Radiophysics and quantum electronics*, vol. 46, no. 8-9, pp. 604–617, 2003.

[8] W. Bennett, "Sources and properties of electrical noise," *Electrical Engineering*, vol. 73, no. 11, pp. 1001–1006, 1954.

[9] R. F. Voss, "1/f (flicker) noise: A brief review," in *33rd Annual Symposium on Frequency Control. 1979*, pp. 40–46, IEEE, 1979.

[10] F. Ellinger, *Radio frequency integrated circuits and technologies*. Springer Science & Business Media, 2008.

[11] D. M. Pozar, *Microwave engineering*. John Wiley & Sons, 2009.

[12] G. Gonzalez, *Microwave transistor amplifiers: analysis and design*, vol. 61. Prentice-Hall Englewood Cliffs, NJ, 1984.

[13] E. Kollberg and S. Yngvesson, "Quantum noise contribution to the receiver noise temperature of heb thz heterodyne receivers," in *Proc. 13th Int. Space Terahertz Technol. Symp*, pp. 73–84, 2002.

[14] G. Tan, B. Jackson, B. Lazareff, J. Adema, A. Baryshev, R. Hesper, T. Klapwijk, M. Kroug, S. Mahieu, D. Maier, *et al.*, "The european receivers for alma," *The Messenger*, vol. 118, p. 18, 2004.

[15] C. Groppi, C. Walker, C. Kulesa, D. Golish, J. Kloosterman, S. Weinreb, G. Jones, J. Barden, H. Mani, T. Kuiper, *et al.*, "Supercam: A 64 pixel heterodyne array receiver for the 350 ghz atmospheric window," in *20th Int. Space Terahertz Technol. Symp*, pp. 90–96, 2009.

[16] J. a. Buckle, R. Hills, H. Smith, W. Dent, G. Bell, E. Curtis, R. Dace, H. Gibson, S. Graves, J. Leech, *et al.*, "Harp/acsis: a submillimetre spectral imaging system on the james clerk maxwell telescope," *Monthly Notices of the Royal Astronomical Society*, vol. 399, no. 2, pp. 1026–1043, 2009.

[17] K. Rohlfs, "Tools of radio astronomy," *Berlin and New York, Springer-Verlag, 1986, 332 p.*, vol. 1, 1986.

[18] D. S. Russell, *Technology advances for radio astronomy*. PhD thesis, California Institute of Technology, 2012.

[19] M. Sieth, K. Devaraj, P. Voll, S. Church, R. Gawande, K. Cleary, A. C. Readhead, P. Kangaslahti, L. Samoska, T. Gaier, *et al.*, "Argus: a 16-pixel millimeter-wave spectrometer for the green bank telescope," in *Millimeter, Submillimeter, and Far-Infrared Detectors and Instrumentation for Astronomy VII*, vol. 9153, p. 91530P, International Society for Optics and Photonics, 2014.

[20] A.-L. Fontana, C. Boucher, P. Serres, Y. Bortolotti, F. Cope, I. Stil, B. Lefranc, O. Garnier, G. Butin, F. Mattiocco, *et al.*, "A 3mm multipixel sis receiver for iram 30-m pico veleta telescope," in *Millimeter, Submillimeter, and Far-Infrared Detectors and Instrumentation for Astronomy VI*, vol. 8452, p. 84522E, International Society for Optics and Photonics, 2012.

[21] A. Kerr, B. Eric, T. Crowe, N. Erikson, R. Fisher, P. Goldsmith, C. Gottlieb, C. Groppi, J. Hesler, T. Hunter, *et al.*, "In support of instrument technology development for thz astronomy," in *Astro2010: The Astronomy and Astrophysics Decadal Survey*, vol. 2010, p. 29, 2009.

[22] M. Sieth, S. Church, J. M. Lau, P. Voll, T. Gaier, P. Kangaslahti, L. Samoska, M. Soria, K. Cleary, R. Gawande, *et al.*, "Technology developments for a scalable heterodyne mmic array at w-band," in *Microwave Conference (EuMC), 2011 41st European*, pp. 527–530, IEEE, 2011.

[23] A.-L. Fontana, B. Lazareff, A. Navarrini, and Y. Bortolotti, "Heterodyne array receiver for radio astronomy in the 2mm band," in *Microwave Conference (EuMC), 2010 European*, pp. 906–909, IEEE, 2010.

[24] Y. Kyung-Wan, Y. In-Bok, U. Man-Seok, L. Jae-Hyun, and L. Seong-Pal, "Low noise k-band mmic receiver module," *IEICE transactions on electronics*, vol. 83, no. 5, pp. 750–754, 2000.

[25] P. Puetz, A. Hedden, P. Gensheimer, D. Golish, C. Groppi, C. Kulesa, G. Narayanan, A. Lichtenberger, J. Kooi, N. Wadefalk, *et al.*, "345 ghz prototype sis mixer with integrated mmic lna," *International journal of infrared and millimeter waves*, vol. 27, no. 10, pp. 1365–1379, 2006.

[26] G. Chattopadhyay, N. Llombart, C. Lee, C. Jung, R. Lin, K. B. Cooper, T. Reck, J. Siles, E. Schlecht, A. Peralta, *et al.*, "Terahertz array receivers with integrated antennas," in *Antenna Technology (iWAT), 2012 IEEE International Workshop on*, pp. 319–322, IEEE, 2012.

[27] E. Schlecht, J. V. Siles, C. Lee, R. Lin, B. Thomas, G. Chattopadhyay, and I. Mehdi, "Schottky diode based 1.2 thz receivers operating at room-temperature and below for planetary atmospheric sounding," *IEEE Transactions on Terahertz Science and Technology*, vol. 4, no. 6, pp. 661–669, 2014.

[28] P. H. Siegel, R. P. Smith, M. Graidis, and S. C. Martin, "2.5-thz gaas monolithic membrane-diode mixer," *IEEE Transactions on Microwave Theory and Techniques*, vol. 47, no. 5, pp. 596–604, 1999.

[29] Y. Uzawa, M. Kroug, T. Kojima, M. Takeda, M. Candotti, Y. Fujii, K. Kaneko, W. Shan, T. Noguchi, and Z. Wang, "A sensitive alma band 10 sis receiver engineering model," *Superconductor Science and Technology*, vol. 22, no. 11, p. 114002, 2009.

[30] T. De Graauw, F. Helmich, T. Phillips, J. Stutzki, E. Caux, N. Whyborn, P. Dieleman, P. Roelfsema, H. Aarts, R. Assendorp, *et al.*, "The herschel-heterodyne instrument for the far-infrared (hifi)," *Astronomy & Astrophysics*, vol. 518, p. L6, 2010.

[31] D. Cuadrado-Calle, D. George, B. Ellison, G. A. Fuller, and K. Cleary, "Celestial signals: Are low-noise amplifiers the future for millimeter-wave radio astronomy receivers?," *IEEE Microwave Magazine*, vol. 18, no. 6, pp. 90–99, 2017.

[32] M. S. Reid, *Low-noise systems in the deep space network*. 2008.

[33] M. Varonen, R. Reeves, P. Kangaslahti, L. Samoska, A. Akgiray, K. Cleary, R. Gawande, A. Fung, T. Gaier, S. Weinreb, *et al.*, "A 75–116-ghz lna with 23-k noise temperature at 108 ghz," in *Microwave Symposium Digest (IMS), 2013 IEEE MTT-S International*, pp. 1–3, IEEE, 2013.

[34] D. Cuadrado-Calle, D. George, G. A. Fuller, K. Cleary, L. Samoska, P. Kangaslahti, J. W. Kooi, M. Soria, M. Varonen, R. Lai, *et al.*, "Broadband mmic lnas for alma band 2+ 3 with noise temperature below 28 k," *IEEE Transactions on Microwave Theory and Techniques*, vol. 65, no. 5, pp. 1589–1597, 2017.

[35] K. S. B. M. J. E. M. Pospieszalski, S. Srikanth, "Alma band 1 receiver development study," *NRAO Mem 9145a rev H1*, 2013.

[36] A. H. Akgiray, S. Weinreb, R. Leblanc, M. Renvoise, P. Frijlink, R. Lai, and S. Sarkozy, "Noise measurements of discrete hemt transistors and application to wideband very low-noise amplifiers," *IEEE Transactions on Microwave Theory and Techniques*, vol. 61, no. 9, pp. 3285–3297, 2013.

[37] P. Gibson, "The vivaldi aerial," in *Microwave Conference, 1979. 9th European*, pp. 101–105, IEEE, 1979.

[38] D. Schaubert, E. L. Kollberg, T. Korzeniowski, T. Thungren, J. Johansson, and K. Yngvesson, "Endfire tapered slot antennas on dielectric substrates," *Antennas and Propagation, IEEE Transactions on*, vol. 33, no. 12, pp. 1392–1400, 1985.

[39] D. S. Woo, K. W. Kim, and H.-C. Choi, "A broadband and high gain tapered slot antenna for w-band imaging array applications," *International Journal of Antennas and Propagation*, vol. 2014, 2014.

[40] K. S. Yngvesson, T. Korzeniowski, Y.-S. Kim, E. L. Kollberg, and J. F. Johansson, "The tapered slot antenna-a new integrated element for millimeter-wave applications," *Microwave Theory and Techniques, IEEE Transactions on*, vol. 37, no. 2, pp. 365–374, 1989.

[41] G. W. Kant, P. D. Patel, S. J. Wijnholds, M. Ruiter, and E. van der Wal, "Embrace: A multi-beam 20,000-element radio astronomical phased array antenna demonstrator," *IEEE Transactions on Antennas and Propagation*, vol. 59, no. 6, pp. 1990–2003, 2011.

[42] N. Jastram and D. S. Filipović, "Wideband millimeter-wave surface micromachined tapered slot antenna," *IEEE Antennas and Wireless Propagation Letters*, vol. 13, pp. 285–288, 2014.

[43] A. Rebollo, R. Gonzalo, and I. Ederra, "Full w-band microstrip fed vivaldi antenna," *Journal of Infrared, Millimeter, and Terahertz Waves*, vol. 37, no. 8, pp. 786–794, 2016.

[44] C. Rusch, J. Schäfer, T. Kleiny, S. Beer, and T. Zwick, "W-band vivaldi antenna in ltcc for cw-radar nearfield distance measurements," in *Antennas and Propagation (EUCAP), Proceedings of the 5th European Conference on*, pp. 2124–2128, IEEE, 2011.

[45] N.-W. Chen, C.-T. Chuang, and J.-W. Shi, "A w-band linear tapered slot antenna on rectangular-grooved silicon substrate," *IEEE Antennas and Wireless Propagation Letters*, vol. 6, pp. 90–92, 2007.

[46] H. Ansoft, "ver. 13," *Ansoft Corporation, Pittsburgh, PA*, 2011.

[47] S. Sugawara, Y. Maita, K. Adachi, K. Mori, and K. Mizuno, "Characteristics of a mm-wave tapered slot antenna with corrugated edges," in *Microwave Symposium Digest, 1998 IEEE MTT-S International*, vol. 2, pp. 533–536, IEEE, 1998.

[48] A. Rezaee Jordehi and J. Jasni, "Parameter selection in particle swarm optimisation: a survey," *Journal of Experimental & Theoretical Artificial Intelligence*, vol. 25, no. 4, pp. 527–542, 2013.

[49] J. Robinson and Y. Rahmat-Samii, "Particle swarm optimization in electromagnetics," *IEEE transactions on antennas and propagation*, vol. 52, no. 2, pp. 397–407, 2004.

[50] J. Kennedy and W. M. Spears, "Matching algorithms to problems: an experimental test of the particle swarm and some genetic algorithms on the multimodal problem generator," in *Evolutionary Computation Proceedings, 1998. IEEE World Congress on Computational Intelligence., the 1998 IEEE International Conference on*, pp. 78–83, IEEE, 1998.

[51] S. Sugawara, Y. Maita, K. Adachi, K. Mori, and K. Mizuno, "A mm-wave tapered slot antenna with improved radiation pattern," in *Microwave Symposium Digest, 1997., IEEE MTT-S International*, vol. 2, pp. 959–962, IEEE, 1997.

[52] R. E. Collin, *Antennas and radiowave propagation*. McGraw-Hill, 1985.

[53] S. Maas, "Microwave mixers, 2nd edn.(artech house, boston, 1993)," tech. rep., ISBN 0-89006-605-1.

[54] R.-Y. Fang and C.-L. Wang, "Wideband slotline-to-rectangular waveguide transition using truncated bow-tie antenna," in *Microwave Conference, 2006. APMC 2006. Asia-Pacific*, pp. 1395–1398, IEEE, 2006.

[55] B. Shuppert, "Microstrip/slotline transitions: Modeling and experimental investigation," *IEEE Transactions on microwave theory and techniques*, vol. 36, no. 8, pp. 1272–1282, 1988.

[56] J. Kooi, G. Chattopadhyay, F. Rice, J. Zmuidzinas, S. Withington, and G. Yassin, "A full-height waveguide to thinfilm microstrip transition," in *Ninth International Conference on Therahertz Electronics*, pp. 15–16, 2001.

[57] M. Van der Merwe and J. de Swardt, "The design and evaluation of a harmonic mixer using an anti-parallel diode pair," *evaluation*, vol. 2, no. 1, p. 6, 1998.

[58] S. A. Maas, *Nonlinear microwave and RF circuits*. Artech House, 2003.

[59] S. A. Maas, "Microwave mixers," *Norwood, MA, Artech House, Inc., 1986, 368 p.*, 1986.

[60] T. Mimura, "The early history of the high electron mobility transistor (hemt)," *IEEE Transactions on microwave theory and techniques*, vol. 50, no. 3, pp. 780–782, 2002.

[61] M. W. Pospieszalski, "Extremely low-noise amplification with cryogenic fets and hfets: 1970-2004," *Microwave Magazine, IEEE*, vol. 6, no. 3, pp. 62–75, 2005.

[62] M. W. Pospieszalski, "Cryogenic amplifiers for jansky very large array receivers," in *Microwave Radar and Wireless Communications (MIKON), 2012 19th International Conference on*, vol. 2, pp. 748–751, IEEE, 2012.

[63] J. Kooi, G. Chattopadhyay, S. Withington, F. Rice, J. Zmuidzinas, C. Walker, and G. Yassin, "A full-height waveguide to thin-film microstrip transition with exceptional

rf bandwidth and coupling efficiency," *International Journal of Infrared and Millimeter Waves*, vol. 24, no. 3, pp. 261–284, 2003.

[64] L. Samoska, M. Varonen, R. Reeves, K. Cleary, R. Gawande, P. Kangaslahti, T. Gaier, R. Lai, and S. Sarkozy, "W-band cryogenic inp mmic lnas with noise below 30k," in *Microwave Symposium Digest (MTT), 2012 IEEE MTT-S International*, pp. 1–3, IEEE, 2012.

[65] L. Belostotski, A. Sutinjo, R. H. Johnston, M. Okoniewski, M. A. Petursson, and T. Burgess, "Study of thermal noise generated in a vivaldi antenna using the improved wheeler cap method," *Antennas and Wireless Propagation Letters, IEEE*, vol. 10, pp. 1047–1050, 2011.

[66] P. F. Goldsmith, I. of Electrical, E. Engineers, M. Theory, and T. Society, *Quasioptical systems: Gaussian beam quasioptical propagation and applications*. IEEE press New York, 1998.

[67] A. Skalare, J. Johansson, E. Kollberg, and R. Murowinski, "Integrated slot-line antennas with sis mixers for focal plane applications," in *17th Eur. Micr. Conf*, pp. 461–465, 1987.

[68] D. Winkler *et al.*, "A new submillimeter wave sis quasi-particle receiver for 750 ghz," in *Proceedings of the 11th International Conference on Infrared Millimeter Waves*, 1986.

[69] E. W. Reid, L. Ortiz-Balbuena, A. Ghadiri, and K. Moez, "A 324-element vivaldi antenna array for radio astronomy instrumentation," *Instrumentation and Measurement, IEEE Transactions on*, vol. 61, no. 1, pp. 241–250, 2012.

[70] P. Hall, "The square kilometre array: An international engineering perspective," in *The Square Kilometre Array: An Engineering Perspective*, pp. 5–16, Springer, 2005.

[71] N. Ghassemi and K. Wu, "Planar high-gain dielectric-loaded antipodal linearly tapered slot antenna for e-and w-band gigabyte point-to-point wireless services," *IEEE Transactions on Antennas and Propagation*, vol. 61, no. 4, pp. 1747–1755, 2013.

[72] B. Alderman, M. Henry, H. Sanghera, H. Wang, S. Rea, B. Ellison, and P. de Maagt, "Schottky diode technology at rutherford appleton laboratory," in *Microwave Technology & Computational Electromagnetics (ICMTCE), 2011 IEEE International Conference on*, pp. 4–6, IEEE, 2011.

[73] Z. Chen, B. Zhang, Y. Fan, X. Yang, and F. Cheng, "Design of a subharmonic mixer with plannar schottky diodes at 300–350 ghz," in *Microwave and Millimeter Wave Circuits and System Technology (MMWCST), 2012 International Workshop on*, pp. 1–3, IEEE, 2012.

[74] B. Thomas, A. Maestrini, J. Gill, C. Lee, R. Lin, I. Mehdi, and P. de Maagt, "A broadband 835–900-ghz fundamental balanced mixer based on monolithic gaas membrane schottky diodes," *IEEE Transactions on Microwave Theory and Techniques*, vol. 58, no. 7, pp. 1917–1924, 2010.

[75] A. A. Note, "Noise figure measurement accuracy–the y-factor method," *Agilent Technology, Palo Alto, CA*, 2001.